GLOBAL CHANGE AND REGIONAL AIR QUALITY: IMPACTS OF CLIMATE, LAND-USE, AND EMISSIONS CHANGES

By

JEREMY CHARLES AVISE

A dissertation submitted in partial fulfillment of
the requirements for the degree of

DOCTOR OF PHILOSOPHY

WASHINGTON STATE UNIVERSITY
Department of Civil and Environmental Engineering

DECEMBER 2007

To the Faculty of Washington State University:

The members of the Committee appointed to examine the dissertation of JEREMY CHARLES AVISE find it satisfactory and recommend that it be accepted.

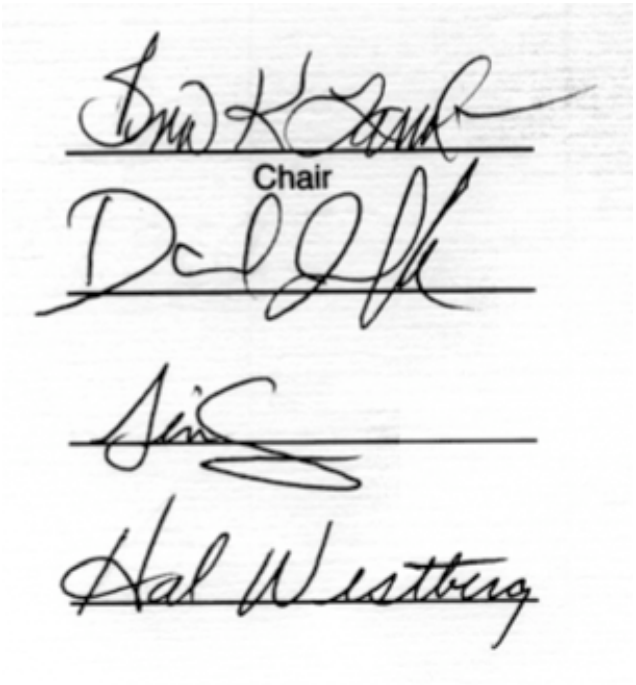

ACKNOWLEDGMENT

I would first and foremost like to thank my graduate advisor, Dr. Brian Lamb, for his mentoring and kindness throughout my time at Washington State University. He has been a tremendous inspiration to me. I would also like to acknowledge the U.S. EPA Science to Achieve Results Fellowship Program for their financial support.

I would like to thank my committee members Dr. Hal Westberg, Dr. Dan Jaffe, and Dr. Serena Chung for their helpful comments and suggestions on this dissertation, as well as Dr. George Mount for all of his suggestions leading up to my defense.

Special thanks goes to all of the LAR graduate students, and in particular, Jack Chen for collaborating on various projects, and Ying Xie for sharing an office with me for the past five years.

Most importantly, I would like to thank my parents for all of their support and guidance, and for teaching me to believe in myself. Lastly, I would like to thank my wife for all of her support and encouragement.

GLOBAL CHANGE AND REGIONAL AIR QUALITY: IMPACTS OF CLIMATE, LAND-USE, AND EMISSIONS CHANGES

Abstract

by Jeremy Charles Avise, Ph.D.
Washington State University
December 2007

Chair: Brian K. Lamb

This dissertation examines the impact that projected future (2050's) global changes have on regional air quality in the U.S. (i.e., ozone and $PM_{2.5}$ concentrations), where the future climate and emissions are based on the Intergovernmental Panel on Climate Change (IPCC) A2 scenario. Specifically, we examine the impact of changes in climate, anthropogenic emissions, chemical boundary conditions, land-use (i.e., biogenic emissions), and the episodic long-range transport (LRT) of Asian emissions. The impact of global changes in climate and emissions, as well as the LRT of Asian emissions, were simulated using the Parallel Climate Model (PCM) and the MOZART-2 global chemical transport model. The PCM and MOZART-2 model results were downscaled to the regional scale using the MM5 meteorological model and the EPA Community Multi-scale Air Quality (CMAQ) photochemical grid model. U.S. anthropogenic emissions were projected to the future using the EPA EGAS economic growth model, while the biogenic emissions were projected using the MEGAN model with adjusted land-use from the Community Land Model.

Model results show that changes in chemical boundary conditions have the most significant impact on summertime U.S. ozone concentrations (+5 ppbv), followed by changes in anthropogenic emissions (+3 ppbv), and climate changes (-1.3 ppbv). Changes in July $PM_{2.5}$ concentrations are primarily influenced by changes in anthropogenic emissions (+3 μg m^{-3}), while changes in chemical boundary conditions have a minimal impact and only increase $PM_{2.5}$ concentrations by +0.4 μg m^{-3}. On average, climate change tends to reduce $PM_{2.5}$ concentrations by roughly -0.9 μg m^{-3}, with the largest decreases occurring in the south eastern U.S. (-3 μg m^{-3}) due to increased wet deposition. The episodic LRT of Asian emissions to the western U.S. is found to elevate surface ozone concentrations in the Pacific Northwest 1-2 ppbv above the average (~48 ppbv) during present-day events, and 1-3 ppbv above the average (~58 ppbv) in the future. In California, surface ozone increases slightly during wintertime LRT events in both the present-day and future cases, but ozone decrease during summertime events due to the meteorological conditions associated with LRT events.

TABLE OF CONTENTS

Page

LIST OF TABLES

CHAPTER TWO

CHAPTER THREE

APPENDIX

LIST OF FIGURES

CHAPTER ONE

CHAPTER TWO

CHAPTER FOUR

APPENDIX

ATTRIBUTION

This dissertation consists of four chapters. Chapter 1 is a general introduction to air quality and the impact that global changes may have on future air quality. Chapters 2 and 3 are independent manuscripts that will be submitted for publication. Chapter 4 contains a general summary and conclusions from this work. All of the research presented in this dissertation was conducted under the guidance of Dr. Brian Lamb. Although I am the primary author of this dissertation, and conducted the majority of model simulations and analyses myself, this work was only made possible through a collaborative effort between myself and many other people. Details of this collaboration for each manuscript is discussed below.

Attribution of projected changes in U.S. ozone and $PM_{2.5}$ concentrations to specific global changes

Jeremy Avise, Jack Chen, and Brian Lamb

Washington State University, Pullman, Washington, USA

Eric Salathé and Clifford Mass
University of Washington, Seattle, Washington, USA

Alex Guenther and Christine Wiedinmyer
National Center for Atmospheric Research, Boulder, Colorado, USA

Larry Horowitz
NOAA Geophysical Fluid Dynamics Laboratory, Princeton, New Jersey, USA

This project is a collaborative effort by researchers from several institutions. Dr. Brian Lamb is the principal investigator for the project. Dr. Jack Chen generated all emissions used in this work. Dr. Eric Salathé and Dr. Clifford Mass developed the interface between the global climate and regional meteorological models, as well as performed the regional meteorological model simulations. Dr. Alex Guenther and Dr. Christine Wiedinmyer provided future land-use and land-cover information, and developed the biogenic emissions modeling system. Dr. Larry Horowitz provided the global chemical model results for generating chemical boundary conditions for the regional photochemical model. Funding for this project was provided by the U.S. Environmental Protection Agency (EPA) Science to Achieve Results (STAR) Program, under grant RD83096201.

Impact of episodic long-range transport of Asian emissions on ozone levels in the western U.S., today and in the future

Jeremy Avise, Jack Chen, and Brian Lamb
Washington State University, Pullman, Washington, USA

Eric Salathé and Clifford Mass
University of Washington, Seattle, Washington, USA

Alex Guenther, Christine Wiedinmyer, and Jean-Francois Lamarque
National Center for Atmospheric Research, Boulder, Colorado, USA

This project is a collaborative effort by researchers from several institutions. Dr. Brian Lamb is the principal investigator for the project. Dr. Jack Chen generated all emissions used in this work, as well as assisted in conducting the long-term regional chemical model simulations. Dr. Eric Salathé and Dr. Clifford Mass developed the

interface between the global climate and regional meteorological models, as well as performed the regional meteorological model simulations. Dr. Alex Guenther and Dr. Christine Wiedinmyer provided future land-use and land-cover information, and developed the biogenic emissions modeling system. Dr. Christine Wiedinmyer also assisted in obtaining the global climate and chemical model results from NCAR. Dr. Jean-Francois Lamarque provided the global chemical model results for generating chemical boundary conditions for the regional photochemical model. Funding for this project was provided by the U.S. Environmental Protection Agency (EPA) Science to Achieve Results (STAR) Program, under grant RD83096201.

CHAPTER ONE

Introduction

Elevated levels of surface ozone (O_3) and fine particulate matter ($PM_{2.5}$; defined as particulate matter with an aerodynamic diameter of 2.5 micrometers or less) have been associated with various adverse health effects, such as lung irritation, decreased lung function, aggravated asthma, and even permanent lung damage [Lippman, 1993; Folinsbee, 1993; Brauer et al., 2001]. In order to protect public health, the Environmental Protection Agency (EPA), under the Clean Air Act, established national ambient air quality standards (NAAQS) for O_3, PM (including $PM_{2.5}$), and four other criteria pollutants known to adversely affect human health. The current NAAQS for ozone is 0.08 ppm over an 8-hour averaging period, and for $PM_{2.5}$ is 35 μg m^{-3} over a 24-hour averaging period and 15 μg m^{-3} annually. In 2002, the number of people living in counties with ozone and $PM_{2.5}$ concentrations above the level set by the NAAQS was estimated to be 136.4 million for ozone and 59.2 million for $PM_{2.5}$ (note: in 2002 the NAAQS for $PM_{2.5}$ was 65 μg m^{-3} over a 24-hour averaging period) [U.S. EPA, 2003]. By 2006, the population exposed to NAAQS exceedances for ozone and $PM_{2.5}$ had been reduced significantly to 77.3 million for ozone and 66.9 million for $PM_{2.5}$ (note: if adjusted for the change in $PM_{2.5}$ NAAQS between 2002 and 2006, reductions comparable to ozone would be seen for $PM_{2.5}$) [http://www.epa.gov/airtrends/sixpoll.html]. This improvement in U.S. air quality is a direct result of emissions reductions. Despite significant progress in improving air quality in the U.S. through

emissions control strategies, exposure to elevated levels of ozone and $PM_{2.5}$ is still widespread.

Global changes in climate and emissions are highly uncertain, and are expected to impact air quality in ways that could potentially offset the recent improvements made in U.S. air quality. The goal of this work is to characterize the projected impacts of global changes (e.g., climate changes, population growth and urbanization, emissions changes, land-use changes) on U.S. air quality fifty years into the future (2050's), for a single future scenario. This dissertation contains two manuscripts that will be published in peer reviewed journals. The first manuscript, titled:

- *Attribution of projected changes in U.S. ozone and $PM_{2.5}$ concentrations to specific global changes*

describes modeling work conducted to determine the individual and combined impacts of changes in climate, regional anthropogenic emissions, chemical boundary conditions (i.e., global emissions), and land-use (i.e., biogenic emissions) on regional U.S. ozone and $PM_{2.5}$ concentrations. The second manuscript:

- *Impact of episodic long-range transport of Asian emissions on ozone levels in the western U.S., today and in the future*

describes modeling work aimed at examining the role that the episodic long-range transport of Asian emissions to the western U.S. has on surface ozone concentrations,

and how this role may change in the future due to global changes in climate and emissions.

Chemistry of Ozone in the Troposphere

Ozone is not directly emitted into the atmosphere, but is formed in the troposphere through a set of complex and highly non-linear photochemical reactions. Production of ozone occurs through the chemical reaction of atomic oxygen (O) and molecular oxygen (O_2):

$$O + O_2 + M \rightarrow O_3 + M \qquad \text{(R1)}$$

where M is any third body (primarily nitrogen or oxygen molecules) that absorbs the energy of the reaction. In the troposphere, oxygen atoms are primarily produced in the presence of sunlight through the photolysis of NO_2:

$$NO_2 + h\nu \rightarrow NO + O \qquad \text{(R2)}$$

where the photon $h\nu$ is from the ultraviolet portion of the solar radiation and has a wavelength between 280 and 430 nm. The nitric oxide (NO) produced in reaction R2 rapidly reacts with ozone and regenerates NO_2.

$$NO + O_3 \rightarrow NO_2 + O_2 \qquad \text{(R3)}$$

Reactions R1-R3 determine the “photostationary state” of ozone. In the absence of hydrocarbons, ozone concentrations remain low (approximately 20-30 ppbv for typical

U.S. latitudes). However, when hydrocarbons (RH) are present through anthropogenic or biogenic emissions, they create a pathway that circumvents reaction R3, and converts NO to NO_2 without destroying ozone. This allows ozone to accumulate in the atmosphere. The net process is:

$$RH + OH + 2O_2 \rightarrow\rightarrow\rightarrow RO_2 + HO_2 + H_2O + RCHO \quad \text{(R4)}$$

$$RO_2 + NO \rightarrow RO + NO_2 \quad \text{(R5)}$$

$$HO_2 + NO \rightarrow OH + NO_2 \quad \text{(R6)}$$

The oxidation of hydrocarbon molecules in reaction R4 produces peroxy radicals (RO_2) and hydroperoxy radicals (HO_2). The actual number and form of peroxy radicals formed in reaction R4 depends on the composition of the hydrocarbon. The radicals RO_2 and HO_2 are highly reactive and rapidly convert NO to NO_2 through reactions R5 and R6. The end result is that during daylight hours ozone is produced through equations R1 and R2, while equations R5 and R6 dominate equation R3 in converting NO to NO_2, so that more ozone is produced than is destroyed and ozone accumulates in the atmosphere. During the nighttime, when sunlight is not present, reaction R2 no longer produces atomic oxygen, and reaction R3 removes ozone from the atmosphere. A more detailed discussion of ozone chemistry can be found in Seinfeld (1989), Seinfeld and Pandis (1998), or Finlayson-Pitts and Pitts (2000).

The production of ozone is highly sensitive to emissions of hydrocarbons/VOCs (volatile organic compounds) and NO_X (NO + NO_2), and the relative ratio of VOCs to NO_X at a particular location determines whether additional NO_X emissions act to inhibit or increase ozone production. In regions where the VOC/NO_X ratio is low (i.e., NO_X concentrations are large compared to VOC concentrations), additional NO_X emissions tend to inhibit ozone production and may reduce ozone concentrations. In this case, VOCs are the limiting factor in the production of ozone. However, when the VOC/NO_X ratio is high (i.e., NO_X concentrations are small compared to VOC concentrations), additional NO_X emissions tend to increase the production of ozone [Jeffries and Crouse, 1990].

Chemistry of Fine Particulates

Fine particulate matter ($PM_{2.5}$) can be directly emitted to the atmosphere through combustion processes (e.g., motor vehicles, power generation, wood stoves, etc ...), or can be formed through chemical processes in the atmosphere. When $PM_{2.5}$ is formed in the atmosphere, it is typically called secondary $PM_{2.5}$ or secondary aerosol. The chemistry involved in the formation of secondary $PM_{2.5}$ is significantly more complex than ozone chemistry, due to the number of chemical species involved and because the reactions involve compounds in the solid, gas, and aqueous phases. Both inorganic and organic gas-phase species can contribute to secondary $PM_{2.5}$ formation, however, the mechanisms for the formation of secondary inorganic aerosols is better understood

than for secondary organic aerosols (SOA) due to the complexity of organic compounds in the atmosphere.

Secondary inorganic $PM_{2.5}$ is primarily made up of sulfate, nitrate, and ammonium. Sulfate is produced when sulfur dioxide (SO_2) is oxidized by OH to produce sulfuric acid (H_2SO_4):

$$SO_2 + OH + M \rightarrow \rightarrow H_2SO_4 + M \quad \text{(R7)}$$

which can nucleate in the presence of water vapor and ammonia to form new sulfate particles. If particles are already present in the atmosphere, the newly formed sulfate may also condense onto an existing particle. When ammonia is abundant in the atmosphere, or sulfate concentrations are low, ammonia will be available to react with nitric acid to form ammonium nitrate (NH_4NO_3) in the solid or aqueous phase:

$$NH_3 + HNO_3 \leftrightarrow NH_4NO_3(s) \quad \text{(R8)}$$

$$NH_3 + HNO_3 \leftrightarrow NH_4^+(aq) + NO_3^-(aq) \quad \text{(R9)}$$

If relative humidity is low, NH_4NO_3 is a solid and reaction R8 is followed. At higher relative humidity (above the deliquescence), NH_4NO_3 will be in the aqueous state and reaction R9 is followed.

Formation of SOA occurs when VOCs, from biogenic and anthropogenic sources, undergo oxidation by atmospheric oxidants such as OH, O_3, or NO_3 (nitrate radical) to

form semi-volatile products that can condense to form aerosols. Monoterpenes (e.g., pinenes) are the primary biogenic VOC involved in SOA formation, while aromatics (e.g., toluene and xylene) are the largest contributors from anthropogenic sources. Typically, a two-product model is used to parameterize SOA formation:

$$VOC + [OH, O_3, NO_3] \rightarrow \alpha_{aero}G_{aero} + \alpha_{gas}G_{gas} \quad \text{(R10)}$$

where VOC represents the precursor hydrocarbon, α is a production coefficient, and G is the semi-volatile product in either aerosol (less volatile) or gas (highly volatile) phase. The partitioning between aerosol and gas phase is a complex process that is influenced by many physical and chemical properties, such as temperature and VOC/NO_X ratio [Odum et al., 1996; Tsigaridis et al., 2006] such that higher temperatures and lower ratios result in greater yields of highly volatile products, while lower temperatures and higher ratios result in greater yields of less volatile products. Readers are referred to Seinfeld and Pandis (1998), or Finlayson-Pitts and Pitts (2000) for a more detailed discussion of secondary aerosol formation.

Global Change and Air Quality

One of the key issues facing air quality planners in the U.S., is how to adapt air quality management plans to account for global changes in climate and trace gas emissions. This is not a trivial issue, since changes in either of these parameters can have a significant impact on ozone and $PM_{2.5}$ chemistry. Changes in climate can directly influence air quality in a number of ways. The first, and most obvious, is change

in regional temperature. In a warmer climate (as projected by the Intergovernmental Panel on Climate Change (IPCC), see Figure 1), reaction rates will increase, which will speed up the reactions involved in the production of ozone and $PM_{2.5}$. For ozone, this means increased production and higher levels of ozone. Dawson et al. [2007] used a chemical transport model to analyze the impact projected climate change would have on a regional ozone episode in the southeastern U.S., and found that temperature change had the single largest impact on 8-hr ozone concentrations, with an increase of approximately 0.34 ppbv / °C increase in temperature. For $PM_{2.5}$, the effect of rising temperatures is more complicated. For example, in terms of SOA, as temperatures increase so does the oxidation of hydrocarbons (reaction R10), but increased temperatures will also push reaction R10 to produce more volatile products, rather than the less volatile ones that contribute to aerosol production.

A second impact of climate change on air quality is through changes in planetary boundary layer (PBL) heights. The height of the PBL is directly related to air quality, because it changes the volume of air available for diluting pollution emitted into the atmosphere. As PBL heights increase, the volume of air available for diluting pollution increases, and air quality tends to improve (i.e, ozone and $PM_{2.5}$ concentrations decrease). PBL heights tend to increase with warmer temperatures, so while increased temperatures may reduce air quality (e.g., increase ozone production), the associated increases in PBL heights may somewhat offset this effect.

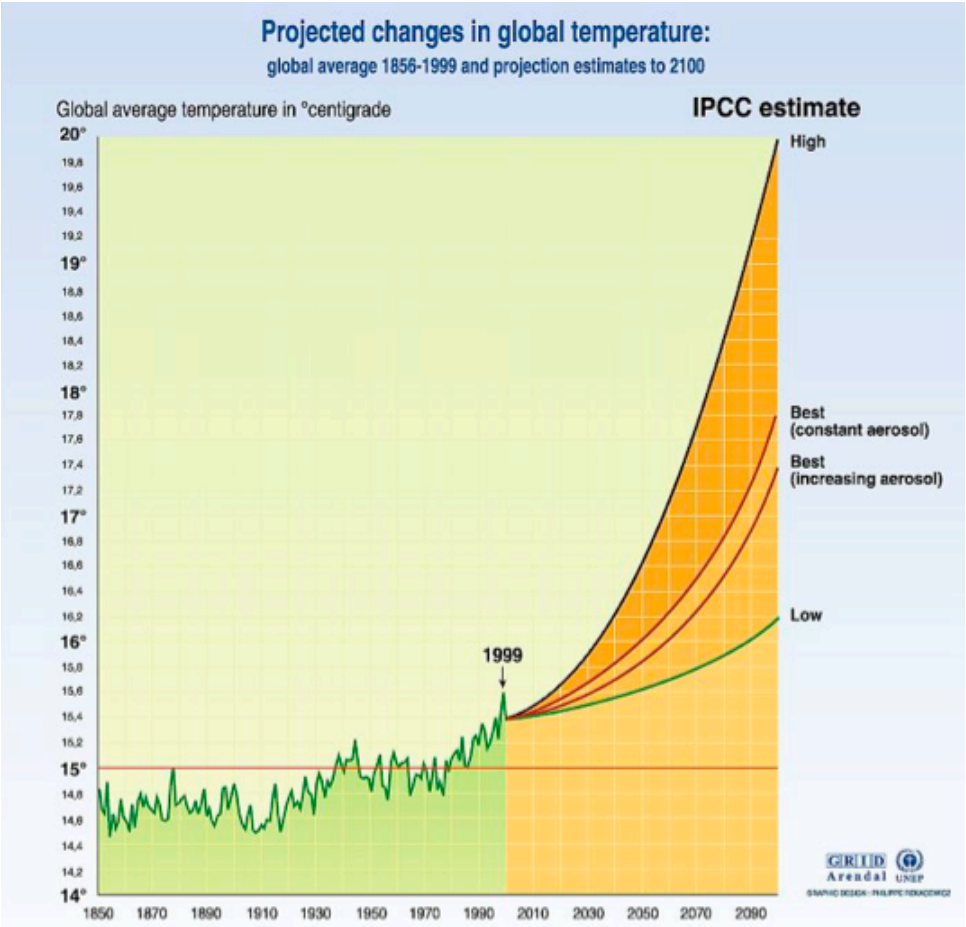

Figure 1. Projected changes in global temperature (from: http://www.grida.no/climate/vital/23.htm)

Climate change may also influence air quality through changes in cloud cover. Cloud cover reduces the amount of solar radiation reaching the surface, which in turn reduces photolysis rates (e.g., reaction R2) and can slow down the production of ozone. Changes in precipitation can also have a significant impact on regional air quality, because precipitation is a mechanism for "cleaning" the atmosphere and removing pollution through wet deposition. For example, Racherla and Adams [2006] projected a decrease in tropospheric $PM_{2.5}$ concentrations in the future due to increased precipitation. Changes in atmospheric water vapor content can also influence air

quality. In a warmer climate, water vapor in the atmosphere is expected to increase, which will likely lead to decreases in ozone through increased removal of the $O(^1D)$ molecule ($O(^1D) + H_2O \rightarrow 2OH$) [Stevenson et al., 2000]. Racherla and Adams [2006] found that on a global scale, water vapor increases in a future climate based on the IPCC A2 scenario would more than offset increases in ozone due to temperature changes, and projected that the global tropospheric ozone burden would decrease by 5% by the year 2050.

Changes in large scale circulation patterns as a result of global climate change may also influence regional air quality. Circulation patterns are responsible for transporting pollution from one region to another. For example, large scale circulation patterns are responsible for the transport of Asian emissions across the Pacific Ocean to the western United States. Consequently, changes in circulation patterns may influence the amount of Asian emissions reaching the U.S., which in turn will effect regional ozone and $PM_{2.5}$ concentrations. Finally, changes in wind speed may also impact regional air quality. Higher wind speeds cause enhanced mixing within the PBL, resulting in improved air quality. In contrast, lower wind speeds are associated with stagnation events that allow pollution to accumulate in a region and significantly increase ozone and $PM_{2.5}$ concentrations. Using global model climate simulations, Mickley et al. [2004] projected that the severity and duration of summertime pollution episodes in the midwest and northeastern U.S. will increase significantly due to increased stagnation events from a decline in the frequency of mid-latitude cyclones

tracking across Southern Canada. Hogrefe et al. [2004] projected that future climate change will increase maximum 8-hr ozone concentrations in the eastern U.S. by as much as 4.2 ppbv by the year 2050. In the western U.S., Steiner et al. [2006] suggest that climate change will result in an increase in summertime ozone of up to 5 ppbv in California's urban areas.

In addition to changes in climate, anthropogenic and biogenic emissions changes are expected to have a significant impact on future air quality, with increased emissions resulting in increased production of both ozone and $PM_{2.5}$. On the global scale, changes in anthropogenic emissions are primarily driven by changes in population. The Intergovernmental Panel on Climate Change (IPCC) estimates that the global population will grow from 5.3 billion in 1990 to between 8.7 and 11.3 billion by the year (Figure 2) 2050 [Nakićenović et al., 2000]. As a direct result of population growth, global emissions of NO_X and non-methane VOCs (both ozone and secondary $PM_{2.5}$ precursors) are projected to increase up to 310% and 230%, respectively, by the year 2050 (Figure 3) [Nakićenović et al., 2000]. Horowitz [2006] conducted global chemical model simulations out to 2100 for various anthropogenic emissions scenarios, and found that anthropogenic emissions alone would change the atmospheric ozone burden by -6% to + 43%, while sulfate aerosols are projected to increase over the next several decades before decreasing to below 2000 levels by 2100. Similarly, Bauer et al. [2007] project that by 2030, nitrate aerosols are expected to become more important due to the expected increase in nitrate precursor emissions. On the regional level, Steiner et al.

[2006] found that projected reductions in anthropogenic emissions in California will lead to a decrease in ozone of 8-15% in the future. Similarly, Tagaris et al. [2007] project that the combined effect of emissions reductions and climate change will lead to a 20% decrease in mean summer maximum 8-hr ozone and will reduce the mean annual $PM_{2.5}$ concentration by 23% over the United States.

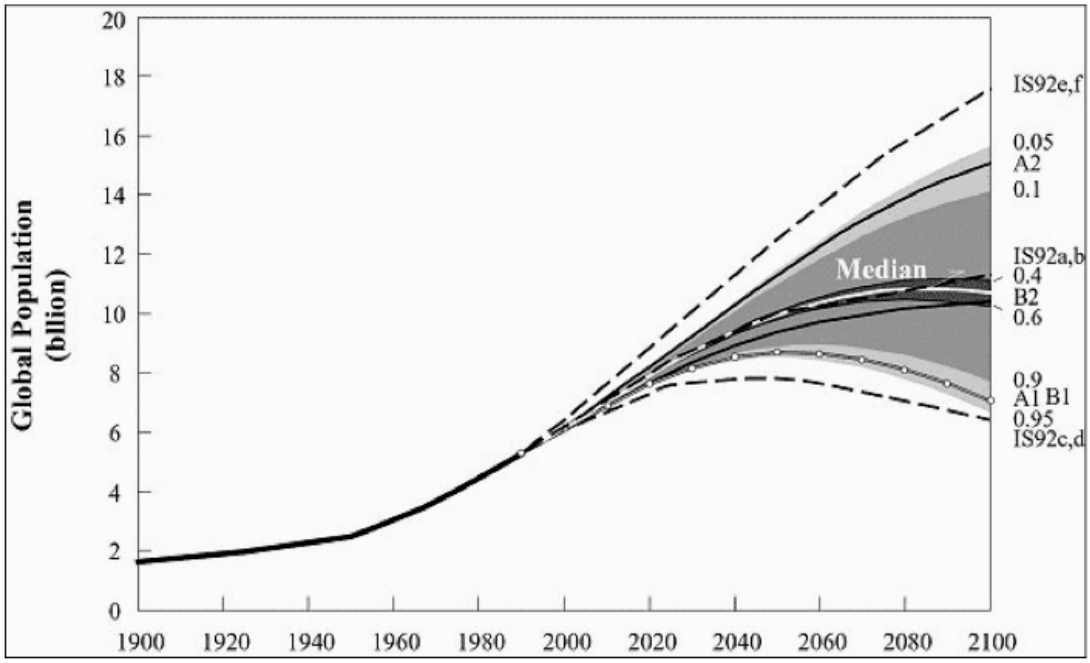

Figure 2. Projected changes in global population, based on IPCC scenario [adapted from Nakićenović et al., 2000].

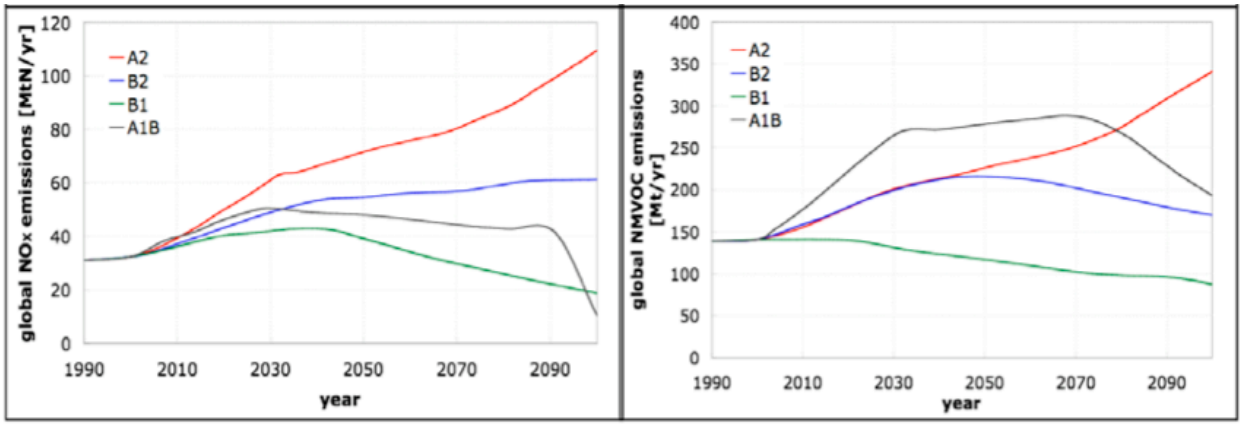

Figure 3. Projected changes in global anthropogenic emissions, based on IPCC scenario [adapted from Nakićenović et al., 2000].

Even if the U.S. does not see such dramatic increases in precursor emissions (possibly even decreases), increases in other regions of the earth, such as Asia, may have a dramatic impact on U.S. air quality due to the long-range transport of those emissions across the Pacific Ocean to North America. Using a global three-dimensional chemical transport model, Jacob et al. [1999] found that a tripling of Asian emissions from 1985 to 2010 resulted in an increase in U.S. monthly mean ozone concentrations of 1-6 ppbv, with the largest increases occurring in the western half of the country.

While population growth results in increased anthropogenic emissions, urbanization works to relocate and concentrate those emissions in urban centers (see Figure 4 for recent urbanization in the Seattle, WA region). Since the majority of the population (particularly in industrialized nations such as the U.S.) live in urban areas, this means a larger number of people will be impacted by the poor air quality associated with the urban environment.

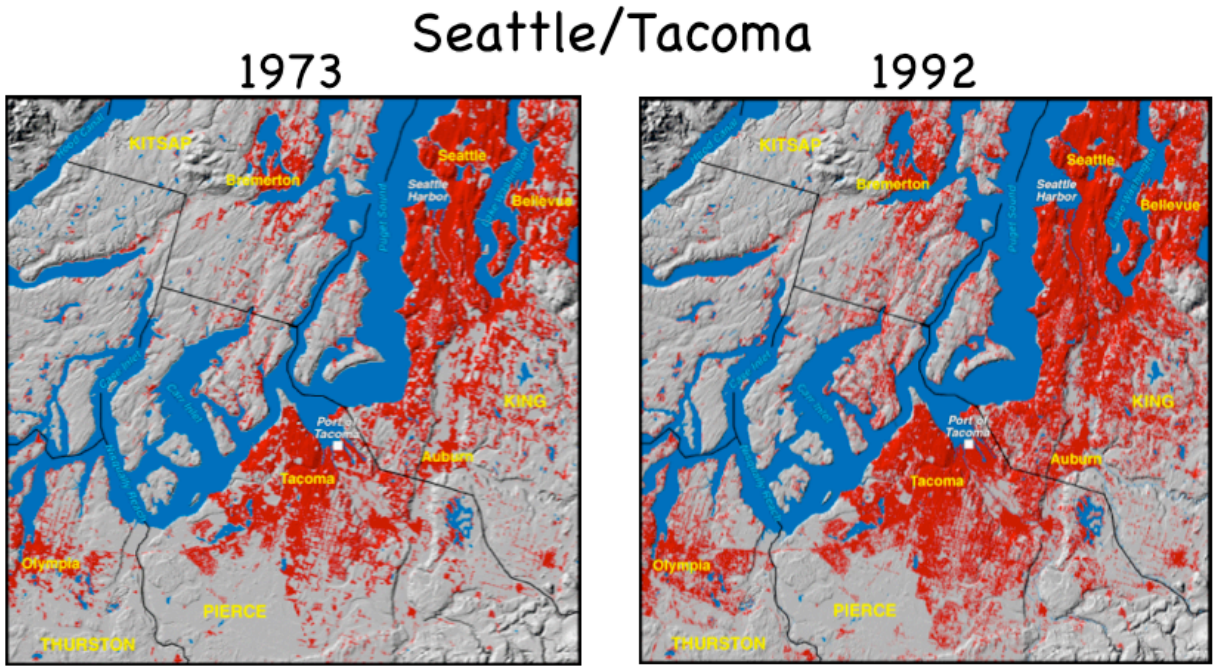

Figure 4. Urbanization in Seattle, WA from 1973 to 1992, where the red areas represents developed land [adapted from http://pubs.usgs.gov/circ/2004/circ1252/15.html].

Future changes in biogenic emissions are also expected to have a significant impact on U.S. air quality. Biogenic VOC emissions are primarily influenced by temperature, but also by the amount of solar radiation reaching the surface, and by precipitation and soil moisture distributions. Consequently, changes in climate may have a profound impact on biogenic emissions. In particular, under a warmer future climate, biogenic VOC emissions are expected to increase, which may result in reduced air quality in regions with high biogenic emissions such as the southeastern United States. In addition, biogenic VOC emissions may also be influenced through such human forces as urbanization and land management practices, as well as naturally through climate driven changes in regional vegetation patterns [Constable et al., 1999;

Wiedinmyer et al., 2006]. Recent modeling work by Tsigaridis and Kanakidou [2007] suggests that projected changes in future biogenic emissions due to temperature change, will significantly increase biogenic SOA production in the atmosphere, making SOA as important as sulfate in terms of total $PM_{2.5}$ concentrations. Racherla and Adams [2007] project the severity and frequency of ozone episodes in the eastern U.S. to increase in the future, due to increases in biogenic emissions in response to climate changes.

References

Bauer, S. E., D. Koch, N. Unger, S. M. Metzger, D. T. Shindell, and D. G. Streets (2007), Nitrate aerosols today and in 2030: a global simulation including aerosols and tropospheric ozone, *Atmos. Chem. Phys.*, 7, 5043-5059.

Brauer, M., S. T. Ebelt, T. V. Fisher, J. Brumm, A. J. Petkau, and S. Vedal (2001), Exposure of Chronic Obstructive Pulmonary Disease Patients to Particles: Respiratory and Cardiovascular Health Effects, *J. Expo. Anal. Environ. Epidmiol.*, 11(6), 490-500.

Constable, J., A. Guenther, D. Schimel, R. Monson (1999), Modeling changes in VOC emission in response to climate change in the continental United States, *Global Change Biology, 5,* 791-806.

Dawson, J. P., P. J. Adams, and S. N. Pandis (2007), Sensitivity of ozone to summertime climate in the eastern USA: A modeling case study, *Atmos. Environ.*, 41, 1494-1511.

Finlayson-Pitts, B. J. and J. N. Pitts (2000), Chemistry of the Upper and Lower Atmosphere: Theory, Experiments, and Applications, Academic Press, San Diego, CA.

Folinsbee, L. J. (1993), Human Health-Effects of Air-Pollution, *Env. Health Persp.*, 10045-56.

Hogrefe, C., B. Lynn, K. Civerolo, J.-Y. Ku, J. Rosenthal, C. Rosenzweit, R. Goldberg, S. Gaffin, K. Knowlton, and P. L. Kinney (2004), Simulating changes in regional air pollution over the eastern United States due to changes in global and regional climate and emissions, *J. Geophys. Res.*, 109, D22301, doi:10.1029/2004JD004690.

Horowitz, L. W. (2006), Past, present, and future concentrations of tropospheric ozone and aerosols: Methodology, ozone evaluation, and sensitivity to aerosol wet removal, *Journal of Geophysical Research*, 111, D22211, doi:10.1029/2005JD006937.

Jacob, D. J., J. A. Logan, and P. P. Murti (1999), Effect of rising Asian emissions on surface ozone in the United States, *Geophys. Res. Lett.*, 26(14), 2175-2178, 10.1029/1999GL900450.

Jeffries and Crouse (1990), Scientific and technical issues related to the application of incremental reactivity. Department of Environmental Sciences and Engineering, University of North Carolina, Chapel Hill, NC.

Lippmann, M. (1993), Health effects of tropospheric ozone: review of recent research findings and their implications to ambient air quality standards, *J. Expo. Anal. Environ. Epidemiol.*, 3, 103-129.

Mickley, L. J., D. J. Jacob, and B. D. Field (2004), Effects of future climate change on regional air pollution episodes in the United States, *Geophys. Res. Lett.*, 31, L24103, doi:10.1029/2004GL021216.

Nakićenović, N., et al. (2000). *Emissions Scenarios: A Special Report of Working Group III of the Intergovernmental Panel on Climate Change,* 599 pp., Cambridge Univ. Press, New York.

Odum, J. R., T. Hoffmann, F. Bowman, D. Collins, R. C. Flagan, and J. H. Seinfeld (1996), Gas/particle partitioning and secondary aerosol formation, *Environ. Sci. Technol.*, 30, 2580-2585.

Racherla, P. N. and P. J. Adams (2006), Sensitivity of global tropospheric ozone and fine particulate matter concentrations to climate change, *J. Geophys. Res.*, 111, D24103, doi:10.1029/2005JD006939.

Racherla, P. N. and P. J. Adams (2007), The Response of surface ozone to climate change over the Eastern United States, *Atmos. Chem. Phys. Discuss.*, 7, 9867-9897.

Seinfeld, J. H. (1989), Urban Air Pollution: State of the Science, *Science*, 243(4892), 745-752.

Seinfeld, J. H. and S. N. Pandis (1998), Atmospheric Chemistry and Physics - from Air Pollution to Climate Change, John Wiley and Sons, New York, NY.

Steiner, A. L., S. Tonse, R. C. Cohen, A. H. Goldstein, and R. A. Harley (2006), Influence of future climate and emissions on regional air quality in California, *J. Geophys. Res.*, 111, D18303, doi:10.1029/2005JD006935.

Stevenson, D. S., C. E. Johnson, W. J. Collins, R. G. Derwent, and J. M. Edwards (2000), Future estimates of tropospheric ozone radiative forcing and methane turnover - the impact of climate change, *Geophys. Res. Lett.*, 105(14), 2073-2076, 10.1029/1999GL010887.

Tagaris, E., K. Manomaiphiboon, K.-J. Liao, L. R. Leung, J.-H. Woo, S. He, P. Amar, and A. G. Russel (2007), Impacts of global climate change and emissions on regional ozone and fine particulate matter concentrations over the United States, *J. Geophys. Res.*, 112, D14312, doi:10.1029/2006JD008262.

Tsigaridis, K., M. Krol, F. J. Dentener, Y. Balkanski, J. Lathiere, S. Metzger, D. A. Hauglustaine, and M. Kanakidou (2006), Change in global aerosol composition since preindustrial times, *Atmos. Chem. and Phys.*, 6, 5585-5628.

Tsigaridis, K. and M. Kanakidou (2007) Secondary organic aerosol importance in the future atmosphere, *Atmos. Env.*, 41, 4682-4692.

U.S. EPA (2003), National Air Quality and Emissions Trends Report (Special Studies Edition) [found online at: http://www.epa.gov/air/airtrends/aqtrnd03/].

Wiedinmyer, C., X. Tie, A. Guenther, R. Neilson, C. Granier (2006), Future changes in biogenic isoprene emissions: how might they affect regional and global atmospheric chemistry?, *Earth Interactions, 10,* paper 3, 1-19.

CHAPTER TWO

Attribution of projected changes in U.S. ozone and $PM_{2.5}$ concentrations to specific global changes

Jeremy Avise, Jack Chen, and Brian Lamb
Washington State University, Pullman, Washington, USA

Eric Salathé and Clifford Mass
University of Washington, Seattle, Washington, USA

Alex Guenther and Christine Wiedinmyer
National Center for Atmospheric Research, Boulder, Colorado, USA

Larry Horowitz
NOAA Geophysical Fluid Dynamics Laboratory, Princeton, New Jersey, USA

Abstract:

The impact that projected changes in future (i.e., 2050's) July climate, anthropogenic emissions, chemical boundary conditions, and land-use have on regional U.S. ozone and $PM_{2.5}$ concentrations is examined through a matrix of regional air quality simulations using the Community Multi-scale Air Quality (CMAQ) model. Projected regional scale changes in meteorology due to climate change under the Intergovernmental Panel on Climate Change (IPCC) A2 scenario are derived through the downscaling of Parallel Climate Model (PCM) output with the MM5 meteorological model. Projected future chemical boundary conditions are obtained through the downscaling of MOZART-2 (Model for Ozone and Related Chemical Tracers, version 2.4) global chemical model simulations based on the SRES IPCC A2 emissions scenario. Projected changes in future U.S. anthropogenic emissions are estimated using the EPA Economic Growth Analysis System (EGAS), and changes in land-use are projected using data from the Community Land Model (CLM) and the Spatially Explicit Regional Growth Model (SERGOM). Land-use changes are projected to have a significant influence on regional air quality due to the impact these changes can have on biogenic hydrocarbon emissions. Changes in chemical boundary conditions are found to have the most significant impact (+5 ppbv) on average daily maximum 8-hr (ADM8-hr) ozone, followed by anthropogenic emissions changes coupled with land-use changes (+3 ppbv), and climate changes (-1.3 ppbv). When climate changes and land-use (i.e.,, biogenic emissions) changes are considered simultaneously, the average decrease in ADM8-hr ozone is even greater (-2.6 ppbv). Changes in average 24-hr (A24-hr) $PM_{2.5}$ concentrations are dominated by projected changes in anthropogenic

emissions (+3 μg m^{-3}), while changes in chemical boundary conditions have a negligible effect (+0.4 μg m^{-3}). On average, climate change reduces A24-hr $PM_{2.5}$ concentrations by -0.9 μg m^{-3}, but this reduction is more than tripled in the south eastern U.S. (-3 μg m^{-3}) due to increased precipitation and wet deposition.

1. Introduction

Reduced air quality due to increased levels of ozone and $PM_{2.5}$ is the result of a complex mix of chemical reactions and physical processes in the atmosphere. These reactions and processes are predominantly influenced by pollutant emissions and meteorological conditions. Consequently, global changes in climate and trace gas emissions from both anthropogenic and biogenic sources may have a profound impact on future air quality. In particular, global climate change can directly affect air quality through changes in regional temperatures, which will influence chemical reaction rates in the atmosphere (Sillman and Samson, 1995). The work of Dawson et al. (2007) found that during a July ozone episode over the eastern U.S., temperature was the meteorological parameter that had the most influence on 8-hr ozone concentrations, with an average increase in 8-hr ozone of 0.34 ppb / ^{o}K. In addition to temperature, global climate changes may directly impact other boundary layer parameters that are important to regional air quality, such as boundary layer heights, cloud formation, and the occurrence of stagnation events. Leung and Gustafson Jr. (2005) investigated the potential effects of climate change on U.S. air quality, and found that changes in temperature, downward solar radiation, rainfall frequency, and the frequency of stagnation events were likely to negatively impact air quality in some regions and positively impact it in others. The work of Mickley et al. (2004) also examined the impact of climate change on regional air quality in the U.S., and found that summertime air quality in the midwest and northeastern U.S. was projected to decline due to a decrease in the frequency of mid-latitude cyclones across southern Canada.

Changes in anthropogenic and biogenic emissions may also have a substantial influence on future air quality. If we ignore control-related reductions, then changes in anthropogenic emissions are primarily driven by population growth and urbanization. The IPCC (Intergovernmental Panel on Climate Change) estimates the global population will grow from 5.3 billion in 1990 to between 8.7 and 11.3 billion by the year 2050 (Nakićenović et al., 2000). As a result of this global population increase, the IPCC SRES (Special Report on Emission Scenarios) projects that over the next 50 years global emissions of the ozone precursors NO_X and non-methane volatile organic compounds (NMVOCs) will increase up to 310% and 230%, respectively (Nakićenović et al., 2000). Although the suite of IPCC SRES emission projections are highly variable and uncertain, nearly all of the estimates predict an increase in ozone precursor emissions through the 2050's. It is already well documented that global ozone concentrations have increased significantly over the past century due to increased anthropogenic emissions (Marenco et al., 1994; Staehelin et al., 1994; Varotsos and Cartalis, 1991). As these emission continue to increase, ozone related air quality issues can be expected to become more pronounced. In regions such as the west coast of North America, there is already evidence that regional air quality is influenced by increasing global anthropogenic emissions, and in particular, increasing Asian emissions. Jaffe et al. (2003) found that surface and airborne measurements of ozone in the springtime air transported from the Eastern Pacific to the west coast of the United States showed ozone increasing by 30% (approximately 10 ppbv) from the mid 1980's to 2002. Similarly, Vingarzan and Thomson (2004) observed an increase of approximately 3.5 ppbv in the ozone levels of marine air transported into southwestern

British Columbia from 1991 to 2000. The increase was attributed to a combination of increased global background levels and direct influence from Asian emissions.

Changes in biogenic emissions are also expected to play a key role in determining future air quality. Biogenic volatile organic compound (BVOC) emissions are primarily influenced by temperature, the intensity of surface level solar radiation (i.e., cloud cover), and to a lesser extent precipitation patterns and soil moisture distributions. Consequently, changes in climate may have a profound impact on regional BVOC emissions. In addition, BVOC emissions may also be influenced through human forces such as urbanization and land management practices, as well as naturally through climate driven changes in regional vegetative patterns. (Constable et al., 1999; Wiedinmyer et al., 2006).

Recent modeling studies have shown the importance of an integrated approach to studying the impacts of global changes on regional air quality. Hogrefe et al. (2004) investigated the impact of global changes (IPCC A2 scenario) in the 2050's on regional air quality in the eastern U.S., and found that summertime average daily maximum 8-hr ozone concentrations were most significantly influenced by changes in chemical boundary conditions (+5.0 ppb) followed by meteorological changes (+4.2 ppb) and anthropogenic emissions (+1.3 ppb). The work of Steiner et al. (2006) investigated the impact of changes in climate and emissions reductions on ozone levels in central California, and found that projected reductions in anthropogenic emissions has the single largest impact on air quality, reducing ozone by 8-15% in urban areas, while

climate change is projected to increase ozone 3-10%. Similarly, Tagaris et al. (2007) found that the projected impact of climate change on U.S. air quality in the 2050's is small compared to the impact of control-related reductions in emissions, and that the the combined effect of climate change and emissions leads to a decrease in mean summertime daily maximum 8-hr ozone of 20% and a reduction of 23% in the mean annual $PM_{2.5}$ concentration.

Although it is known that the global environment is changing and that these changes may have a profound impact on air quality, the magnitude and spatial distribution of these impacts remains highly uncertain. In this work, we apply the EPA Community Multi-scale Air Quality (CMAQ) version 4.4 photochemical grid model (Byun and Schere, 2006) to examine the individual and combined impacts that global changes (projected to the 2050's) have on regional air quality in the United States (this work follows the same approach as Chen et al. [2007]). Specifically, we examine how changes in climate, regional anthropogenic emissions, global emissions (as chemical boundary conditions into CMAQ), and land-use (as biogenic emissions) affect regional ozone and $PM_{2.5}$ concentrations. Section 2 describes the methodology and models used in this study. In section 3, we discuss our results, and in section 4 we present our conclusions.

2. Methodology

In order to quantify the impact of projected global changes on surface ozone and $PM_{2.5}$ concentrations, we conducted a matrix of CMAQ "attribution" simulations based

on six different combinations of model inputs (Table 1). Each of the six attribution cases were comprised of five separate month long simulations using meteorological conditions representative of July for either present-day (1990-1999) or future (2045-2054) time periods. July conditions from five separate years were simulated to ensure our results were representative of average July conditions for each climate period. We first simulated present-day levels of ozone and $PM_{2.5}$ with CMAQ driven by meteorology, chemical boundary conditions, anthropogenic emissions, and land-cover (i.e., biogenic emissions) that reflect present-day conditions (CURall case). Future levels of ozone and $PM_{2.5}$ were simulated using CMAQ driven by model inputs that reflect projected conditions for the 2045-2054 (hereinafter referred to as future-2050) time period (FUTall case), where future-2050 conditions were based on the IPCC SRES A2 scenario (Nakićenović et al., 2000). To examine the individual effects of projected global change parameters on ozone and $PM_{2.5}$ concentrations, an additional four cases were simulated. Specifically, these four cases examined the impact of future chemical boundary conditions alone (futBC simulation), future anthropogenic emissions combined with future land-cover (futEMISfutLU simulation), future climate alone(futMETcurLU), and future climate combined with future land-cover (futMETfutLU). All modeling results were grouped and analyzed by EPA region (see Figure 1). For simplicity, we have combined results from regions 1, 2, and 3, and will treat them as a single region (R1-3).

2.1. Model Setup

2.1.1. Chemical Transport Model

In this work, the CMAQ version 4.4 photochemical grid model was run on a 36-km by 36-km grid, centered over the continental U.S., with 17 vertical sigma levels from the surface to the tropopause (first layer height approximately 18 m; Table A1). Gas-phase chemistry was modeled using a condensed version of the SAPRC-99 chemical mechanism (Carter 2000a,b) available with the CMAQ distribution, which includes 72 model species and 214 chemical reactions. Aerosol processes were simulated using a modal approach with the AERO3 aerosol module (Byun and Schere, 2006) for model species including sulfates, nitrates, primary and secondary organics, and elemental carbon. The model was driven using MM5 meteorological fields processed through the Meteorology-Chemistry Interface Processor (MCIP version 3.0).

2.1.1. Meteorology

To generate the meteorological fields used to drive CMAQ, MM5 version 3 (Grell et al., 1994) was used to downscale present-day and future-2050 global climate model results from the NCAR-DOE Parallel Climate Model (PCM; Washington et al., 2000). The PCM model couples atmospheric, land surface, ocean, and sea-ice modules to form an earth system model for current and future climate scenario projections. The future-2050 PCM simulations were based on the IPCC SRES A2 “business as usual” greenhouse gas emission scenario. The A2 emissions scenario is characterized by a very heterogeneous world based on regional self-reliance. An emphasis on family and community results in a relatively slow decline in fertility rates. As a result, the A2

scenario has the largest population increase of all the IPCC scenarios (approximately 11 billion by 2050). In addition, while some attention is given to environmental issues on a regional basis, overall global environmental concerns are relatively weak in the A2 scenario (Nakićenović et al., 2000). As a result, the A2 scenario ranks as one of the more severe scenarios in terms of future population growth, temperature change, and increases in ozone and $PM_{2.5}$ precursor emissions.

The MM5 simulations were performed in non-hydrostatic mode with 28 vertical sigma levels, and a one-way nested configuration at 108-km and 36-km grid resolutions. Model parameterizations include: MRF (Hong-Pan) PBL scheme (Hong and Pan, 1996), simple 5-layer soil model with land-use information from 1-km USGS data (Chen and Dudhia, 2001a,b), Kain-Fritsch cumulus parameterization scheme (Kain and Fritsch, 1990), explicit moisture (including simple ice physics, but no mixed phase processes), and the CCM2 radiation scheme. This model configuration was chosen to capture large scale meteorological processes at the 36-km grid scale, as well as to optimize computational speed. In order to maintain simulation stability and mass conservation, nudging was employed on the outer 108-km domain (108-km) towards the PCM output. This constrains MM5 to the global model and results in a smooth transition from the global model to the continental scale MM5 simulations.

Model configuration for the current and future decade simulations was identical except for the 1-km land-use data used. For the present-day simulations, land-use information was based on the 1-km USGS dataset with 24 land-cover categories. Since

variations in land-use and land-cover are known to significantly influence regional meteorology and air quality through surface energy flux perturbations (Civerolo et al., 2000), land-use for the future-2050 simulations was updated with data from the Community Land Model (CLM; Bonan et al., 2002) and the Spatially Explicit Regional Growth Model (SERGOM; Theobald, 2005). The CLM predicted changes in vegetation distribution by plant functional types for the 2050 climate, while the SERGOM model provided projected urban and suburban population density distributions out to the year 2030. Figure 2 depicts the land-use information provided to MM5 for the present-day and future-2050 simulations. The most striking projected changes are the predominance of dryland crop and sparsely vegetated lands in the future. The majority of the forested lands in the eastern U.S. and grasslands in the central U.S. are projected to be converted to pastures and dryland crops in the future. The southwestern states are projected to shift from predominantly shrubland to barren and sparsely vegetated land with small areas of grass and shrubland. For the western U.S., much of the evergreen needleleaf regions are converted to crop and grassland mosaic. Table A2 shows a quantitative comparison of the changes in area coverage for each USGS land-use category.

Projected changes in average daily maximum (ADM) surface temperature, boundary layer height, downward solar radiation, and average water vapor content within the boundary layer are shown in Figure 3, and summarized by EPA region in Table 2. ADM surface temperatures are projected to increase across the continental United States, however, the magnitude of the increase varies greatly by region. The

eastern U.S. is expected to have the largest increase in ADM surface temperature, with Region 1-3 having a projected increase of +3.4 ºC and Region 4 projected to increase by +2.6 ºC. The south western U.S. (Region 9) shows comparable changes with Region 4, and the Pacific Northwest (Region 10) shows the smallest increase in ADM surface temperature of +1.0 ºC. Changes in ADM PBL heights are clearly correlated to changes in ADM surface temperature (see Figure 3). Regions with smaller changes in surface temperature (e.g., Texas, California, Oregon) show decreases in PBL heights, while the regions with the largest increase in temperature (southwestern states) correlate to the largest increase in PBL height. On average, ADM PBL height is projected to increase by approximately 100 m or more for most regions, except regions 6 and 7, which show only slight increases due to offsetting increases and decreases in PBL heights within the two regions. Since temperature and PBL height are so highly correlated, on a regional scale any reduction in air quality due to increased temperatures may be offset by increased PBL heights. Note, the larger increases in temperature and PBL heights along the coastlines are due to a slight mismatch in the land surface classifications for the present-day and future-2050 scenarios, and are not the result of climate changes.

Assuming the amount of downward solar radiation can be used as a surrogate to cloud cover (i.e., reduced downward radiation implies increased cloud cover), from Figure 3 we can see that the general trend is towards less cloud cover for much of the U.S., which implies faster photolysis rates in the atmosphere leading to increased production of pollutants such as ozone. There are, however, regions such as portions

of Texas and the Pacific Northwest and south eastern U.S., which are projected to experience more cloud cover in the future, potentially leading to improved air quality in those regions. Water vapor content is generally projected to increase in the eastern U.S., while the western U.S. shows small regions of slight increases and larger areas of decreasing water vapor content. Increases in water vapor in the eastern U.S. is likely to lead to decreases in ozone (Stevenson et al., 2000) due to the destruction of ozone through photolysis and the removal of the $O(^1D)$ molecule through its subsequent reaction with water vapor in the atmosphere ($O(^1D) + H_2O \rightarrow 2OH$).

2.1.3. Chemical Boundary Conditions

Both present-day and future-2050 sets of chemical boundary conditions were obtained through the downscaling of output from the MOZART-2 (Model for Ozone and Related Chemical Tracers, version 2.4) global chemical transport model. The MOZART-2 output used here was previously described by Horowitz (2006). Horowitz (2006) applied MOZART-2 to estimate tropospheric ozone and aerosol concentrations from 1860 to 2100 based on historical and projected changes in emissions, while the feedbacks from climate change and trends in stratospheric ozone were ignored. The historical simulations (1860-1990) were based on the EDGAR-HYDE historical emissions inventory (van Aardenne et al., 2001), while the future simulations (1990-2100) were based on emissions projections from four different IPCC SRES scenarios (A2, A1B, B1, and A1F1). For the purpose of this work, we obtained daily average model results from the A2 MOZART-2 simulations, for July 2000 and July 2050. Note that the meteorological inputs used to drive these MOZART-2 simulations are not

the same as the PCM results used in this work, so some consistency is lost. However, the MOZART-2 output does provide a realistic set of present-day and projected future-2050 chemical boundary conditions for our CMAQ simulations.

Chemical boundary conditions represent the transport of local emissions from somewhere outside of the modeling domain into the interior of the domain. Due to the predominant westerly flow across the Pacific ocean and continental U.S., the western boundary condition for our domain primarily reflects the transport of emissions from the Asian continent to the western U.S., while the eastern boundary condition reflects the transport of U.S. emissions out over the Atlantic ocean. The northern and southern boundary conditions reflect a mixture of local U.S. emissions with Canadian and Mexican emissions, respectively.

Average present-day and future-2050 vertical profiles along the western boundary are shown in Figure 4, and boundary condition totals from the surface to 500 mbar for all sides are summarized in the appendix (Table A3). A shift towards higher concentrations of ozone, reactive nitrogen species, NMVOCs, and $PM_{2.5}$ can be clearly seen for all vertical levels along the western boundary (similar shifts are evident along all four boundaries; see Figures A1-A3). Generally, we see an increase in ozone of approximately 10 ppbv from the present-day to future 2050 conditions for the west, south, and east boundaries, while the north boundary shows a smaller increase of only 7 ppbv (Table A3). Similarly, NO_X and NO_Y also show the smallest increases along the north boundary (8 pptv and 76 pptv), however the increase along the south boundary

(58 pptv and 228 pptv) is significantly larger than the increase projected along the west and east boundaries (approximately 10 pptv and 130 pptv). Non-methane VOCs increase between 0.6 ppbv and 0.7 ppbv for all four sides. In terms of $PM_{2.5}$, the largest projected increases are along the western and southern boundaries (approximately 0.8 $\mu g\ m^{-3}$), reflecting projected increases in particulate and precursor emissions from Asia and South America. Little to no change in $PM_{2.5}$ is projected along the northern and eastern boundaries.

2.1.4. Regional Emissions

The anthropogenic emissions inventory used in this work is based on the 1999 EPA National Emissions Inventory (NEI-1999; http://www.epa.gov/ttn/chief/net/1999inventory.html), and was processed through the SMOKE (Sparse Matrix Operating Kernel Emissions; Houyoux et al., 2005) emissions system. Future anthropogenic emissions were projected out to 2050 using emission growth factors from the EPA Economic Growth Analysis System (EGAS; U.S. EPA, 2004). EGAS generates emission growth factors based on projections of economic activity variables such as personal income, disposable income, population, employment, and estimated future energy consumption. The EGAS growth factors were applied to area and mobile source categories, but not to point sources. Point source emissions were held constant with the assumption that any increase in future point source emissions (due to new point sources) will be offset by improved control technologies. Future anthropogenic emissions were also updated to account for the expansion of urban areas through projected estimates of population and housing density by the SERGOM model for the

year 2030. Present-day and projected future-2050 anthropogenic emissions are summarized in Table 3. Area source emissions are projected to experience the largest increase, with emissions for all species, excluding CO, increasing by more than 50%. Non-road emissions are projected to increase between 6% and 33%, depending on the species, while mobile emissions are projected to stay relatively unchanged.

Biogenic emissions were generated dynamically using MEGAN-EZ (Model of Emissions of Gases and Aerosols from Nature - EZ version; Guenther et al., 2006). The model uses seasonal vegetation datasets to estimate hourly isoprene, monoterpene, and other VOC emissions from plants as a function of predicted hourly temperature and ground level shortwave radiation from MM5. For the current land-cover case, a 1-km seasonal vegetation dataset, derived from satellite observations, was used (provided by Christine Wiedinmyer from NCAR). The 1-km data were up-sampled to match the 36-km continental U.S. domain. For the future-2050 land-cover case, the vegetation dataset was updated with the Community Land Model to be consistent with the future-2050 land-use dataset used in the MM5 simulations, as well as to account for simulated changes in plant functional types due to projected future-2050 climate change.

Projected changes in land-cover resulted in significant changes in biogenic emissions capacity from the present-day to future-2050 case. Figure 5 shows emissions capacity of isoprene and monoterpenes at 30 ºC for the present-day and future-2050 time periods. In the future, isoprene emitting vegetation has been

significantly reduced in the south and south eastern states, as well as in the northern mid-west and along the west coast of California. Similarly, significant reduction of monoterpene emitting plants are projected along the west coast of the U.S. and into Canada, as well as in the south and south eastern U.S. and eastern Canada. The projected reduction of isoprene and monoterpene emitting plants is significant enough to negate any increase in emissions due to increased future temperatures, and actually results in a net reduction in total future-2050 BVOC emissions compared to the present-day. Table 4 shows a comparison of total continental U.S. biogenic emissions for the case of present-day land-cover combined with present-day meteorology (CURall and futBC cases), the case of future-2050 land-cover and present-day meteorology (futEMIS case), the case of present-day land-cover combined with future-2050 meteorology (futMETcurLU case), and the case of future-2050 land-cover combined with future-2050 meteorology (FUTall and futMETfutLU cases). When we consider both changes in meteorology and future land-cover we see a net reduction in U.S. BVOC emissions of -53 ktons-day^{-1} compared to the present-day. However, if we consider changes in meteorology alone, and do not account for future changes in land-cover, we see a net increase in BVOC emissions of +32 ktons-day^{-1}. When present-day meteorology is combined with future-2050 land-cover, the net result is a decrease in BVOC emissions of -60 ktons-day^{-1} compared to the present-day.

3. Results and Discussion

In the following sections, we first compare simulated surface ozone and $PM_{2.5}$ concentrations from the present-day (CURall) simulations to measurements made at

monitoring sites throughout the United States. We then analyze and discuss the results of our attribution CMAQ simulations in terms of 8-hr ozone, 24-hr $PM_{2.5}$ concentrations, and exceedances of the ozone and $PM_{2.5}$ standards.

3.1. Ozone and $PM_{2.5}$ Evaluation

CMAQ has undergone extensive evaluation for both ozone and $PM_{2.5}$ model predictions for the continental U.S. (e.g: Eder and Yu, 2006; Phillips and Finkelstein, 2006), and has shown good performance for most regions (i.e., within a factor of 2 of observations). For this work, model performance is evaluated through a comparison of modeled and observed daily maximum 8-hr (DM8-hr) ozone and daily $PM_{2.5}$ concentrations (Figures 6 and 7, and Table A4 in the appendix). Since our CMAQ simulations were driven by MM5 results that were nudged towards climate model output and not observations, our present-day (CURall) simulations represent a realization of present-day air quality and are not representative of air quality at any specific time (i.e., we cannot do a direct day-to-day or hour-to-hour comparison with observations). Hourly ozone and daily $PM_{2.5}$ observations were obtained from the EPA's AIRS database (http://www.epa.gov/ttn/airs/airsaqs/) for the five July's from 1999-2003. The 1999-2003 time period was chosen to best match the NEI-1999 used in this work. A total of 1,349 ozone and 1,277 $PM_{2.5}$ monitoring sites were used (see Figure A6). Figure 6 compares ranked modeled and observed DM8-hr ozone concentrations averaged across all sites within each EPA region. Model performance for average DM8-hr ozone is fairly consistent across all regions, ranging from an over-prediction of +15% in Region 8 to +39% in Region 4. Peak DM8-hr ozone, represented by the 98th percentile value,

shows better performance than the average, and ranges from -2% in Region 9 to +24% in Region 4 (DM8-hr ozone performance results are shown in Table A4). Figure 7 compares ranked modeled and observed daily $PM_{2.5}$ concentrations averaged across all sites within each EPA region. Modeled $PM_{2.5}$ performance for the average of the daily $PM_{2.5}$ concentrations is relatively consistent across all regions, ranging from an under-prediction of -11% in Region 9 to -24% in Region 6. The only exception to this is in Region 8, which under-predicts the average by -44%. The peak (98^{th} percentile) daily $PM_{2.5}$ concentrations show much more variability compared to the average, and range from under-predictions of -7% to -17% for Regions 4, 5, 6, and 7 to under-predictions of -41% to -62% in Regions 1-3, 8, 9, and 10.

3.2. Ozone results

The impact of projected future-2050 global changes on surface ozone concentrations is large, but spatially highly variable. Some regions experience increases in ozone greater than 10 ppbv (west-central U.S.), while others see reductions of a few ppbv (southeastern U.S.). Figure 8 shows a map of the average daily maximum 8-hr (ADM8-hr) ozone concentration for the CURall base case simulation with difference maps for the five attribution simulations. Table 4 summarizes these results by EPA region.

On average, projected changes in chemical boundary conditions (futBC simulation) have the largest impact on U.S. ADM8-hr ozone levels (+5 ppbv). The boundary condition impact is more pronounced in the west (+6 ppbv) than in the east

(+4 ppbv), due to the predominant westerly flow across the U.S. (i.e., the further away from the boundary the less impact the boundary conditions have on ozone levels). This result is consistent with Hogrefe et al. [2004] who showed that changes in chemical boundary conditions following the IPCC A2 scenario had the largest impact on ozone levels.

Future emissions changes (futEMIS) are projected to increase ADM8-hr ozone levels across the U.S. by an average of +3 ppbv. The most significant increases in ADM8-hr ozone are projected to occur in regions that combine increases in anthropogenic emissions with sufficient future biogenic emissions. In particular, Region 9 in the west and Region 4 in the southeast show the largest increase in ADM8-hr ozone (+5 ppbv). The smallest increase in ADM8-hr ozone (+2 ppbv) is projected to occur in the Regions 5 and 8, which combine relatively smaller increases in anthropogenic emissions with lower future biogenic emissions. Hogrefe et al. [2004] project a smaller increase in ozone due to future anthropogenic emissions, based on the IPCC A2 scenario, with an increase of only 1.3 ppbv in the eastern United States. The discrepancy between Hogrefe et al. [2004] and the results presented here is most likely due to how future regional anthropogenic emissions are projected. Hogrefe et al. [2004] projected future U.S. emissions based on the IPCC A2 scenario, while emissions in this work are projected using the EPA's EGAS model. In contrast, Tagaris et al. [2007] found that under the A1b scenario the simulated 20% reduction in ozone was primarily due to control-related reductions in emissions. Similarly, Tao et al. [2007] found that under the IPCC B1 scenario, the 4-12% modeled reduction in ozone was

dominated by emissions changes, while Steiner et al. [2006] found that projected reductions in California's anthropogenic emissions had the single largest effect on reducing ozone.

Projected meteorological changes (futMETcurLU simulation) result in an overall decrease (-1.3 ppbv) in U.S. ADM8-hr ozone. The meteorological impacts are spatially highly variable, so some regions show increases in ADM8-hr ozone, while others show a decrease. The largest increases in ADM8-hr ozone (approximately +4 ppbv), are found in the northeast and west central regions. Our results for the northeast are in agreement with Hogrefe et al. [2004] who found that climate change resulted in an increase of roughly 4 ppbv in ADM8-hr ozone, as well as, Racherla and Adams [2007] who found that climate change based on the A2 scenario increased 95th percentile ozone in the eastern U.S. by approximately 5 ppbv. In the west central region, increased temperature is somewhat offset by increases in daytime PBL height, and the increase in ADM8-hr ozone appears to be due to a combination of decreased water vapor and less cloud cover in the future atmosphere (Figure 3). A decrease in water vapor is expected to increase ozone concentrations, while less cloud cover means increased photolysis rates in the atmosphere and increased ozone production. In the northeast, increased ADM8-hr ozone appears to be due to a combination of increased temperature with only small increases in daytime PBL heights, as well as decreased cloud cover, which offset any reduction in ozone due to increased water vapor in the atmosphere. The largest decreases in ADM8-hr ozone appear in the south and southwestern regions (-6 ppbv), with smaller decreases occurring along the west coast

and northern regions (approximately -1 ppbv). The decreases in ADM8-hr ozone in the south and southwest regions are the result of increased water vapor in the atmosphere combined with increased cloud cover. The smaller decrease along the west coast cannot be attributed to specific meteorological changes, and is in contrast with Steiner et al. [2006] who found that climate change alone would increase ozone 3-10% throughout California.

When projected changes in future land-use are combined with future meteorological conditions (futMETfutLU case), the future ADM8-hr ozone is spatially very similar to when only meteorological changes are considered (futMETcurLU case). Accounting for changes in future land-use (i.e., reduced biogenic emissions) has the effect of enhancing the projected decrease in ADM8-hr ozone due to climate change. This enhancement is most pronounced in Region 4, where the largest decreases in BVOC emissions are expected. In Region 4, ADM8-hr ozone is projected to decrease an additional 3 ppbv from -5 ppbv to -8 ppbv. On average across the U.S., the decrease in ADM8-hr ozone is projected to double from -1.3 ppbv, when climate change alone is considered, to -2.6 ppbv when climate change and future land-use changes are accounted for simultaneously.

The combined effects of projected changes in chemical boundary conditions, emissions, land-use, and climate (FUTall simulation) on ADM8-hr ozone results in the largest increases in the west central U.S. (e.g., +12 ppbv in Region 9) and in the northeastern U.S. (e.g., +12 ppbv in Region 1-3). In Region 1-3, all of the global

changes accounted for in this study increase ADM8-hr ozone. The same is true for the eastern portion of Region 9, however in the western portion of Region 9 (California) changes in chemical boundary conditions and emissions increase AMD8-hr ozone, while climate change tends to decrease AMD8-hr ozone. The largest projected decreases in AMD8-hr ozone occur in the south and southeast regions, where future AMD8-hr ozone is dominated by climate effects. This is reflected in the relatively small increases in AMD8-hr ozone (+3 ppbv) in Regions 4 and 6. On average across the U.S., the combined effects of projected global changes result in a +7 ppbv increase in AMD8-hr ozone, and the changes in ozone are dominated by changes chemical boundary conditions and emissions in most regions, except for the southeast, which is dominated by changes in convective precipitation.

3.2.1. Exceedance of the 8-hr ozone standard

Figure 9 shows the average number of July exceedances per grid of the 8-hr 80 ppbv ozone level. The exceedance results are summarized by EPA region in Table 5. For most regions, projected changes in future chemical boundary conditions (futBC case) and emissions (futEMIS case) contribute nearly equally (i.e., within 1 exceedance/ grid) to increasing exceedances of the 8-hr ozone standard. The exception to this is in Region 4, where emissions changes result in more significant increases in 80 ppbv exceedances compared to chemical boundary conditions, and in Region 8, where changes in chemical boundary conditions increase exceedances more than do changes in emissions. Changes in climate alone (futMETcurLU case) have the smallest effect on 80 ppbv exceedances for all regions except Regions 1-3 and 10, and actually result in a

decrease in Region 4. In Region 1-3, changes in climate result in the largest increase in 80 ppbv exceedances, while in Region 10 climate effects are greater than emissions effects, but smaller than effect of chemical boundary conditions. When climate change and land-use changes are simultaneously accounted for (futMETfutLU case), the change in the number of 80 ppbv exceedances is the smallest for all regions, and decreases for Regions 4, 5, 6, and 9. When all global changes are accounted for simultaneously (FUTall case), the number of 80 ppbv exceedances more than doubles for all regions except Region 4. The largest increases are in Regions 1-3 and 9, where the number of 80 ppbv exceedances increase by approximately +9 exceedances per grid. On average across the entire U.S., 8-hr ozone 80 ppbv exceedances are expected to increase by +5.3 exceedances per grid due to the combined effects of global change.

3.3. $PM_{2.5}$ results

Results for the July average 24-hr (A24-hr) $PM_{2.5}$ concentrations are shown in Figure 10, and summarized by EPA region in Table A5. Changes in emissions (futEMIS case) contribute most to increasing A24-hr $PM_{2.5}$ concentrations across the U.S. (approximately +3 μg m^{-3}). The largest increases in A24-hr $PM_{2.5}$ due to changes in emissions are found in the east and central U.S. (+4 μg m^{-3} for Regions 1-3 and 7; +5 μg m^{-3} for Regions 4 and 5), while the smallest changes occur in the west (+1 μg m^{-3} for Regions 8 and 10; +2 μg m^{-3} for Region 9). Unlike ozone, changes in chemical boundary conditions (futBC case) have very little impact on $PM_{2.5}$ concentrations. A24-hr $PM_{2.5}$ concentrations are influenced most by changes in chemical boundary

conditions along the west coast (Regions 9 and 10), but for all regions the increase in A24-hr $PM_{2.5}$ is less than +1 μg m^{-3}.

Changes in meteorology (futMETcurLU simulation) result in a slight decrease in A24-hr $PM_{2.5}$ concentrations across the U.S. (approximately -1 μg m^{-3}). The largest decrease in A24-hr $PM_{2.5}$ occurs in Region 4 (-3 μg m^{-3}), and is primarily due to increased wet deposition in the region (Figure A7). Changes across the rest of the U.S. range from +0.2 μg m^{-3} in Region 1-3 to -1 μg m^{-3} in Regions 5, 6, and 7. Results for the future meteorology and future land-use simulations (futMETfutLU case) show very little difference in A24-hr $PM_{2.5}$ to those of the future meteorology and current land-use simulations (futMETcurLU case), which suggests that the effect of meteorological changes on A24-hr $PM_{2.5}$ dominate the effect that changes in future biogenic emissions, due to land-use changes, has on A24-hr $PM_{2.5}$.

In the FUTall case, the largest increase in A24-hr $PM_{2.5}$ occurs in Region 1-3 (+4 μg m^{-3}) and is almost entirely due to changes in emissions. Region 4 shows the smallest increase in A24-hr $PM_{2.5}$ (+1 μg m^{-3}) due to the combined effects of changes in emissions, which tends to increase A24-hr $PM_{2.5}$, and changes in meteorology, which decreases A24-hr $PM_{2.5}$. On average, across the continental U.S. the A24-hr $PM_{2.5}$ concentration is projected to increase by +2 μg m^{-3}.

3.3.1. Exceedance of the 24-hr $PM_{2.5}$ standard

Exceedance results for the 24-hr 35 μg m^{-3} $PM_{2.5}$ standard are shown in Figure 11 and summarized by EPA region in Table A6. Similar to the A24-hr $PM_{2.5}$ concentrations, changes in emissions (futEMIS case) are expected to have the most significant impact on exceedances, with the largest increases occurring within Regions 1-3, 4, and 5. On average, across the U.S., changes in emissions alone are projected to increase 24-hr $PM_{2.5}$ exceedances by +4,441 (or +1007%) in the month of July. Boundary conditions are projected to have the least impact on exceedances and only increase the total number of U.S. exceedances in July by +43 (or +10%). Changes in meteorology (futMETcurLU case) work towards decreasing the number of $PM_{2.5}$ exceedances in all regions. When changes in land-use are accounted for along with changes in meteorology (futMETfutLU case), the number of $PM_{2.5}$ exceedances also decreases in most regions, but the decrease is less than what is seen for the future meteorology case (futMETcurLU). The differing results from the futMETfutLU and futMETcurLU cases are the result of a decrease in BVOC emissions in the futMETfutLU case, due to projected land-use changes. This decrease in BVOC emissions leads to a decrease in biogenic secondary organic aerosol (SOA) formation, but an increase in OH concentrations. Higher OH leads to increases in sulfate (formed by SO_2 reacting with OH), as well as increased HNO_3 (formed by NO_2 reacting OH), which subsequently leads to increases in nitrate and ammonium (formed by HNO_3 reacting with NH_3). The increases in sulfate, nitrate, and ammonium aerosols offset the decrease in biogenic SOA resulting in a small overall increase in $PM_{2.5}$ for the futMETfutLU case compared to

the futMETcurLU case (see Figures A8 and A9 for difference plots of the relevant species involved).

4. Conclusions

Changes in future ozone and $PM_{2.5}$ concentrations compared to the present-day, are due to the synergistic effects of changes in chemical boundary conditions, regional anthropogenic emissions, land-use (biogenic emissions), and climate. Overall, U.S. July ADM8-hr ozone concentrations in the 2050's are projected to increase by an average of +7 ppbv compared to the present-day. However, these results are spatially highly variable, and some regions may experience larger increases in ADM8-hr ozone, while other regions may experience decreases in ADM8-hr ozone. Projected changes in chemical boundary conditions are found to have the single largest impact on ADM8-hr ozone, and increase ozone levels in all regions. The second largest impact on ozone levels is due to changes in anthropogenic emissions combined with future land-use (i.e., reduced BVOC emissions), which increase ozone in most regions, except in large urban centers, where ozone decreases. Climate change alone is projected to increase ADM8-hr ozone in some regions (north east and west central), and decrease it in others (west coast and south/south east), but results in an overall decrease in ozone. When projected changes in climate and land-use are simultaneously accounted for, ADM8-hr ozone is decreased even further.

Projected increases in future A24-hr $PM_{2.5}$ concentrations are primarily driven by by increases in inorganic aerosol concentrations, due to changes in anthropogenic

emissions, which more than offset any decreases in biogenic SOA due to reduced BVOC emissions (from projected land-use changes). Projected changes in chemical boundary conditions result in a negligible increase (< 1 μg m^{-3}) in A24-hr $PM_{2.5}$ concentrations. Climate change tends to reduce $PM_{2.5}$ concentrations in most regions, with the largest reductions coming in the south eastern U.S. due to more removal through wet deposition from enhanced precipitation.

The results from this work show that although climate change may play an important role in defining future air quality in certain regions, on a larger scale, changes in chemical boundary conditions and emissions appear to play a much more important role. However, recent work by Tao et al. (2007) suggests that the importance of specific global changes to projected air quality may change depending on which future climate/ emissions scenario is assumed. To examine the relationship between specific global changes and regional air quality more thoroughly, we plan to conduct a matrix of additional model runs, which will include multiple future climate, global/regional anthropogenic emissions, and land-use/land-cover scenarios.

References

Bonan, G. B., Oleson, K. W., Vertenstein, M., Levis, S., Zeng, X. B., Dai, Y. J., Dickinson, R. E., and Yang, Z. L. (2002), The Land Surface Climatology of the Community Land Model Coupled to the NCAR Community Climate Model, *Journal of Climate*, 15(22), 3123-3149.

Byun, D. and K. L. Schere (2006), Review of the Governing Equations, Computational Algorithms, and Other Components of the Models-3 Community Multiscale Air Quality (CMAQ) Modeling System, *Applied Mechanics Reviews*, 59, 51-77.

Carter, W., 2000a: Documentation of the SAPRC-99 Chemical Mechanism for VOC Reactivity Assessment, Draft report to the California Air Resources Board, Contracts 92-329 and 95-308, May 8 (available at http://www.cert.ucr.edu/~carter/absts.htm#saprc99).

Carter, W., 2000b: Implementation of the SAPRC-99 Chemical Mechanism into the Models-3 Framework, Report to the United States Environmental Protection Agency, January 29 (available at http://www.cert.ucr.edu/~carter/absts.htm#s99mod3).

Chen, F., and J. Dudhia (2001a), Coupling an advanced land-surface/hydrology model with the Penn State/NCAR MM5 modeling system. Part I: Model implementation and sensitivity, *Mon. Wea. Rev.*, 129, 569-585.

Chen, F., and J. Dudhia (2001b), Coupling an advanced land-surface/hydrology model with the Penn State/NCAR MM5 modeling system. Part I: Preliminary model validation, *Mon. Wea. Rev.*, 129, 587-604.

Chen, J., J. Avise, B. Lamb, C. Mass, E. Salathé, A. Guenther, C. Wiedinmyer, D. McKenzie, N. Larkin, and S. O'Neill (2007), Global Change Impacts on Future Regional Air Quality in the United States, *Atmos. Chem. Phys.*, submitted.

Civerolo, K. L., Sistla, G., Rao, S. T., and Nowak, D. J. (2000), The Effects of Land Use in Meteorological Modeling: Implications for Assessment of Future Air Quality Scenarios, *Atmospheric Environment*, 34(10), 1615-1621.

Constable, J., A. Guenther, D. Schimel, R. Monson (1999), Modeling changes in VOC emission in response to climate change in the continental United States, *Global Change Biology, 5,* 791-806.

Dawson, J. P., P. J. Adams, and S. N. Pandis (2007), Sensitivity of ozone to summertime climate in the eastern USA: A modeling case study, *Atmos. Environ.*, 41, 1494-1511.

Eder, B. and S. Yu (2006), A performance evaluation of the 2004 release of Models-3 CMAQ, *Atmospheric Environment*, 40, 4811-4824.

Grell, G. A., J. Dudhia, D. R. Stauffer (1994), A Description of the Fifth-Generation Penn State/NCAR Mesoscale Model (MM5), National Center for Atmospheric Research, Boulder, CO; NCAR/TN-398+STR, 122 pp.

Guenther, A., T. Karl, P. Harley, C. Wiedinmyer, P. I. Palmer, and C. Geron (2006), Estimates of global terrestrial isoprene emissions using MEGAN (Model of Emissions of Gases and Aerosols from Nature). *Atmospheric Chemistry and Physics Discussions*, 6, 107-173.

Hogrefe, C., B. Lynn, K. Civerolo, J.-Y. Ku, J. Rosenthal, C. Rosenzweit, R. Goldberg, S. Gaffin, K. Knowlton, and P. L. Kinney (2004), Simulating changes in regional air pollution over the eastern United States due to changes in global and regional climate and emissions, *J. Geophys. Res.*, 109, D22301, doi:10.1029/2004JD004690.

Hong, S.-Y., and H. L. Pan (1996), Nonlocal boundary layer vertical diffusions in a medium-range forecast model. *Mon. Wea. Rev.*, 124, 2322-2339.

Horowitz, L. W. (2006), Past, present, and future concentrations of tropospheric ozone and aerosols: Methodology, ozone evaluation, and sensitivity to aerosol wet removal, *Journal of Geophysical Research*, 111, D22211, doi:10.1029/2005JD006937.

Houyoux, Marc, Vukovich, Jeff, and Brandmeyer, J. E. (2005), Sparse Matrix Operator Kernel Emissions Modeling System User Manual. [online] http://cf.unc.edu/cep/empd/products/smoke.

Jaffe, D., T. Anderson, d. Covert, R. Kotchenruther, B. Trost, J. Danielson, W. Simpson, T. Berntsen, S. Karlsdottir, D. Blake, J. Haris, G. Carmichael, and I. Uno (1999), Transport of Asian Air Pollution to North America, *Geophys. Res. Lett., 26*, 711-714.

Kain, J. S., and J. M. Fritsch (1990), A one-dimensional entraining/detraining plume model and its application in convective parameterization. *J. Atmos. Sci.*, 47, 2784-2802.

Leung, L. R., and W. I. Gustafson Jr. (2005), Potential regional climate and implications to U.S. air quality, *Geophys. Res. Lett.*, 32, L16711, doi:10.1029/2005GL022911.

Marenco, A., H. Gouget, P. Nédélec, J.-P. Pagés, and F. Karcher (1994), Evidence of a long term increase in tropospheric ozone from Pic du Midi data series: Consequences: positive radiative forcing, *J. Geophys. Res.*, 99, 16617-16632.

Mickley, L. J., D. J. Jacob, and B. D. Field (2004), Effects of future climate change on regional air pollution episodes in the United States, *Geophys. Res. Lett.*, 31, L24103, doi:10.1029/2004GL021216.

Nakićenović, N., et al. (2000). *Emissions Scenarios: A Special Report of Working Group III of the Intergovernmental Panel on Climate Change,* 599 pp., Cambridge Univ. Press, New York.

Olivier, J. G.J., J. J.M. Berdowski, J. A.H.W. Peters, J. Bakker, A. J.H. Visschedijk, and J.P. J. Bloos (2000), Applications of EDGAR. Including a Description of EDGAR V3.0: Reference Database with Trend Data for 1970-1995. NRP report no. 410200 051 / RIVM report no. 773301 001, RIVM, Bilthoven, the Netherlands.

Phillips, S. B. and P. L. Finkelstein (2006), Comparison of spatial patterns of pollutant distribution with CMAQ predictions, *Atmospheric Environment*, 40, 4999-5009.

Sillman S. and P. J. Samson (1995), Impact of temperature on oxidant photochemistry in urban, polluted rural, and remote environments, *J. Geophys. Res., 100,* 11497-11508.

Staehelin, J., J. Thudium, R. Buehler, A. Volz-Thomas, W. Graber (1994), Trends in Surface Ozone Concentrations at Arosa (Switzerland), *Atmos. Environ.*, 28, 75-87.

Steiner, A. L., S. Tonse, R. C. Cohen, A. H. Goldstein, and R. A. Harley (2006), Influence of future climate and emissions on regional air quality in California, *J. Geophys. Res.*, 111, D18303, doi:10.1029/2005JD006935.

Stevenson, D. S., C. E. Johnson, W. J. Collins, R. G. Derwent, and J. M. Edwards (2000), Future estimates of tropospheric ozone radiative forcing and methane turnover - the impact of climate change, *Geophys. Res. Lett.*, 105(14), 2073-2076, 10.1029/1999GL010887.

Tagaris, E., K. Manomaiphiboon, K.-J. Liao, L. R. Leung, J.-H. Woo, S. He, P. Amar, and A. G. Russel (2007), Impacts of global climate change and emissions on regional ozone and fine particulate matter concentrations over the United States, *J. Geophys. Res.*, 112, D14312, doi:10.1029/2006JD008262.

Tao, Z., A. Williams, H.-C. Huang, M. Caughey, and X.-Z. Liang (2007), Sensitivity of U.S. surface ozone to future emissions and climate changes, *Geophys. Res. Lett.*, 34, L08811, 10.1029/2007GL029455.

Theobald, D. M. (2005), Landscape Patterns of Exurban Growth in the USA From 1980 to 2020, *Ecology and Society,* 10(1), [online] http://www.ecologyandsociety.org/vol10/iss1/art32/.

U.S. EPA (2004), Economic Growth Analysis System (EGAS) version 5.0 User Manual, U.S. Environmental Protection Agency, [online] http://www.epa.gov/ttn/ecas/egas5.htm

van Aardenne, J. A., G. R. Carmichael, H. Levy II, D. Streets, and L. Hordijk (1999), Anthropogenic NOx emissions in Asia in the period 1990-2020. *Atmos. Environ.*, 33, 633-646.

Varotsos, C., C. Cartalis (1991), Re-evaluation of surface ozone over Athens, Greece, for the period 1901-1940. *Atmospheric Research*, 26, 303-310.

Vingarzan, R. and B. Thomson (2004), Temporal variation in daily concentrations of ozone and acid related substances at Saturna Island, British Columbia. *Journal of the Air and Waste Management Association*, 54, 459-472.

Washington, W. M., J. W. Weatherly, G. A. Meehl, A. J. Semtner, T. W. Bettge, A. P. Craig, W. G. Strand, J. Arblaster, V. B. Wayland, R. James, and Y. Zhang (2000), Parallel Climate Model (PCM) control and transient simulations. *Climate Dyn.*, 16, 10/11, 755-774.

Wiedinmyer, C., X. Tie, A. Guenther, R. Neilson, C. Granier (2006), Future changes in biogenic isoprene emissions: how might they affect regional and global atmospheric chemistry?, *Earth Interactions, 10,* paper 3, 1-19.

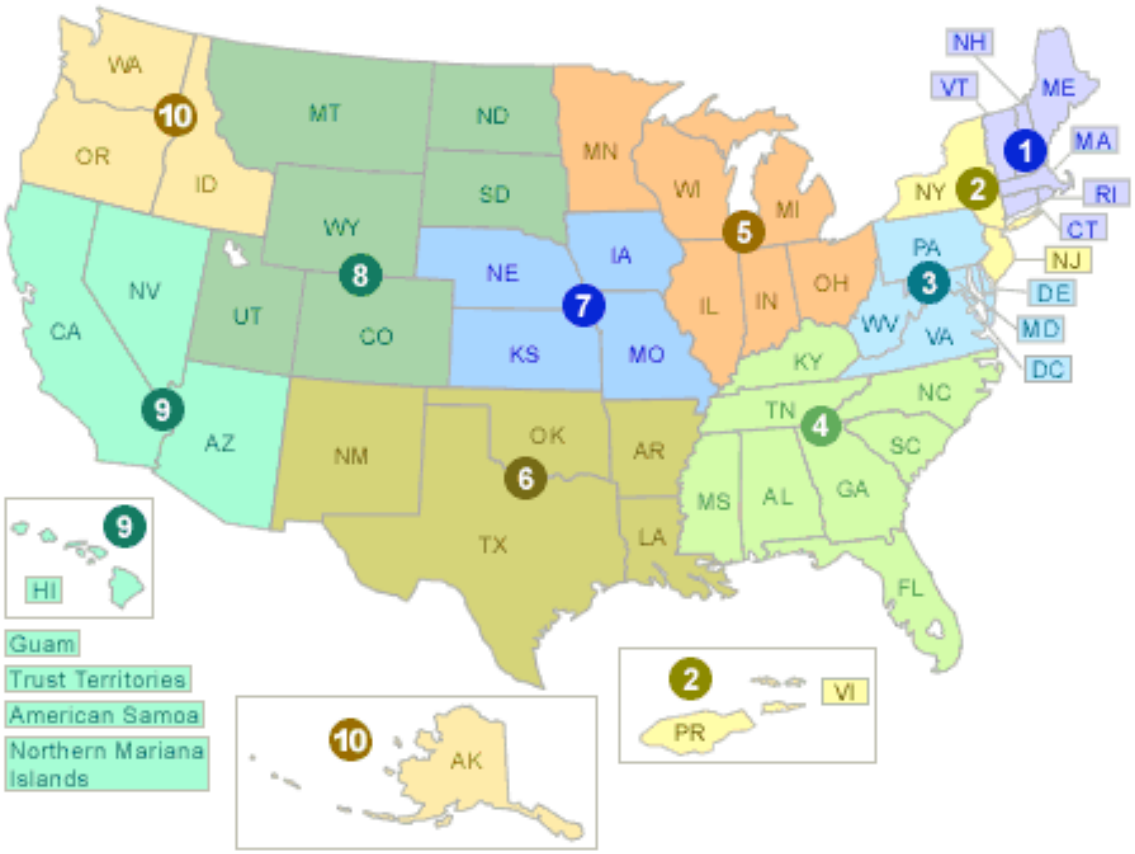

Figure 1.
EPA regions for the continental United States. Note that for simplicity we are treating Regions 1, 2, and 3 as a single region when discussing our results (from http://www.epa.gov/epahome/locate2.htm).

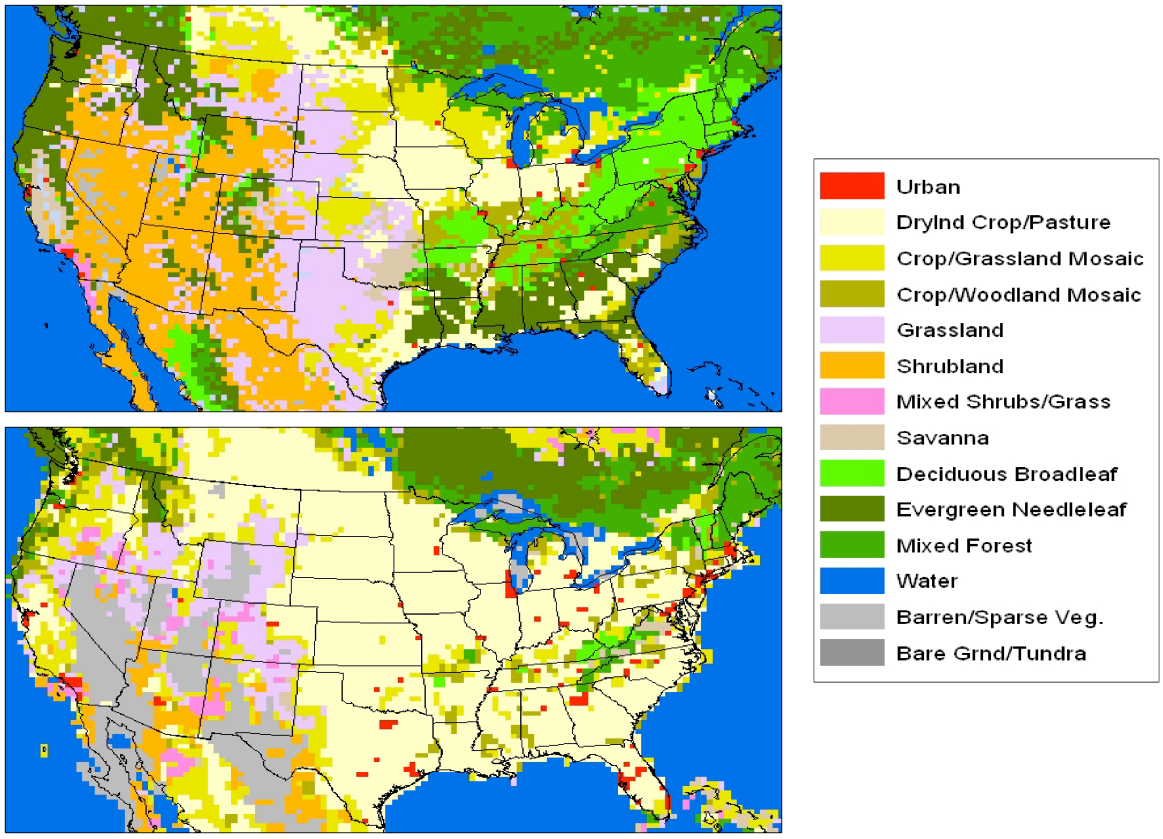

Figure 2.
MM5 land-use by USGS category for the present-day (top) and future-2050 (bottom) simulations.

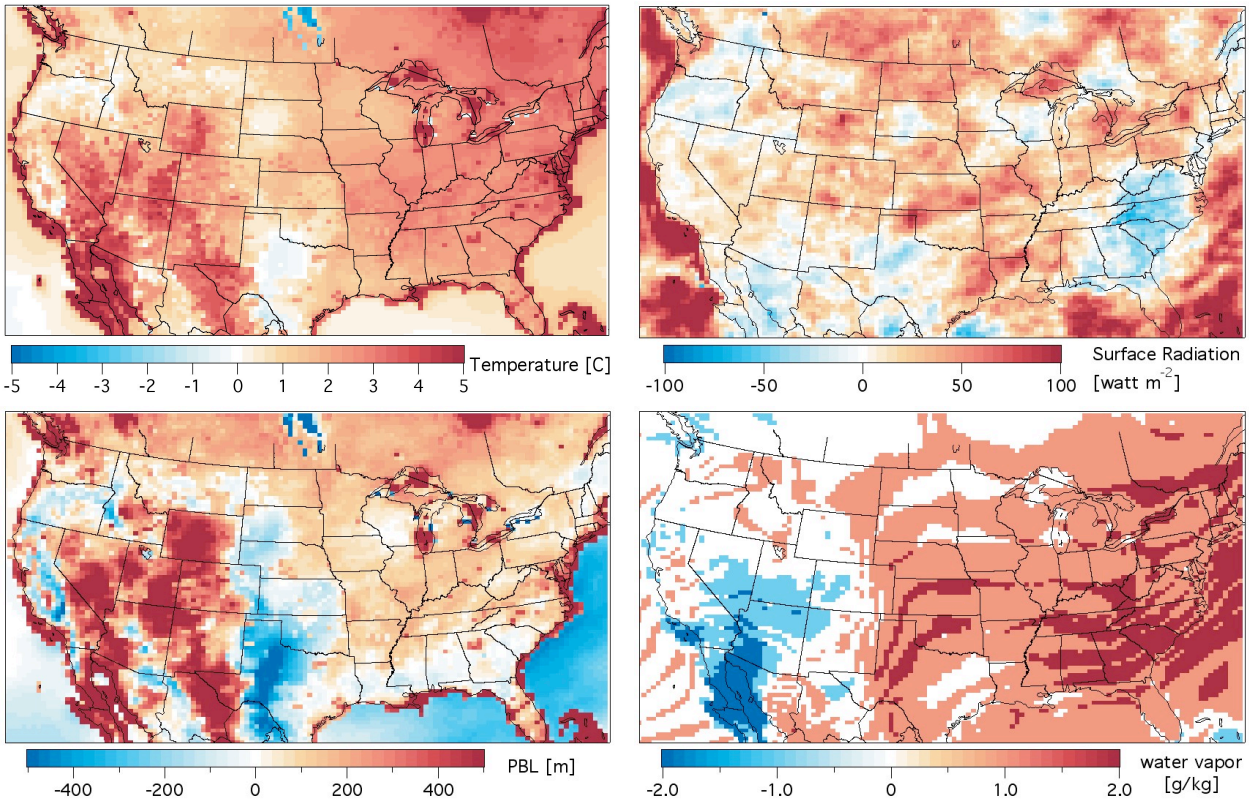

Figure 3.
Projected change from the present-day to the 2050's for (upper left) average daily maximum surface temperature, (lower left) average daily maximum boundary layer height, (upper right) average daily maximum downward solar radiation, and (lower right) average daily water vapor content within the boundary layer.

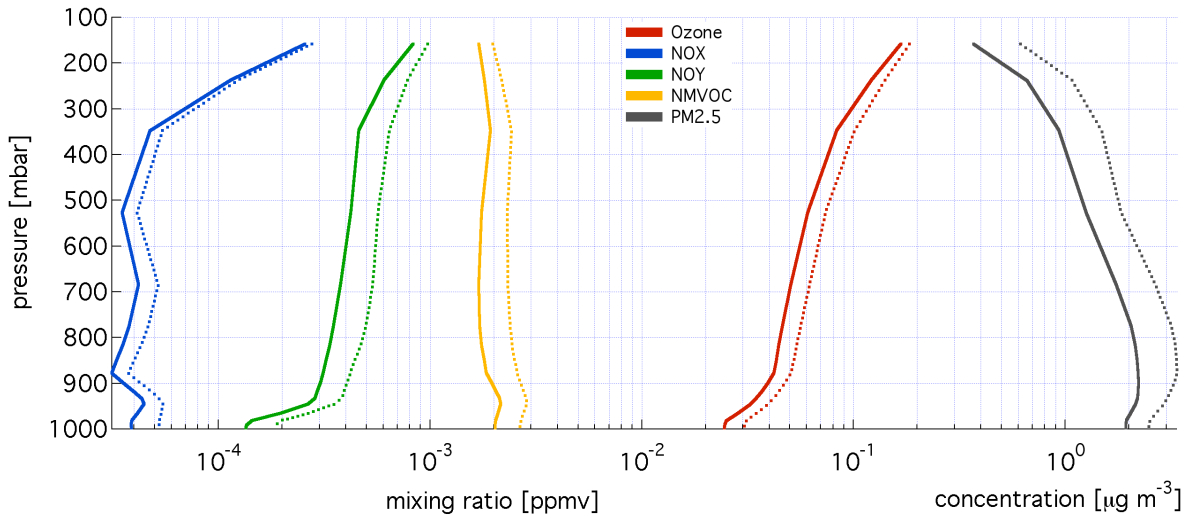

Figure 4.
Comparison of predicted present-day (solid line) to projected future-2050 (dashed line) chemical boundary conditions along the western boundary of the modeling domain.

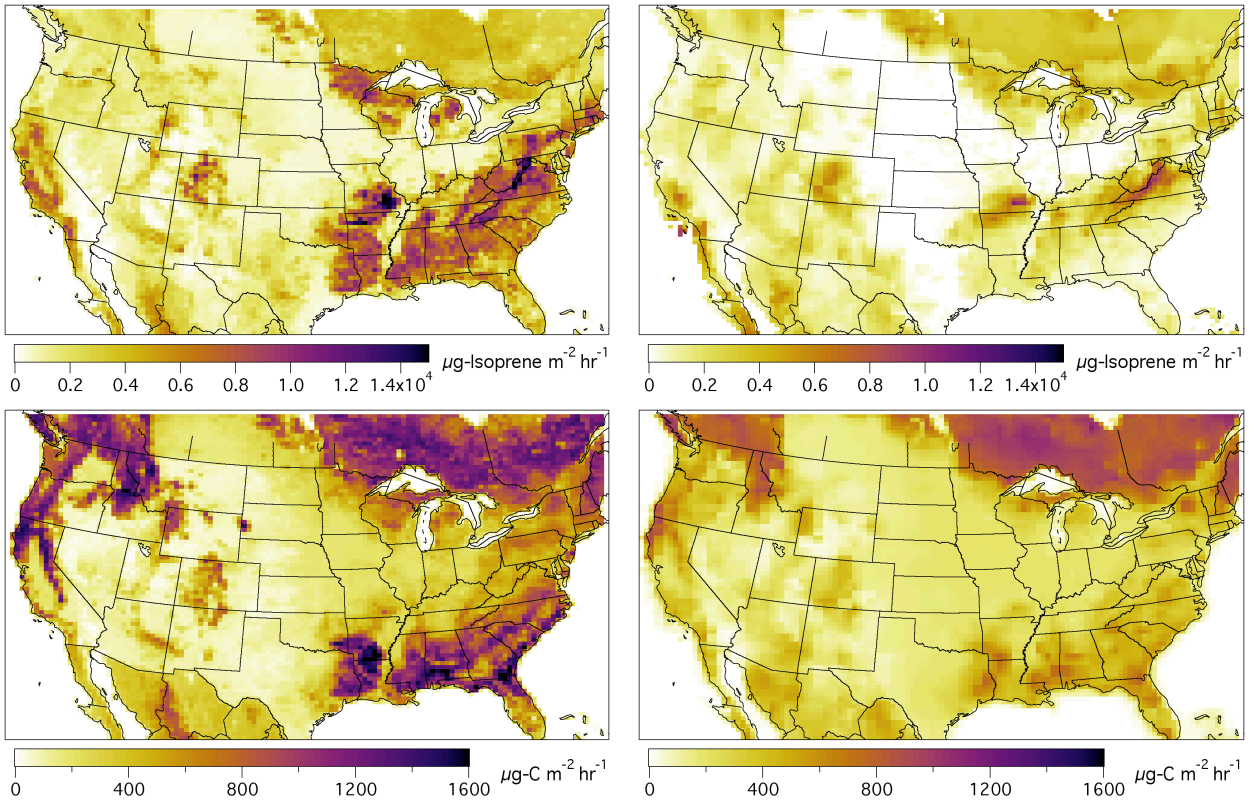

Figure 5.
Biogenic emissions capacity maps (normalized to 30 ºC) for present-day isoprene (upper left), future-2050 isoprene (upper right), present-day monoterpenes (lower left), and future-2050 monoterpenes (lower right).

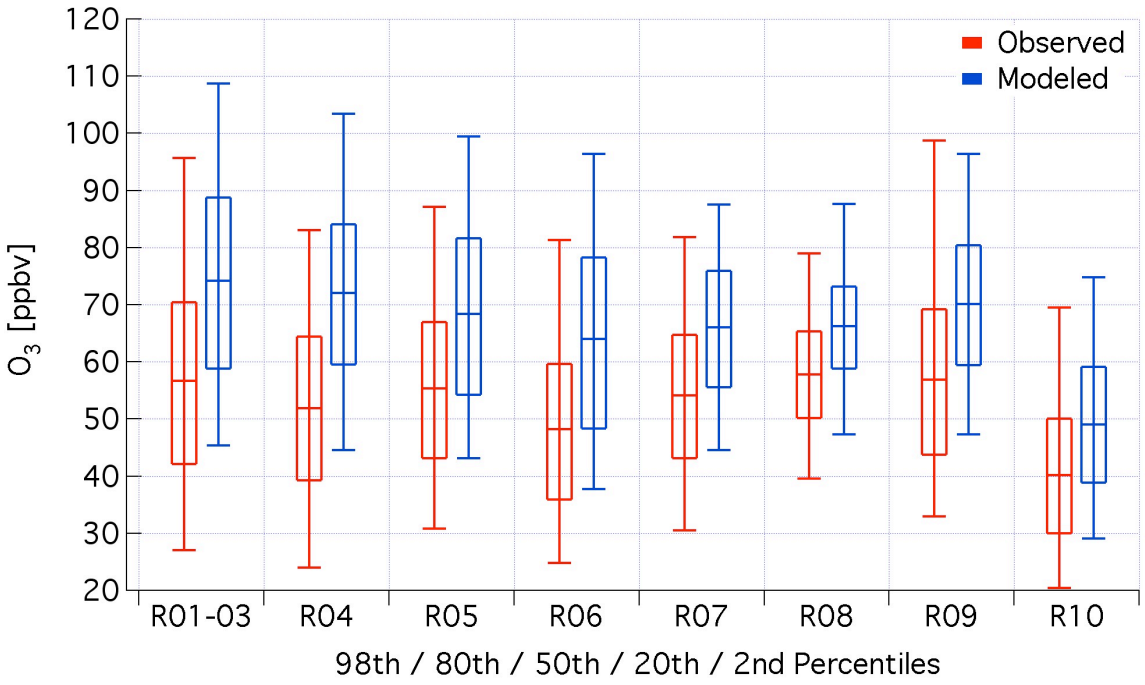

Figure 6.
Comparison of modeled to observed daily maximum 8-hr ozone concentrations.

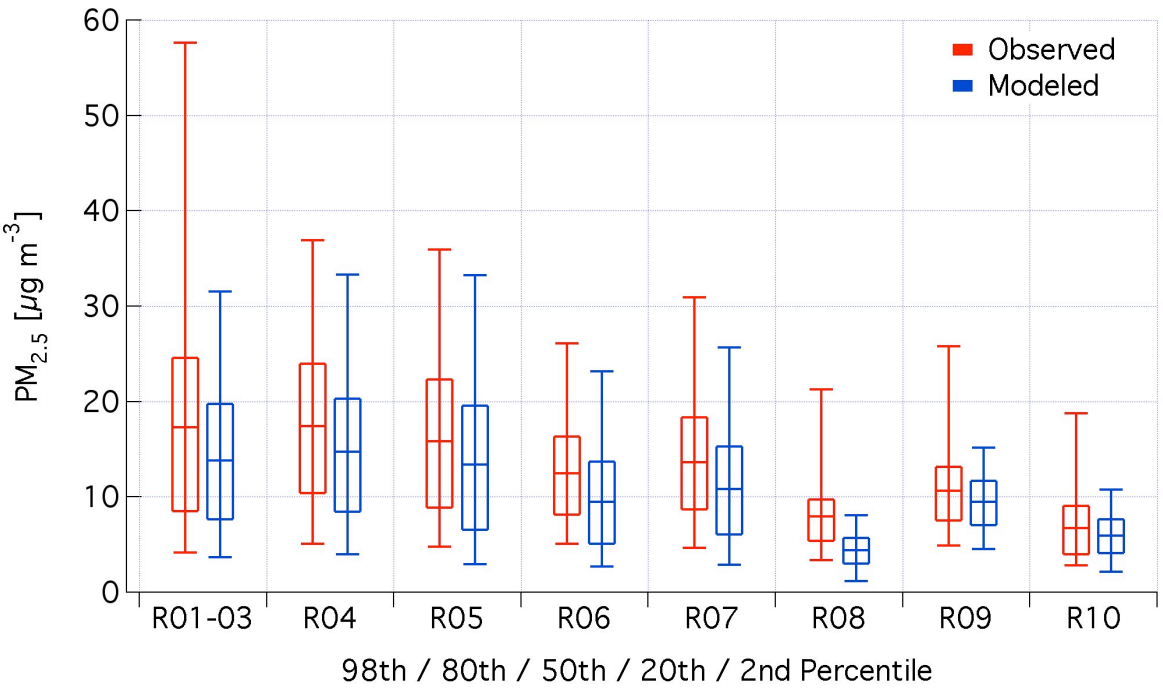

Figure 7.
Comparison of modeled to observed 24-hr average $PM_{2.5}$ concentrations.

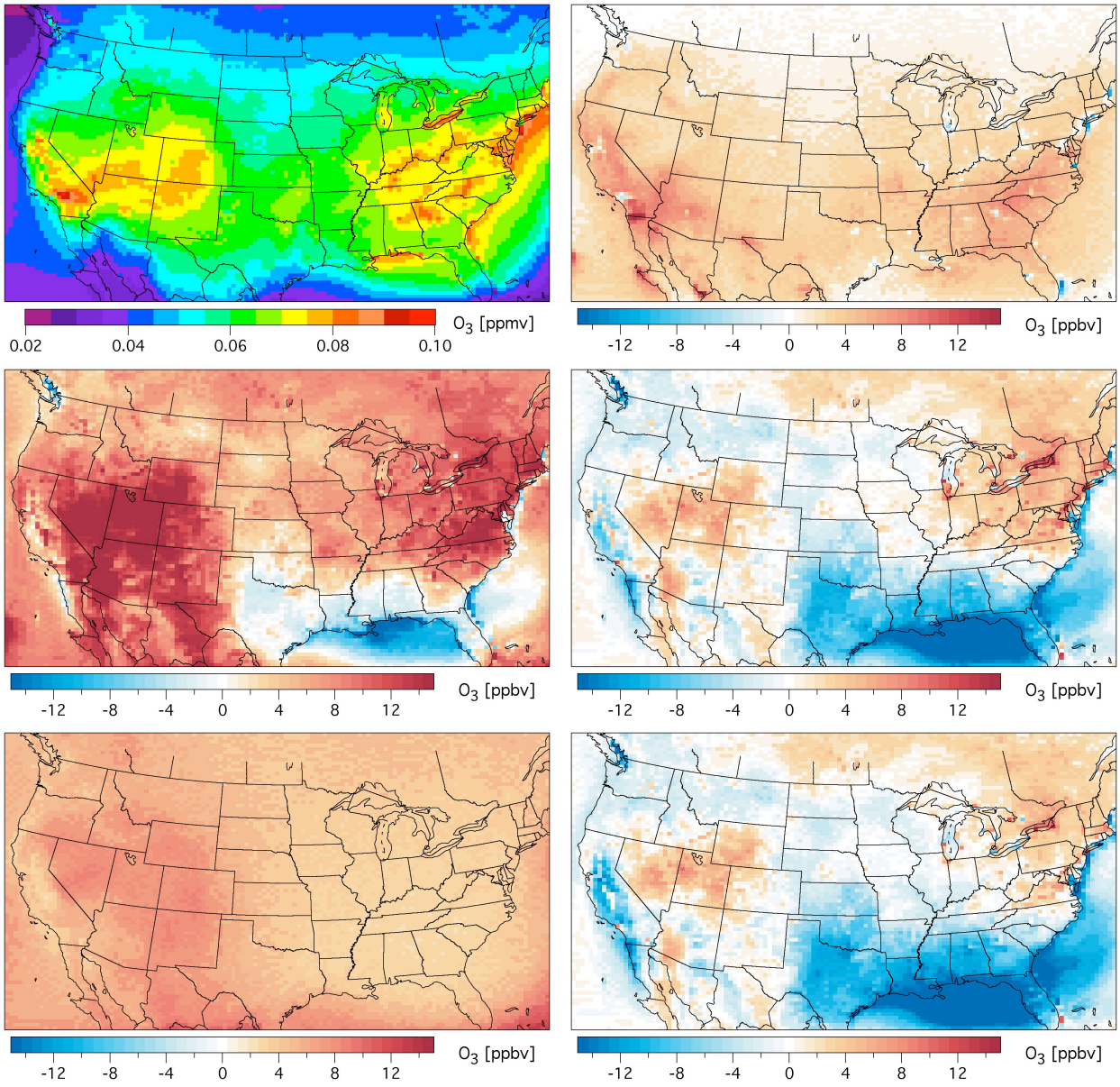

Figure 8.
Average daily maximum 8-hr ozone for (upper left) the CURall simulation, (middle left) difference between the FUTall and CURall simulations, (lower left) difference between the futBC and CURall simulations, (upper right) difference between the futEMIS and CURall simulations, (middle right) difference between the futMETcurLU and CURall simulations, and (lower right) difference between the futMETfutLU and CURall simulations.

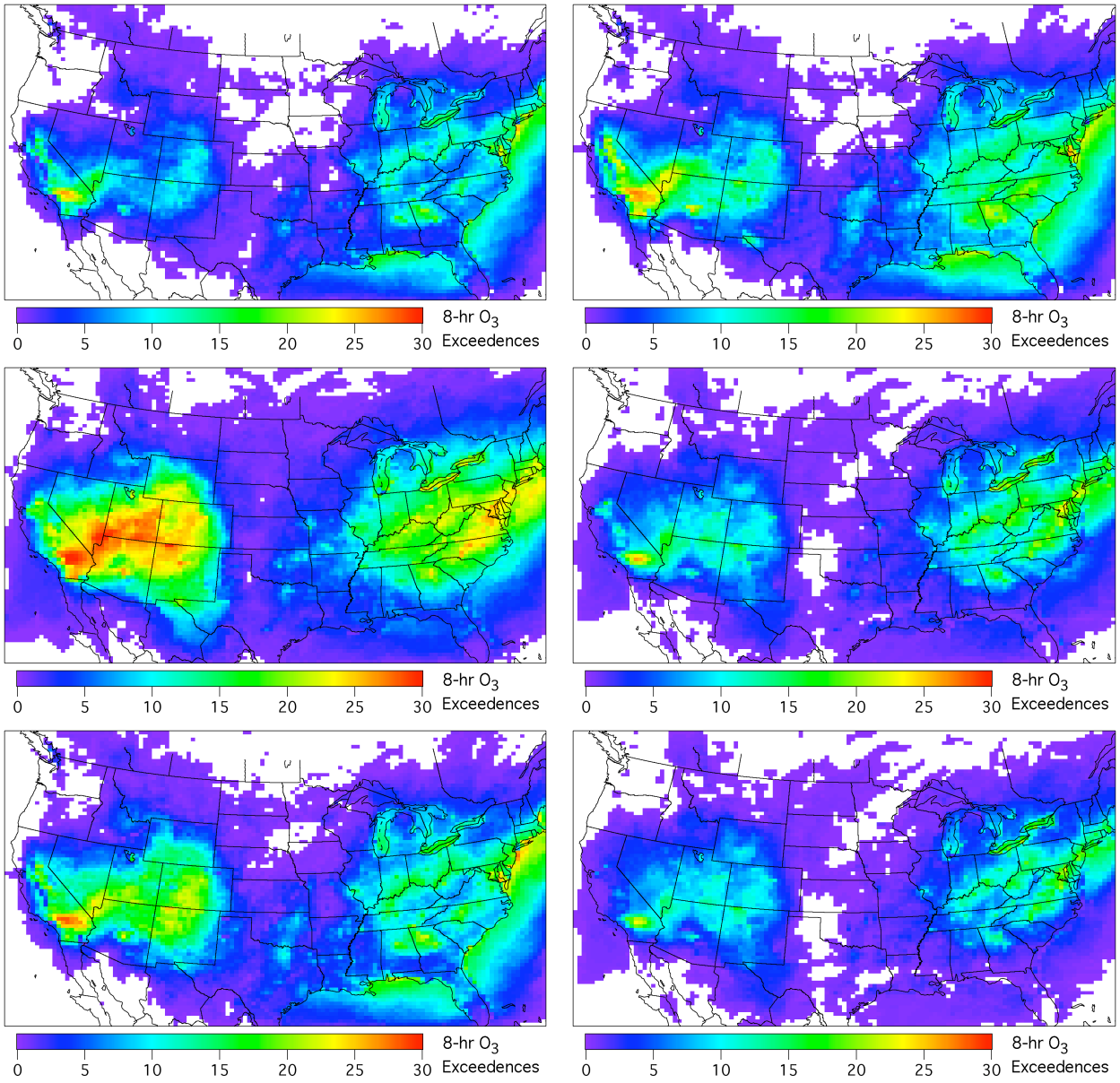

Figure 9.
Average number of days in July in which the daily maximum 8-hr ozone level exceeded the 80 ppbv standard for (upper left) the CURall simulation, (middle left) the FUTall simulation, (bottom left) the futBC simulation, (upper right) the futEMIS simulation, (middle right) the futMETcurLU simulation, and (lower right) the futMETfutLU simulation.

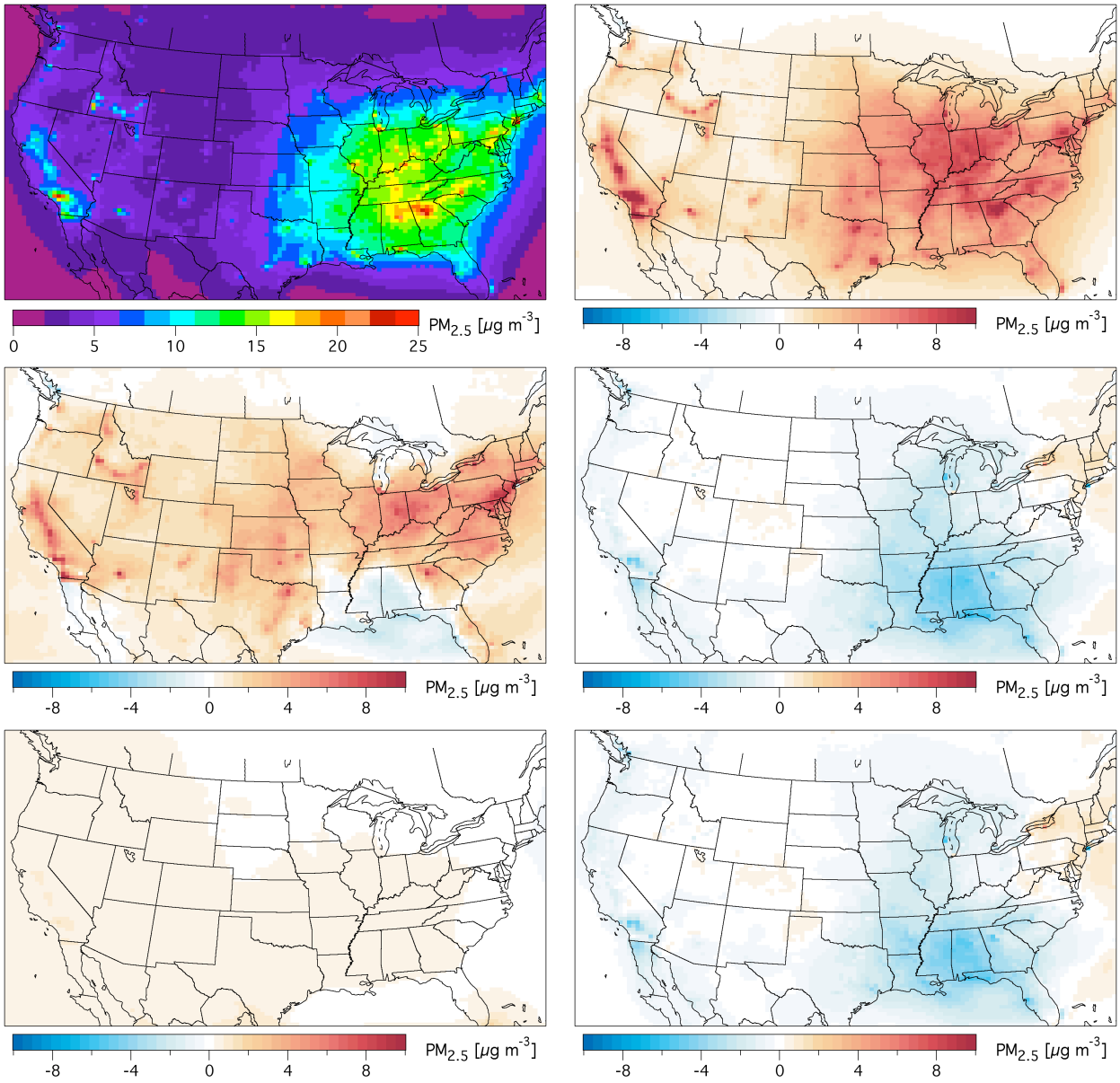

Figure 10.
Average maps of 24-hr PM2.5 concentration for (upper left) the CURall simulation, (middle left) difference between the FUTall and CURall simulations, (lower left) difference between the futBC and CURall simulations, (upper right) difference between the futEMIS and CURall simulations, (middle right) difference between the futMETcurLU and CURall simulations, and (lower right) difference between the futMETfutLU and CURall simulations.

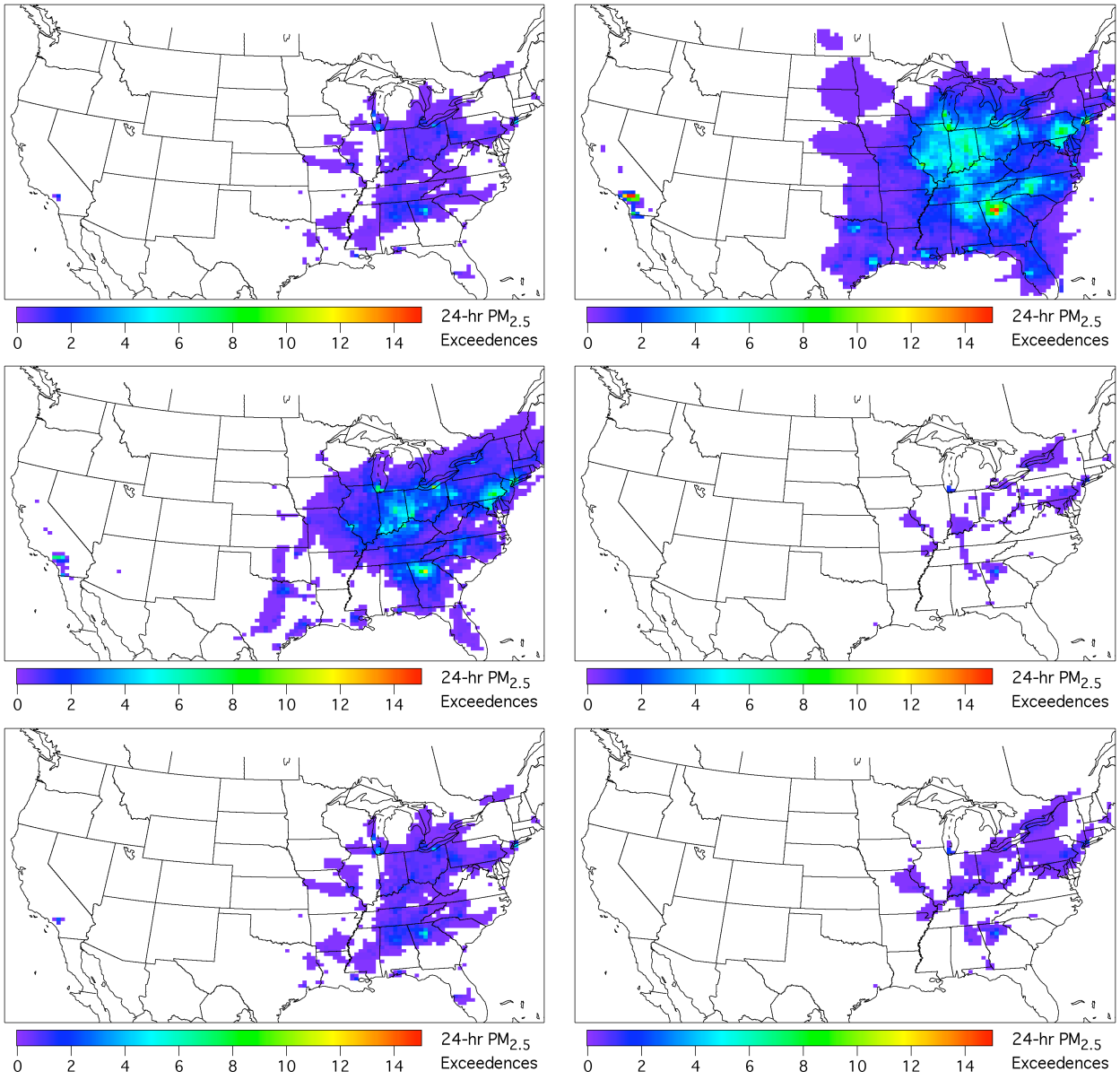

Figure 11.
Average number of days in July in which the 24-hr PM2.5 level exceeded the 35 ug/m3 standard for (upper left) the CURall simulation, (middle left) the FUTall simulation, (bottom left) the futBC simulation, (upper right) the futEMIS simulation, (middle right) the futMETcurLU simulation, and (lower right) the futMETfutLU simulation.

Table 1.
Designated model inputs for the six attribution cases. The “present-day” parameters refer to input representative of the 1990’s, while “future-2050” refers to input parameters representative of the 2050’s. Each case is comprised of five separate month long simulations representative of July meteorological conditions.

Simulation Name	Chemical boundary conditions	Anthropogenic emissions	Land-use / land-cover*	Meteorology
CURall	present-day	present-day	present-day	present-day
FUTall	future-2050	future-2050	future-2050	future-2050
futBC	future-2050	present-day	present-day	present-day
futEMIS	present-day	future-2050	future-2050	present-day
futMETcurLU	present-day	present-day	present-day	future-2050
futMETfutLU	present-day	present-day	future-2050	future-2050

* surrogate for biogenic emissions

Table 2.
Projected changes in meteorology from the present-day to the 2050 time period, where the delta change from the present-day is shown in parenthesis.

Region	Maximum surface temperature [C]	Maximum boundary layer height [m]	Maximum radiation reaching the surface [watt m^{-2}]	Average water vapor mixing ratio [g/kg]	Average wind speed [m/s]
R1-3	24.4 (+3.4)	1934 (+153)	865 (+10)	8.6 (+1.3)	2.3 (+0.0)
R04	29.2 (+2.6)	1976 (+93)	889 (+2)	11.4 (+1.5)	2.2 (+0.0)
R05	25.1 (+2.3)	1982 (+115)	834 (+23)	8.5 (+0.9)	2.4 (+0.0)
R06	29.6 (+1.5)	2288 (+13)	934 (+17)	10.3 (+0.7)	2.2 (+0.1)
R07	26.6 (+1.8)	2039 (+18)	852 (+32)	9.3 (+1.1)	2.4 (-0.1)
R08	22.2 (+1.7)	2509 (+184)	875 (+25)	6.9 (+0.3)	2.1 (+0.1)
R09	27.5 (+2.6)	2501 (+233)	1023 (+10)	7.9 (-0.6)	1.9 (+0.2)
R10	22.8 (+1.0)	2282 (+92)	937 (+5)	6.5 (+0.2)	2.1 (+0.2)

Table 3.
Summary of U.S. present-day (PD) and projected future-2050 (F2050) anthropogenic and biogenic emissions. Fractional change (future-2050 / present-day) is shown in parentheses for anthropogenic emissions. Note, for this work anthropogenic point source emissions were assumed constant between the two time periods.

species	units	anthropogenic				biogenic			
		point	area	non-road	mobile	PD meteorology, PD land-cover	PD meteorology, F2050 land-cover	F2050 meteorology, PD land-cover	F2050 meteorology, F2050 land-cover
CO	ktons/day	11.4 (1.0)	40.2 (1.20)	72.5 (1.11)	161.4 (0.99)	--	--	--	--
NO_X		24.1 (1.0)	3.7 (1.58)	12.6 (1.10)	22.4 (0.99)	4.1	4.1	4.2	4.2
VOC		4.5 (1.0)	19.9 (2.11)	8.1 (1.30)	15.6 (0.98)	156	96	188	103
NH_3		0.2 (1.0)	15.2 (2.50)	0.01 (1.06)	0.8 (0.99)	--	--	--	--
SO_2		42.7 (1.0)	2.8 (1.57)	1.5 (1.33)	0.8 (0.99)	--	--	--	--
PM_{10}		4.5 (1.0)	57.1 (1.93)	1.1 (1.17)	0.7 (0.99)	--	--	--	--
$PM_{2.5}$		3.6 (1.0)	13.9 (1.79)	1.0 (1.17)	0.5 (0.99)	--	--	--	--

Table 4.
Average daily maximum 8-hr ozone level (ppbv) for each EPA region.

Region	CURall	FUTall	futBC	futEMIS	futMET-curLU	futMET-futLU
R1-3	70	+12	+4	+3	+4	+2
R04	70	+3	+3	+5	-5	-8
R05	63	+7	+4	+2	+1	+0
R06	63	+3	+5	+3	-6	-7
R07	61	+5	+4	+3	-1	-2
R08	62	+9	+6	+2	+0	+0
R09	68	+12	+6	+5	+0	-1
R10	53	+7	+6	+3	-1	-1
U.S.	64	+7	+5	+3	-1.3	-2.6

Table 5.
Average number of 8-hr ozone 80 ppbv exceedances per grid per month.

Region	# grid cells	CURall	FUTall	futBC	futEMIS	futMET-curLU	futMET-futLU
R1-3	494	8.0	+8.9	+2.3	+2.6	+3.8	+1.5
R04	788	7.0	+4.1	+2.0	+4.6	-0.7	-2.6
R05	680	4.0	+4.0	+1.3	+1.3	+1.0	-0.5
R06	1119	2.9	+3.9	+3.1	+2.0	-0.3	-0.8
R07	558	0.7	+2.6	+1.0	+0.8	+0.6	+0.1
R08	1173	2.5	+7.0	+4.0	+1.2	+1.0	+0.9
R09	774	5.8	+9.6	+4.3	+3.9	+0.7	-0.6
R10	508	0.4	+1.6	+0.6	+0.2	+0.4	+0.4
U.S.	6094	3.9	+5.3	+2.6	+2.1	+0.6	-0.3

CHAPTER THREE

Impact of episodic long-range transport of Asian emissions on ozone levels in the western U.S., today and in the future

Jeremy Avise, Jack Chen, and Brian Lamb
Washington State University, Pullman, Washington, USA

Eric Salathé and Clifford Mass
University of Washington, Seattle, Washington, USA

Alex Guenther, Christine Wiedinmyer, and Jean-Francois Lamarque
National Center for Atmospheric Research, Boulder, Colorado, USA

Abstract:

This work examines the impact that present-day (1990-1999) episodic long-range transport (LRT) of Asian emissions has on ozone levels in the western United States, and how this impact may change in the future (2045-2054) due to global changes in climate and emissions. The transport of Asian emissions to the western U.S. is modeled using the MOZART-2 three-dimensional global chemical model for the present-day and future decades, where the future decade results are based on the IPCC A2 scenario. Regional impacts of the episodic LRT events are analyzed through the downscaling of MOZART-2 using the CMAQ regional photochemical grid model. In this work, a LRT event is defined as a CO concentration exceeding the monthly 85th percentile value for a minimum of 18 consecutive hours. LRT events in the lower (< 2 km) and mid-tropsophere (2-6 km) are examined. For the present-day, 1 to 3 LRT lower and mid-troposphere events occur every month depending on season, and the number of events does not change by more than 40% either way in the future. Enhancements of CO and PAN are found in the LRT air masses regardless of season, while measurable ozone enhancement only occurs in the late spring and summer months. The enhancement for all species is projected to increase in the future. In the Northwest U.S. (Oregon and Washington), surface ozone increases roughly 1-2 ppbv during present-day lower-troposphere LRT events for most seasons. In the future, surface ozone is projected to increase an additional 1 ppbv above present-day increases during LRT events. In California, wintertime surface ozone tends to increase during lower and mid-troposphere LRT events, for both the present-day and future cases, but surface ozone tends to decrease during summertime events. The decrease in ozone during

summer events is most likely due to the meteorological conditions associated with these LRT events. Overall, we project background concentrations of CO, PAN, and ozone to increase roughly 40 ppbv, 0.13 ppbv, and 9 ppbv, respectively.

1. Introduction

Air quality in any region is highly influenced by the chemical composition of the air being transported into that region. In the western United States, the concentrations of pollutants in the incoming air from the Pacific Ocean are often enhanced by emissions from the Asian continent, and these enhancements have the potential to adversely affect air quality in the region. In recent years, interest in assessing the long-range transport (LRT) of Asian emissions to North America has increased. Air masses leaving the Asia Pacific region have been characterized through intensive field studies such as the 2001 Transport and Chemical Evolution over the Pacific (TRACE-P) study [Jacob et al., 2003], which examined the chemical composition and transport of Asian air masses, and the 2001 Asia Pacific Aerosol Characterization Experiment (ACE-Asia) [Huebert et al., 2003] that focused on quantifying the distribution of aerosol concentrations and properties within these same air masses. The LRT of these polluted air masses from Asia to the western U.S. has been well documented over the past twenty years [e.g., Andreae et al., 1988; Parrish et al., 1992; Jaffe et al., 1999, 2003a; Takemura et al., 2002]. Intensive field campaigns such as the Intercontinental Transport and Chemical Transformation 2002 (ITCT 2K2) study [Parrish et al., 2004] and the Photochemical Ozone Budget of the Eastern North Pacific Atmosphere (PHOBEA) I and II [Jaffe et al., 2001; Kotchenruther et al., 2001a; Jaegle et al., 2003] have provided rich data sets for studying the chemical composition of the air reaching the western United States to determine the Asian influence.

The primary mechanism for transporting Asian emissions to the U.S. is the passage of cold fronts over Asia, and then out to the Pacific [Jacob et al., 2003; Liang et al., 2004]. Once Asian pollution reaches the U.S., subsidence is the primary mechanism for influencing surface level ozone [Jacob et al., 1999; Hudman et al., 2004]. Using GEOS-CHEM global chemical transport model simulations, Hudman et al. [2004] estimated the influence of Asian emissions on springtime surface ozone at Trinidad Head, California to be roughly 6 ppbv. Similarly, Fiore et al. [2002] found that anthropogenic Asian emissions contribute between 4-7 ppbv to surface ozone across the U.S., with larger contributions occurring in the west. Hudman et al. [2004] estimated LRT events to increase surface ozone in the western U.S. an additional 2 ppbv [Hudman et al., 2004] based on subsidence dilution factors from Jaffe et al. [2003a, 2003b]. However, the influence of the episodic transport of Asian emissions to the U.S. is not as well understood, and is likely highly variable. Price et al. [2004] examined 11 LRT events between 1997 and 2002 off the coast of Washington State, and found that ozone enhancements during LRT events were highly variable due to mixing with upper tropospheric air and variations in the presence of mineral dust.

The work presented here examines two decades (1990-1999 and 2045-2054) of global and regional chemistry model output as described by Chen et al. [2007] to determine the potential impacts that episodic Asian LRT events have on regional air quality in the western U.S., and how these impacts may change in the future due to global changes in climate and emissions. Section 2 describes the methodology and models used in this study. In section 3 we examine the frequency of episodic Asian

LRT events using elevated CO concentrations as a measure of when an event occurs. We then examine the enhancements above mean seasonal values during the LRT events for CO, PAN, and ozone, and end with an analysis of the impacts that these LRT events have on regional ozone levels in California, Oregon, and Washington. Summary and conclusions are presented in section 4.

2. Methodology

A multi-scale modeling approach is used to examine the impact of the episodic LRT of Asian emissions on present-day air quality in the western U.S., and to project how the impact of these events may change in the future due to global changes in climate and emissions. The transport of Asian emissions across the Pacific Ocean to the western U.S. is simulated using the MOZART-2 (Model of Ozone and Related Chemical Tracers, version 2) [Horowitz et al., 2003] global chemical transport model, driven by meteorological fields generated with the Parallel Climate Model (PCM) [Washington et al., 2000], for a current decade spanning 1990-1999 (present-day) and a future decade spanning 2045-2054 (future-2050). Output from MOZART-2 is examined to determine how the LRT of Asian emissions to the western U.S. may change in the future, in terms of the frequency, timing, and severity of these events. LRT events in two vertical regions are examined: from the surface to 2-km above the surface (lower-troposphere events), and from 2-6 km above the surface (mid-troposphere events). Although LRT events do occur in the upper-troposphere (> 6 km) [Liang et al., 2004; Bernsten et al., 1999], the impact of these events on regional ozone concentrations in the western U.S. is expected to be minimal.

We define a LRT event to have occurred when the CO concentration exceeds the monthly 85th percentile CO concentration for a given grid-cell for a minimum of 18 consecutive hours. Weiss-Penzias et al. [2004] used a similar method to identify LRT events from GEOS-CHEM model output and found good agreement with observations in predicting and quantifying LRT events. CO is a useful species to use for representing the LRT of Asian emissions, because its atmospheric lifetime (months) is sufficiently longer than typical transport times across the Pacific Ocean (4-8 days), and its source regions are relatively well known [Goldstein et al., 2004]. Additional measures were also examined (e.g., 75th percentile, as well as 12-hour and 24-hour events for both CO and PAN), and we found that our results were similar using all measures.

LRT events are analyzed in terms of lower and mid-troposphere events for each of the seven MOZART-2 grid cells (rows 12-18) off of the coast of the western U.S. from southern California to Washington State (Figure 1). To analyze the impact that LRT events have on both present-day and future-2050 regional ozone concentrations for the western U.S., CMAQ simulations were conducted for both the present-day and future-2050 decades for the continental U.S. at a 36-km grid resolution. The influence of the LRT events is incorporated into the CMAQ simulations by using MOZART-2 output as dynamic chemical boundary conditions for the CMAQ simulations. Further details of this implementation can be found in Chen et al. [2007] and Chapter 2 of this dissertation.

2.1. Global Models

Global model simulations were conducted at NCAR using MOZART-2 [Horowitz et al., 2003]. MOZART-2 is a global three-dimensional chemical transport model that has been implemented and evaluated in numerous studies [e.g., Lamarque et al., 2003; Lamarque and Hess, 2004; Chandra et al., 2004; Beig and Brasseur, 2006; Arellano and Hess, 2006; Tie et al., 2006], including inter-continental transport studies [Liu and Mauzerall, 2005; Goldstein et al., 2004], as well as for investigating the impact of projected emissions changes on future air quality [Horowitz, 2006].

In this application of MOZART-2, the model was run on a 2.8° latitude x 2.8° longitude horizontal grid, with 18 vertical hybrid levels extending from the surface to 4 hPa. Model results were archived at three hour intervals. MOZART-2 simulations were driven using meteorological fields from PCM [Washington et al., 2000] simulations for two ten year time periods: present-day (1990-1999) and future-2050 (2045-2054). The future-2050 PCM simulations represent a future climate based on the IPCC A2 scenario, which is one of the more pessimistic future scenarios.

Present-day MOZART-2 emissions are from the POET (Precursors of Ozone and their Effects in the Troposphere) database [Granier et al., 2004], which includes anthropogenic emissions based on the EDGAR (Emissions Database for Global Atmospheric Research) version 3.2 inventory [Olivier et al., 2000] and the Global Emissions Inventory Activity (GEIA) datasets [http://geiacenter.org]. Oceanic emissions are based on IMAGES [Muller and Brasseur, 1995, 1999]. The inventory includes

emissions from fossil fuel combustion, industrial processes, agricultural waste, biomass burning, lightening, aircraft, soil, and oceanic volatile organic compounds. Global biogenic emissions were generated using algorithms adapted from Guenther et al. [1995] and global land cover data generated by the Community Land Model (CLM) [Bonan et al., 2002]. For the future-2050 simulations, global anthropogenic emissions were projected to 2050 by geopolitical region (OECD90, REF, ASIA, and ALM) based on the IPCC SRES A2 scenario [Nakićenović et al., 2000].

2.2. Regional Models

To examine the impact the LRT of Asian emissions has on regional air quality in the western U.S., it is necessary to downscale the global model simulations using regional meteorological and photochemical grid models. The present-day and future-2050 global model simulations were downscaled to the regional scale using the MM5 version 3 meteorological model [Grell et al., 1994] and the EPA Community Multi-scale Air Quality (CMAQ) version 4.4 photochemical grid model [Byun and Schere, 2006]. Model simulations were conducted on a Lambert Conformal projection centered over the continental U.S. with a central latitude of 97 °W, central longitude of 40 °N, and first and second parallels of 33 °N and 45 °N, respectively. The MM5 simulations were conducted in non-hydrostatic mode with 28 full-sigma vertical levels in a one-way nested configuration for 108-km and 36-km grid resolution. The following model parameterizations were used: MRF (Hong-Pan) PBL scheme [Hong and Pan, 1996], simple 5-layer soil model with land-use information from 1-km USGS data [Chen and Dudhia, 2001a,b], Kain-Fritsch cumulus parameterization scheme [Kain and Fritsch,

1990], explicit moisture (including simple ice physics, but no mixed phase processes), and the CCM2 radiation scheme. Model configurations were chosen to optimize computational speed, while also capturing large scale meteorological processes at the 36-km grid scale. To maintain simulation stability, the outer 108-km domain was nudged towards the PCM output, which constrains MM5 to the global model and results in a smooth transition from the global model to the continental scale (36-km) MM5 simulations.

Model configurations for the present-day and future-2050 MM5 simulations were the same, except for the land-use dataset used. The present-day simulations used land-use information based on the USGS 1-km land-use dataset, which includes 24 land-cover categories. Since variations in land-use and land-cover can significantly influence regional meteorology and air quality through surface energy flux perturbations [Civerolo et al., 2000], land-use for the future-2050 simulations was updated with data from the Community Land Model (CLM) [Bonan et al., 2002] and the Spatially Explicit Regional Growth Model (SERGOM) [Theobald, 2005]. The CLM predicted changes in vegetation distribution due to climate change and changes in land management practices for the 2050 time period, while SERGOM provided projected urban and suburban population density distributions out to the year 2030. For a more detailed description of the changes in land-cover predicted by CLM and SERGOM used in this work, the readers are referred to Chen [2007] and Chen et al. [2007].

Output from the 36-km MM5 simulations was processed through MCIP (Meteorology-Chemistry Interface Processor version 3.0) and used to drive the CMAQ version 4.4 photochemical grid model. Gas-phase chemistry was modeled using a condensed version of the SAPRC-99 chemical mechanism [Carter 2000a,b] available with the CMAQ distribution, while aerosol processes were simulated with the AERO3 aerosol module [Byun and Schere, 2006]. The model was run with 17 vertical sigma levels from the surface to the tropopause, with a first layer height of approximately 36 meters. Present-day anthropogenic emissions were processed through the SMOKE (Sparse Matrix Operating Kernel Emissions) emissions processing system [Houyoux et al., 2005], and were based on the 1999 EPA National Emissions Inventory (NEI-1999; http://www.epa.gov/ttn/chief/net/1999inventory.html).

Future-2050 anthropogenic emissions were projected out to the year 2050 using emissions growth factors, based on projections of economic activity, generated through the EPA Economic Growth Analysis System (EGAS) [U.S. EPA, 2004]. EGAS growth factors were applied to area and mobile source categories, but not to point sources. Due to the uncertainty surrounding future point source locations and emissions, point source emissions were held constant between the present-day and future-2050 time periods. Future-2050 anthropogenic emissions were also updated to account for the expansion of urban areas using the SERGOM model, which projected estimates of population and housing density to the year 2030. Biogenic emissions for both the pesent-day and future-2050 simulations were generated dynamically using the MEGAN-EZ (Model of Emissions of Gases and Aerosols from Nature - EZ version) [Guenther et

al., 2006]. MEGAN-EZ estimates hourly isoprene, monoterpene, and other VOC emissions from plants using seasonal vegetation datasets, along with MM5 predicted hourly temperatures and incident shortwave radiation at the surface. For the present-day case the seasonal vegetation dataset was derived from satellite observations. For the future-2050 case, the present-day vegetation dataset was updated with the Community Land Model to be consistent with the future-2050 land-use dataset used in the MM5 simulations. For a more detailed description and summary of the anthropogenic and biogenic emission inventories used in this work, the readers are referred to Chen [2007] and Chen et al. [2007].

3. Results and Discussion

3.1. Frequency of LRT Events

The number of simulated long-range transport events per month, defined as 18 consecutive hours of CO concentrations exceeding the monthly average 85th percentile value, are shown in Tables 1 (mid-troposphere events) and 2 (lower-troposphere events). The number of monthly predicted events is generally largest in the springtime for both the lower and middle troposphere, which is consistent with the more direct flow across the Pacific Ocean from Asia to the Northern Pacific during spring months [Hess et al., 1996]. The number of monthly transport events also tends to increase from the lower latitudes (row 12) to higher latitudes (row 18), particularly during the summer and fall seasons. The predicted number of LRT events agrees relatively well with measurements made at Cheeka Peak Observatory in Washington State from 2001-2002 and associated GEOS-CHEM simulations, which suggest approximately 1-2

events per month below 2-km, and 2-3 events per month between 2-km and 6-km [Liang et al., 2004]. However, Liang et al. [2004] do show strong seasonal variations in the number of lower-troposphere LRT events, with an increased occurrence of events in the springtime. Although the predicted number of lower-troposphere events in Table 2 does show more events occurring in springtime compared to other seasons, the difference between seasons is small. There are no obvious patterns to the predicted changes in the number of monthly transport events from the present-day to the future-2050, and changes are different for different seasons, latitudes, and the type of event (lower or mid-troposphere). For mid-troposphere events (Table 1), the number of events tends to increase in the lower latitudes and decrease in the higher latitudes in the winter and summer. In the springtime, mid-troposphere events are projected to decrease for nearly all latitudes, while fall events are projected to increase for most latitudes. Lower-troposphere (Table 2) events show a similar trend in springtime, with most latitudes showing a decrease in the number of events, however, the decrease is significantly larger in the higher latitudes compared to lower latitudes. Unlike the mid-troposphere events, lower-troposphere events show a decrease in the number of fall events for most latitudes, with only the lowest latitudes showing some increase. Projected changes in lower-troposphere winter events show an increase in higher latitudes and a decrease in lower latitudes, which is the opposite of what is projected for the mid-troposphere. Summer lower-troposphere events tend to increase in the future for all latitudes, but the increase is larger in the lower latitudes. The significant differences between lower and mid-troposphere in terms of the projected changes of the

number of LRT events in the future suggests that events in the lower and mid-troposphere are not highly coupled and may occur independent of one another.

3.2. Comparison of Modeled to Observed

Observations made during the ITCT 2K2 [Nowak et al., 2004] and PHOBEA [Kotchenruther et al., 2001] experiments are compared to modeled mean springtime values in Table 3. Modeled CO is roughly 20-30 ppbv lower than observed values, which suggests that the magnitude of Asian emissions in the model may not sufficiently capture actual Asian emissions in order to reproduce the observed CO levels. However, MOZART does accurately predict the seasonal variation in CO concentrations (see Figure 2), with CO levels decreasing throughout the spring and early summer and increasing again in the fall, due to seasonal changes in OH concentration and the seasonal variability in industrial emissions [Millet et al., 2004; Granier et al., 1999]. Modeled PAN is significantly higher than observed levels, while ozone is significantly under predicted. The discrepancies in PAN and ozone may be partly due to inaccurate Asian emissions, or possibly that the PCM output used to drive MOZART is predicting lower than actual temperatures across the Pacific, which is resulting in decreased thermal decomposition of PAN and higher PAN concentrations. Consequently, NO_X would be reduced, which may lower ozone levels depending on the ratio of hydrocarbons to NO_X. However, 1999 was also a year with anomalously high incoming ozone [personal communication with Dan Jaffe], which may account for the discrepancy between model predictions and observations.

3.3. Event Concentrations

Average CO, PAN, and ozone concentrations compared to event average concentrations in the lower and mid-troposphere for both the present-day and future-2050 time periods are shown in Figure 2. Because of the way we have defined a LRT event, CO concentrations will be inherently higher during these events, however, we also see significant enhancements in PAN concentrations during events, as well as enhancements in ozone during late-spring and summer months. Table 4 summarizes these results by season. Enhancement of CO, during present-day LRT events, above the seasonal average tends to be largest when CO concentrations are low (e.g., fall for mid-troposphere events and summer for lower-troposphere events), but in general the seasonal variation in not large. This contradicts results from Liang et al. [2004] and Weiss-Penzias et al. [2004], who found that the largest enhancement occurs in the winter and spring months. Enhancements in CO during future-2050 events in the lower-troposphere also tends to be largest when CO concentrations are low, while in the mid-troposphere, CO enhancements are roughly the same for winter, spring, and fall, but are lowest in the summer. For both lower and mid-troposphere events, CO enhancement during events tend to increase from the present-day to the future-2050 by roughly +6 ppbv, suggesting events may increase in severity in the future (this increase is on top of the 30-40 ppbv increase in average CO concentrations from the present-day to the future-2050). Corresponding enhancements in PAN are generally largest in the winter and spring for both the present-day and future-2050 simulations, and tend to increase in magnitude in the future (20 to 120 pptv), with the only exception being fall mid-troposphere events (this increase is on top of the 10-230 pptv increase in PAN from the

present-day to the future-2050). Ozone concentrations show the largest enhancement in the summer months (~ 6 ppbv) during both lower and mid-troposphere events, and this enhancement is projected to increase slightly in the future (+0.5 ppbv for mid-troposphere events and +1.7 ppbv for low-troposphere events). Spring and fall ozone levels show smaller enhancement compared to summer, at 2-3 ppbv in the lower-troposphere, and -5.5 to +1.5 ppbv in the mid-troposphere. Future-2050 event ozone enhancements generally change by less than 1 ppbv for the spring and fall. Changes in ozone enhancements are on top of the 5-12 ppbv increase in average ozone from the present-day to future-2050.

During both lower and mid-troposphere LRT events, CO and PAN concentrations are highly correlated (see Figure 3). Correlation in the mid-troposphere is much stronger than in the lower-troposphere, and in the present-day case ranges from 0.76 in the winter to 0.82 in the fall, while correlation in the lower-troposphere is not as high, and ranges from 0.40 in the winter to 0.71 in the spring. The springtime correlations for both the lower and mid-troposphere events are in agreement with springtime observations made off the coast of Washington State as part of the 1999 PHOBEA experiments [Kotchenruther et al., 2001], which showed a correlation between PAN and CO of 0.66. Hudman et al. [2004] also found a similar correlation between CO and PAN (r=0.61) in Asian pollution plumes measured during ITCT 2K2. CO and PAN correlation is projected to become slightly stronger in the future in the lower-troposphere (0.42 in the winter to 0.76 in the spring), but remains roughly the same in the mid-troposphere, except for in the fall, which shows a decrease from 0.82 in the present-day case to 0.67

for the future-2050 case. Unlike CO and PAN, CO and ozone are not highly correlated during LRT events (Figure 4), due to complexities, such as mixing with high levels of ozone in the upper troposphere. The CO - ozone correlation does not significantly change from the present-day to the future-2050.

3.4. Impact on Surface Ozone Levels

The impact LRT events have on seasonal surface ozone levels in the western U.S. is illustrated in Figures 5-8 for the present-day (results are summarized in Tables 5 and 6 for each region). Southern California shows the largest increase in ozone in the winter time, with both lower and mid-troposphere LRT events increasing ozone levels approximately +1 to +3 ppbv throughout the region. Summer and spring time events tend to have the opposite affect and actually result in a decrease in peak ozone ranging from -1 to -8 ppbv for mid-troposphere events and -2 to -4 ppbv for lower-troposphere events. Although pollutant concentrations in the incoming air during these events are enhanced, the meteorological conditions leading to the LRT events may not be conducive to producing high ozone episodes. Northern California also shows peak summer ozone levels decreasing (-1 to -3 ppbv) during mid-troposphere LRT events, while lower-troposphere events lead to slight increases in ozone levels (+1 to +2 ppbv for peak values and +2 to +3 for average values across the region). Oregon and Washington show similar results for mid-troposphere events for non-summer seasons, with peak and regional average ozone levels increasing by +1 to +2 ppbv. During summer mid-troposphere events, Washington shows a slight decrease in peak ozone levels (-1 to -2 ppbv), while Oregon shows no significant change. Summertime lower-

troposphere events tend to increase surface ozone in Oregon and Washington, with Oregon having slightly larger increases in ozone (+1 to + 3 ppbv) compared to Washington (-1 to +2 ppbv).

Results for the future-2050 case are shown in Figures 9-12 and summarized in Tables 7 and 8. For southern California, the impact of mid-troposphere events on peak surface ozone is similar for both the present-day and future-2050 cases. The only significant difference is in the summertime, where future-2050 events cause between no change and a -4 ppbv decrease in peak ozone level compared to the present-day case which shows up to a -8 ppbv decrease. However, on average across all of southern CA, the future-2050 events result in significantly larger increases in surface ozone during the winter (+3 ppbv compared to +1 ppbv for the present-day cases) and summer months (+1 ppbv compared to -3 ppbv for the present-day cases). Similarly, the impact of lower-troposphere events is not significantly different between the present-day and future-2050 in regards to peak ozone levels. On average across all of southern California, the future-2050 events cause an additional +1 to +2 ppbv increase in surface ozone during the winter and sumer months above present-day events. In northern California, future-2050 lower and mid-troposphere events tend to increase ozone more in the winter months compared to the present-day, but show the opposite trend for other months. Oregon and Washington both show larger increases in surface ozone (+1 to + 2 ppbv) under LRT conditions for both lower and mid-troposphere events compared to the present-day case.

4. Summary

We examined the influence of the episodic LRT of Asian emissions on CO, PAN, and ozone concentrations within the incoming air to the western U.S. for a present-day (1990-1999) and future-2050 (2045-2054) decade using the MOZART-2 global chemistry model, and evaluated the impact of these events on surface ozone levels throughout the western U.S. through regional CMAQ model simulations. The number of LRT events (defined as 18 consecutive hours of CO concentrations exceeding the monthly 85th percentile for CO) ranges from 1-3 events per month depending on the season, and the number of events tends to increase with latitude (e.g., southern California experiences fewer events than does Washington). Projected changes in the number of LRT events in the future is highly variable, and depends on the season, latitude, and whether the LRT event occurs in the lower or mid-troposphere. However, the number of events generally does not change by more than 40% for any given latitude and season.

The enhancement of pollutant concentrations during LRT events tends to increase in the future for both lower and mid-troposphere events. This is particularly true for lower-troposphere events, which see an increase in CO enhancement from the present-day of +16 to +18 ppbv, to a future-2050 enhancement of +22 to +27 ppbv (the increase in CO enhancement from the present-day to future-2050 is in addition to the 30-40 ppbv increase in average CO concentration). Similarly, PAN and ozone enhancements increase in magnitude from the present-day case to the future-2050 case, again in addition to increases in average ozone and PAN concentrations. The

increase in magnitude of the ozone and PAN enhancement is potentially a concern, because subsidence of ozone and PAN (followed by ozone production) are two of the primary mechanisms for Asian influence on surface ozone in the U.S. [e.g. Jacob et al., 1999; Hudman et al., 2004].

The impact of Asian LRT events was found to have a minimal impact on surface level ozone concentrations along the U.S. west coast. LRT events generally led to increases of roughly +1 to +2 ppbv in present-day surface level ozone throughout Oregon and Washington for most seasons. In the future-2050 case, the influence of LRT events resulted in ozone increases of roughly +1 to +3 ppbv. In California, LRT events tended to increase wintertime ozone by several ppbv in the present-day case, with slightly larger increases for the future-2050 case. Despite an increase in pollutant concentrations within the LRT air masses, summertime events in California were associated with a decrease in surface ozone levels for both the present-day and future-2050 cases. The decrease in ozone that occurs in California during summertime LRT events is most likely due to the local meteorological conditions associated with these events.

The work presented here is unique in that we have examined both the present-day and projected future episodic transport of Asian emissions to the U.S. west coast to determine how global changes may impact these episodic events, and what implications this has on U.S. air quality. Previous work has primarily focused on present-day episodic transport only, or on how increases in Asian emissions will impact U.S. air

quality through enhanced background concentrations, but not changes in the episodic LRT transport of these emissions. Although we found that Asian LRT events do not influence ozone levels along the U.S. west coast by more than several ppbv, this does not mean that Asian emissions play an insignificant role in defining U.S. air quality. One potential flaw within this study is that we did not determine the source of the CO enhancement observed in MOZART-2, so we have no way of distinguishing whether the enhancement was due to the LRT of Asian emissions or transport from some other region. Furthermore, it is far more likely that the most significant impact of Asian emissions on U.S. ozone levels will occur through an increase in the background ozone concentrations that enter the U.S. from the Pacific. For example, Chapter 2 of this dissertation showed that as global emissions increase (including Asian emissions) based on the IPCC SRES A2 scenario, surface ozone in the western U.S. will increase by 6 ppbv.

References

Arellano Jr., A. F. and P. G. Hess (2006), Sensitivity of top-down estimates of CO sources to GCTM transport, *Geophys. Res. Lett.*, 33, doi:10.1029/2006GL027371.

Andrae, M. O., H. Berresheim, T. W. Andrae, M. A. Kritz, T. S. Bates, and J. T. Merrill (1988), Vertical distribution of dimethylsulfide, sulfur dioxide, aerosol ions, and radon over the Northeast Pacific Ocean, *J. Atmos. Chem.*, 6, 149-173.

Beig, G. and G. P. Brasseur (2006), Influence of anthropogenic emissions on tropospheric ozone and its precursors over the Indian tropical region during a monsoon, *Geophys. Res. Lett.*, 33, doi:10.1029/2005GL024949.

Bonan, G. B., K. W. Oleson, M. Vertenstein, S. Levis, X. B. Zeng, Y. J. Dai, R. E. Dickinson, and Z. L. Yang (2002), The Land Surface Climatology of the Community Land Model Coupled to the NCAR Community Climate Model, *J. Climate*, 15(22), 3123-3149.

Byun, D. and K. L. Schere (2006), Review of the Governing Equations, Computational Algorithms, and Other Components of the Models-3 Community Multiscale Air Quality (CMAQ) Modeling System, *Applied Mechanics Reviews*, 59, 51-77.

Carter, W., 2000a: Documentation of the SAPRC-99 Chemical Mechanism for VOC Reactivity Assessment, Draft report to the California Air Resources Board, Contracts 92-329 and 95-308, May 8 (available at http://www.cert.ucr.edu/~carter/absts.htm#saprc99).

Carter, W., 2000b: Implementation of the SAPRC-99 Chemical Mechanism into the Models-3 Framework, Report to the United States Environmental Protection Agency, January 29 (available at http://www.cert.ucr.edu/~carter/absts.htm#s99mod3).

Chandra, S., J. R. Ziemke, X. Tie, and G. Brasseur (2004), Elevated ozone in the troposphere over the Atlantic and Pacific oceans in the Northern Hemisphere, *Geophys. Res. Lett.*, 31, doi:10.1029/2004GL020821.

Chen, F., and J. Dudhia (2001a), Coupling an advanced land-surface/hydrology model with the Penn State/NCAR MM5 modeling system. Part I: Model implementation and sensitivity. *Mon. Wea. Rev.*, 129, 569-585.

Chen, F., and J. Dudhia (2001b), Coupling an advanced land-surface/hydrology model with the Penn State/NCAR MM5 modeling system. Part I: Preliminary model validation. *Mon. Wea. Rev.*, 129, 587-604.

Chen, J. C.-M., Short-term air quality forecasts for the Pacific Northwest and long-range global change predictions for the U.S., PhD Dissertation, Washington State University, Department of Civil & Environmental Engineering, Pullman, WA, 2007.

Civerolo, K. L., Sistla, G., Rao, S. T., and Nowak, D. J. (2000), The Effects of Land Use in Meteorological Modeling: Implications for Assessment of Future Air Quality Scenarios, *Atmospheric Environment*, 34(10), 1615-1621.

Fiore, A. M., D. J. Jacob, I. Bey, R. M. Yantosca, B. D. Field, A. C. Fusco, and J. G. Wilkinson (2002), Background ozone over the United States in summer: Origin, trend, and contribution to pollution episodes, *J. Geophys. Res.*, 107(D15), 4275, doi:10.1029/2001JD000982.

Granier, C., J. F. Müller, G. Pétron, and G. Brasseur (1999), A three-dimensional study of the global CO budget, *Chemosphere: Global Change Science*, 1, 255-261.

Granier, C. et al. (2004), Present and future surface emissions of atmospheric compounds, European Commission report EVK 2199900011 (Available at http://www.aero.jussieu.fr/project/ACCENT/POET.php).

Grell, G. A., J. Dudhia, D. R. Stauffer (1994), A Description of the Fifth-Generation Penn State/NCAR Mesoscale Model (MM5), National Center for Atmospheric Research, Boulder, CO; NCAR/TN-398+STR, 122 pp.

Guenther, A., C. N. Hewitt, D. Erickson, R. Fall, C. Geron, T. Graedei, L. Klinger, M. Lerdau, W. A. McKay, T. Pierce, B. Scholes, R. Steinbracher, R. Taliamaraju, J. Taylor, and P. Zimmerman (1995), A Global-Model of Natural Volatile Organic-Compound Emissions, *J. Geophys. Res.*, 100(D5), 8873-8892.

Guenther, A., T. Karl, P. Harley, C. Wiedinmyer, P. I. Palmer, and C. Geron (2006), Estimates of global terrestrial isoprene emissions using MEGAN (Model of Emissions of Gases and Aerosols from Nature), *Atmospheric Chemistry and Physics Discussions*, 6, 107-173.

Goldstein, A. H., D. B. Millet, M. McKay, L. Jaeglé, L. Horowitz, O. Cooper, R. Hudman, D. J. Jacob, S. Oltmans, and A. Clarke (2004), Impact of Asian emissions on observations at Trinidad Head, California, during ITCT 2K2, *J. Geophys. Res.*, 109, doi:10.1029/2003JD004406.

Hess, P. G., N. Srimani, and S. J. Flocke (1996), Trajectories and related variations in the chemical composition of air for the Mauna Loa Observatory during 1991 and 1992, *J. Geophys. Res.*, 101, 14, 543-14, 568.

Houyoux, Marc, Vukovich, Jeff, and Brandmeyer, J. E. (2005), Sparse Matrix Operator Kernel Emissions Modeling System User Manual. [online] http://cf.unc.edu/cep/empd/products/smoke.

Hong, S.-Y., and H. L. Pan (1996), Nonlocal boundary layer vertical diffusions in a medium-range forecast model. *Mon. Wea. Rev.*, 124, 2322-2339.

Horowitz L. W., S. Walters, D. L. Mauzerall, L. K. Emmons, P. J. Rasch, C. Granier, X. Tie, J.-F. Lamarque, M. G. Schultz, G. S. Tyndall, J. J. Orlando, and G. P. Brasseur (2003), A global simulation of tropospheric ozone and related tracers: Description and evaluation of MOZART, version 2, *J. Geophys. Res.*, 108(D24), doi:10.1029/2002JD002853.

Horowitz, L. W. (2006), Past, present, and future concentrations of tropospheric ozone and aerosols: Methodology, ozone evaluation, and sensitivity to aerosol wet removal, *J. Geophys. Res.*, 111, doi:10.1029/2005JD006937.

Huebert, B. J., T. Bates, P. B. Russell, G. Shi, Y. J. Kim, K. Kawamura, G. Carmichael, and T. Nakajima (2003), An overview of ACE-Asia: Strategies for quantifying the relationships between Asian aerosols and their climatic impacts, *J. Geophys. Res.*, 108(23), doi:10.1029/2003JD003550.

Jacob, D. J., J. A. Logan, and P. P. Murti (1999), Effect of rising Asian emissions on surface ozone in the United States, *Geophys. Res. Lett.*, 26(14), 2175-2178, 10.1029/1999GL900450.

Jacob, D. J., J. H. Crawford, M. M. Kleb, V. S. Connors, R. J. Bendura, J. L. Raper, G. W. Sachse, J. C. Gille, L. Emmons, and C. L. Heald (2003), Transport and Chemical Evolution over the Pacific (TRACE-P) aircraft mission: Design, execution, and firs results, *J. Geophys. Res.*, 108(D20), doi:10.1029/2002JD003276.

Jaffe, D. A., T. Anderson, D. Covert, B. Trost, J. Danielson, W. Simpson, D. Blake, J. Harris, and D. Streets (2001), Observations of Ozone and Related Species in the Northeast Pacific During the PHOBEA Campaigns: 1. Ground based observations at Cheeka Peak, *J. Geophys. Res.*, 106, 7449-7461.

Jaffe, D. A., I. MacKendry, T. Anderson, and H. Price (2003a), Six “new” episodes of trans-Pacific transport of air pollutants, *Atmos. Environ.*, 37, 391-404.

Jaffe, D., J. Snow, and O. Cooper (2003b), The 2001 Asian dust events: Transport and impact on surface aerosol concentrations in the U.S., *Eos. Trans.*, AGU, 84(46), 501,507.

Jaegle, L., D. A. Jaffe, H. U. Price, P. Weiss-Penzias, P. I. Palmer, M. J. Evans, D. J. Jacob, and I. Bey (2003), Sources and budgets for CO and O3 in the Northeast Pacific during the spring of 2001: Results from the PHOBEA-II Experiment, *J. Geophys. Res.*, 108(D20), doi: 10.1029/2002JD003121.

Kain, J. S., and J. M. Fritsch (1990), A one-dimensional entraining/detraining plume model and its application in convective parameterization. *J. Atmos. Sci.*, 47, 2784-2802.

Kotchenruther, R. A., D. A. Jaffe, H. J. Beine, T. Anderson, J. W. Bottenheim, J. M. Harris, D. Blake, and R. Schmitt (2001), Observations of Ozone and Related Species in the Northeast Pacific During the PHOBEA Campaigns: 2. Airborne observations, *J. Geophys. Res.*, 106, 7463-7483. (Corrected Table 1 published in Vol. 106 (D17), p. 20,507)

Lamarque, J.-F., D. P. Edwards, L. K. Emmons, J. C. Gille, O. Wilhelmi, C. Gerbig, D. Prevedel, M. N. Deeter, J. Warner, D. C. Ziskin, B. Khattatov, G. L. Francis, V. Yudin, S. Ho, D. Mao, J. Chen, and J. R. Drummond (2003), Identification of CO plumes from MOPITT data: Application to the August 2000 Idaho-Montana forest fires, *Geophys. Res. Lett.*, 30(13), doi:10.1029/2003GL017503.

Lamarque, J.-F. and P. G. Hess (2004), Arctic Oscillation modulation of the Northern Hemisphere spring tropospheric ozone, *Geophys. Res. Lett.*, 31, doi: 10.1029/2003GL019116

Liang, Q., L. Jaeglé, D. A. Jaffe, P. Weiss-Penzias, and A. Heckman (2004), Long-range transport of Asian pollution to the northeast Pacific: Seasonal variations and transport pathways of carbon monoxide, *J. Geophys. Res.*, 109, D23S07, doi: 10.1029/2003JD004402.

Liu, J. and D. L. Mauzerall (2005), Estimating the average time for inter-continental transport of air pollutants, *Geophys. Res. Lett.*, 32, doi:10.1029/2005GL022619.

Millet, D. B., et al. (2004), Volatile organic compound measurements at Trinidad Head, California, during ITCT 2K2: Analysis of sources, atmospheric composition, and aerosol residence times, *J. Geophys. Res.*, 109, doi:10.1029/2003JD004026.

Müller, J.-F., and G. Brasseur (1995), IMAGES: A three-dimensional chemical transport model of the global troposphere, *J. Geophys. Res.*, 100(16), 445-16,490.

Müller, J.-F., and G. Brasseur (1999), Sources of upper tropospheric HOx, A three-dimensional study, *J. Geophys. Res.*, 104, 1705-1715.

Nakićenović, N., et al. (2000), *Emissions Scenarios: A Special Report of Working Group III of the Intergovernmental Panel on Climate Change,* 599 pp., Cambridge Univ. Press, New York.

Nowak, J. B. et al. (2004), Gas-phase chemical characteristics of Asian emission plumes observed during ITCT 2K2 over the eastern North Pacific Ocean, *J. Geophys. Res.*, 109, D23S19, doi:10.1029/2003JD004488.

Olivier, J. G.J., J. J.M. Berdowski, J. A.H.W. Peters, J. Bakker, A. J.H. Visschedijk, and J. P. J. Bloos (2000), Applications of EDGAR. Including a Description of EDGAR V3.0: Reference Database with Trend Data for 1970-1995, NRP report no. 410200 051 / RIVM report no. 773301 001, RIVM, Bilthoven, the Netherlands.

Parrish, D. D., C. J. Hahn, E. J. Williams, R. B. Norton, F. C. Fehsenfeld, H. B. Singh, J. D. Shetter, B. W. Gandrud, and B. A. Ridley (1992), Indication of photochemical histories of Pacific air masses from measurements of atmospheric trace species at Point Arena, California, *J. Geophys. Res.*, 97, 15883-15901.

Parrish, D. D., Y. Kondo, O. R. Cooper, C. A. Brock, D. A. Jaffe, M. Trainer, T. Ogawa, G. Hübler, and F. C. Fehsenfeld (2004), Intercontinental Transport and Chemical Transformation 2002 (ITCT 2K2) and Pacific Exploration of Asian Continental Emission (PEACE) experiments: An overview of the 2002 winter and spring intensives, *J. Geophys. Res.*, 109(D23S01), doi:10.1029/2004JD004980.

Price, H. U., D. A. Jaffe, O. R. Cooper, and P. V. Doskey (2004), Photochemistry, ozone production, and dilution during long-range transport episodes from Eurasia to the northwest United States, *J. Geophys. Res.*, 109(D23S13), doi:10.1029/2003JD004400.

Takemura, T. I. Uno, T. Nakajima, A. Higurashi, and I. Sano (2002), Modeling study of long-range transport of Asian dust and anthropogenic aerosols from East Asia, *Geophys. Res. Lett.*, 29, doi:10.1029/2002GL016251.

Theobald, D. M. (2005), Landscape Patterns of Exurban Growth in the USA From 1980 to 2020, *Ecology and Society,* 10(1), [online] http://www.ecologyandsociety.org/vol10/iss1/art32/.

Tie, X., G. P. Brasseur, C. S. Zhao, C. Granier, S. Massie, Y. Qin, P. C. Wang, G. Wang, P. C. Yang, and A. Richter (2006), Chemical characterization of air pollution in Eastern China and the Eastern United States, *Atmos. Env.*, 40, 2607-2625.

U.S. EPA (2004), Economic Growth Analysis System (EGAS) version 5.0 User Manual, U.S. Environmental Protection Agency, [online] http://www.epa.gov/ttn/ecas/egas5.htm

Washington, W. M., J. W. Weatherly, G. A. Meehl, A. J. Semtner, T. W. Bettge, A. P. Craig, W. G. Strand, J. Arblaster, V. B. Wayland, R. James, and Y. Zhang (2000), Parallel Climate Model (PCM) control and transient simulations, *Climate Dyn.*, 16, 10/11, 755-774.

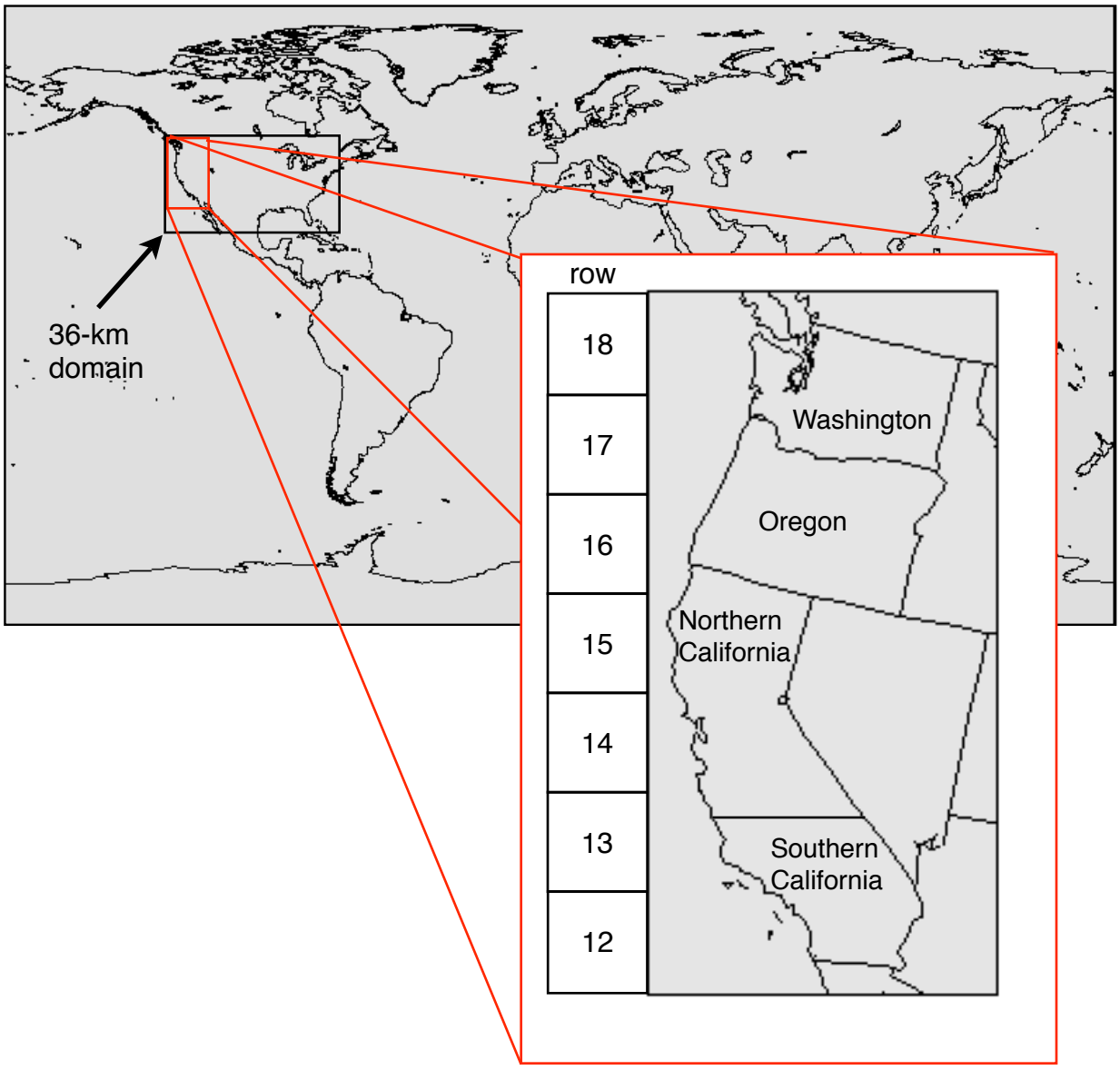

Figure 1.
Global model domain, 36-km regional domain, and the grids used for measuring long-range transport events.

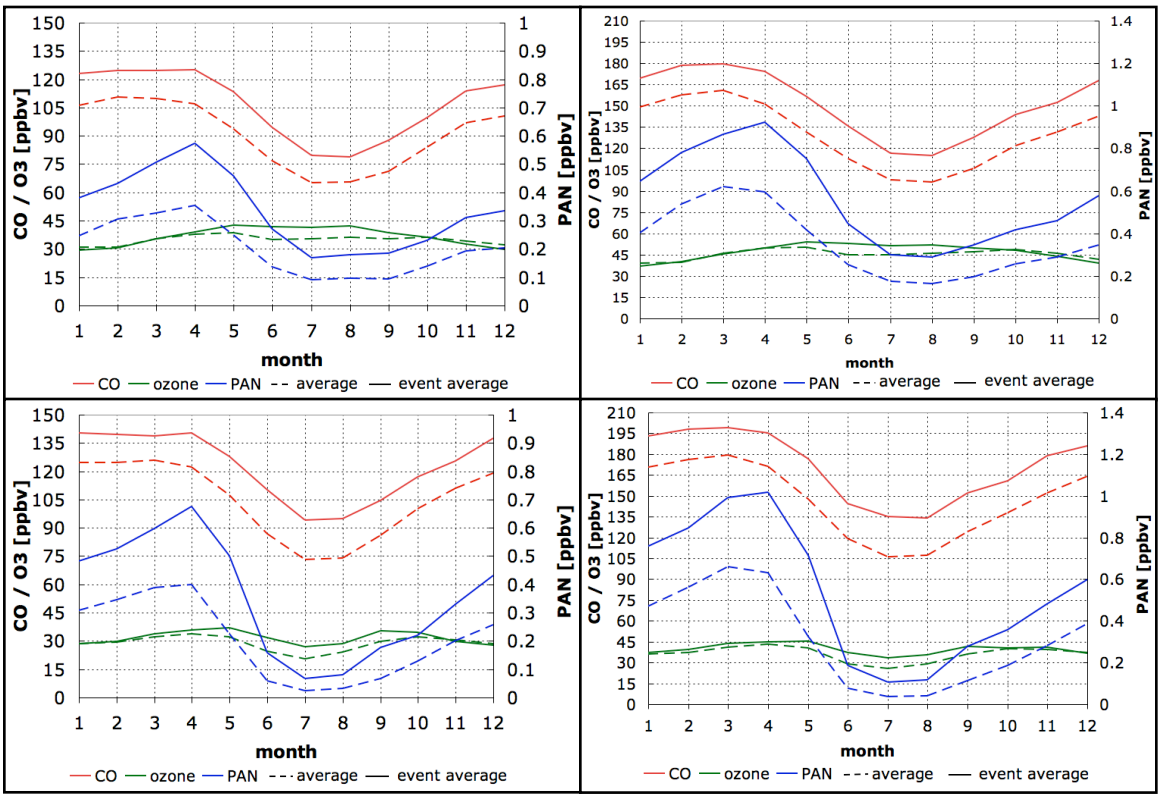

Figure 2.
Monthly average CO, PAN, and ozone concentrations compared to CO, PAN, and ozone concentrations during (upper left) present-day mid-troposphere CO events, (lower left) present-day lower-troposphere events, (upper right) future-2050 mid-troposphere events, and (lower right) future-2050 lower-troposphere events. Concentrations are averaged across all MOZART grids.

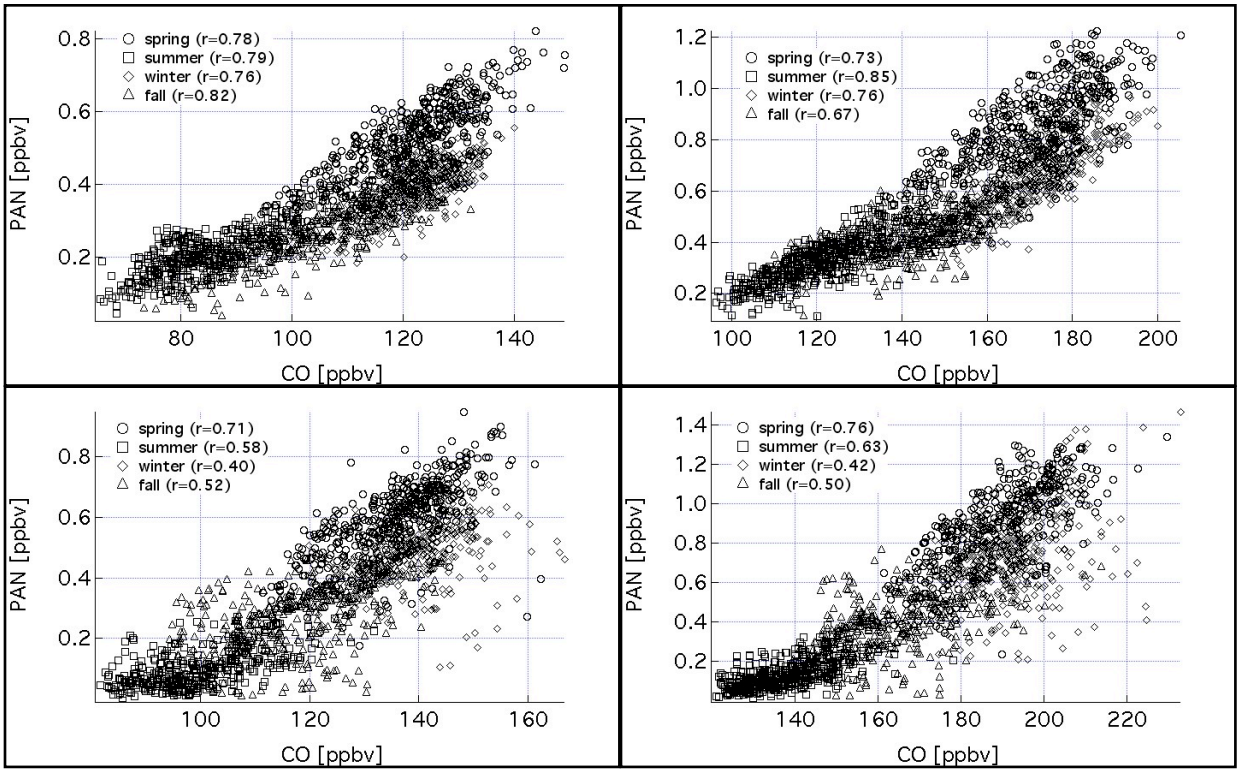

Figure 3.
CO vs PAN during long-range transport events for (upper left) present-day mid-troposphere events, (lower left) present-day lower-troposphere events, (upper right) future-2050 mid-troposphere events, and (lower right) future-2050 lower-troposphere events.

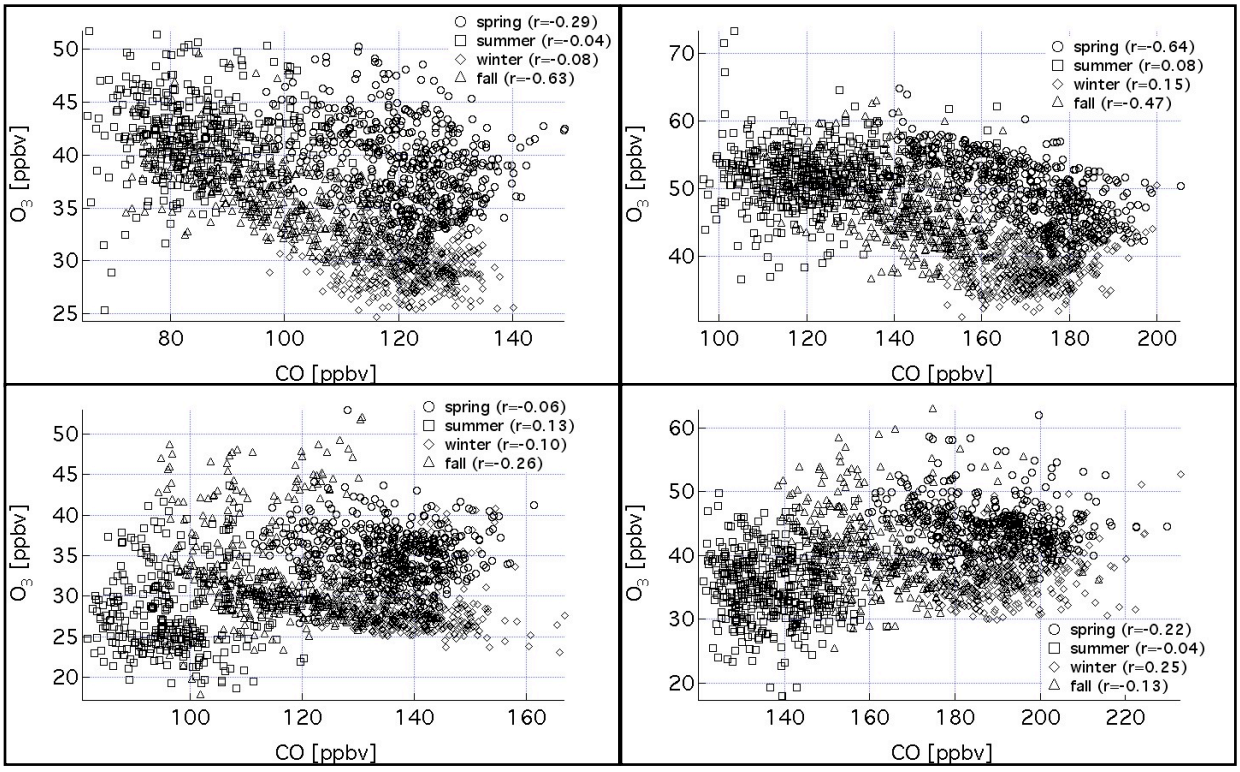

Figure 4.
CO vs ozone during long-range transport events for (upper left) present-day mid-troposphere events, (lower left) present-day lower-troposphere events, (upper right) future-2050 mid-troposphere events, and (lower right) future-2050 lower-troposphere events.

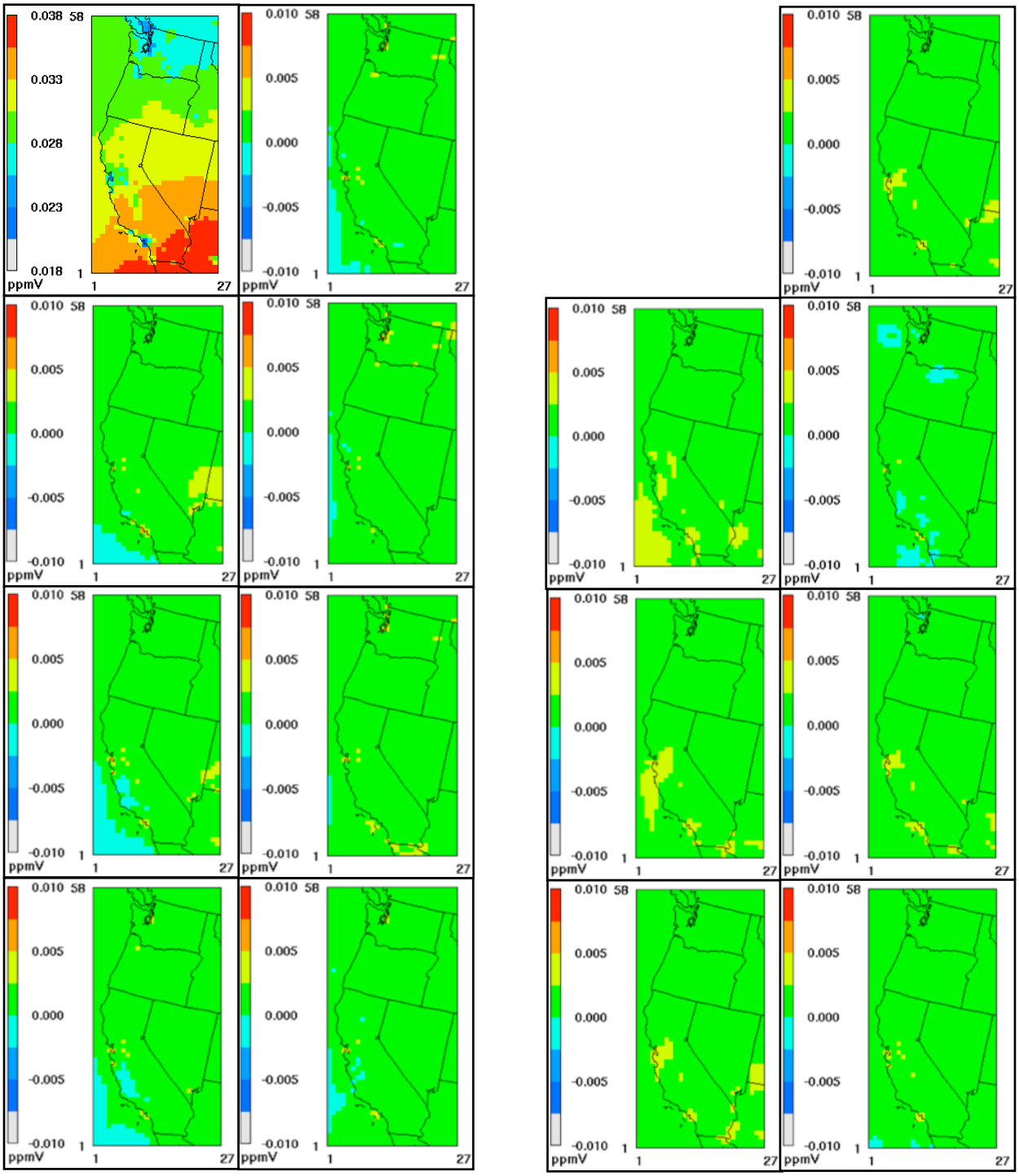

Figure 5.
Present-day winter average daily maximum 1-hr ozone concentration (upper left) and the difference in the daily 1-hr maximum ozone during transport events. Transport events are shown from top to bottom representing events in MOZART rows 12-14 for the left column and 15-18 for the right columns. Mid-troposphere events are shown on the left and lower-troposphere events on the right.

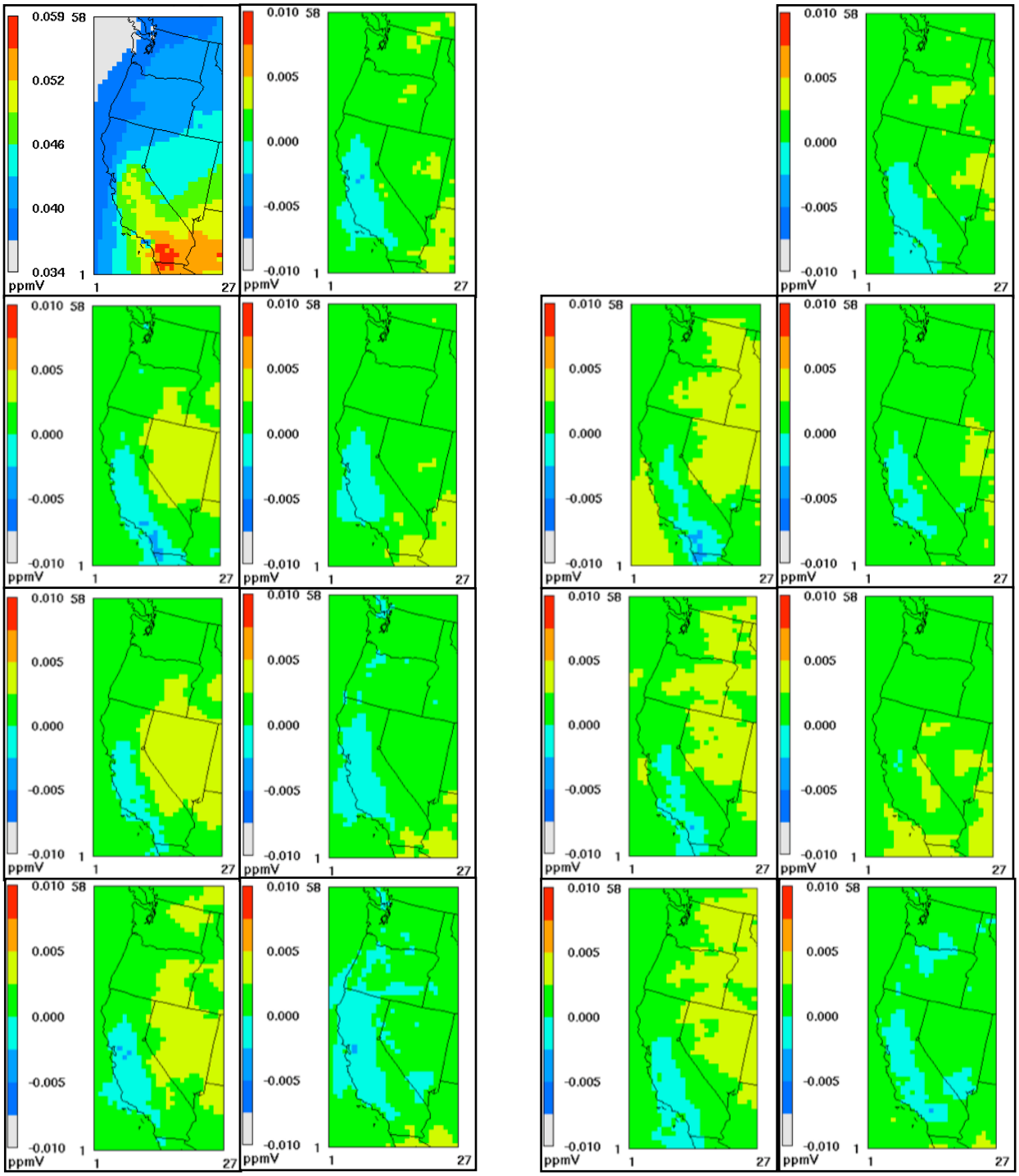

Figure 6.
Present-day spring average daily maximum 1-hr ozone concentration (upper left) and the difference in the daily 1-hr maximum ozone during transport events. Transport events are shown from top to bottom representing events in MOZART rows 12-14 for the left column and 15-18 for the right columns. Mid-troposphere events are shown on the left and lower-troposphere events on the right.

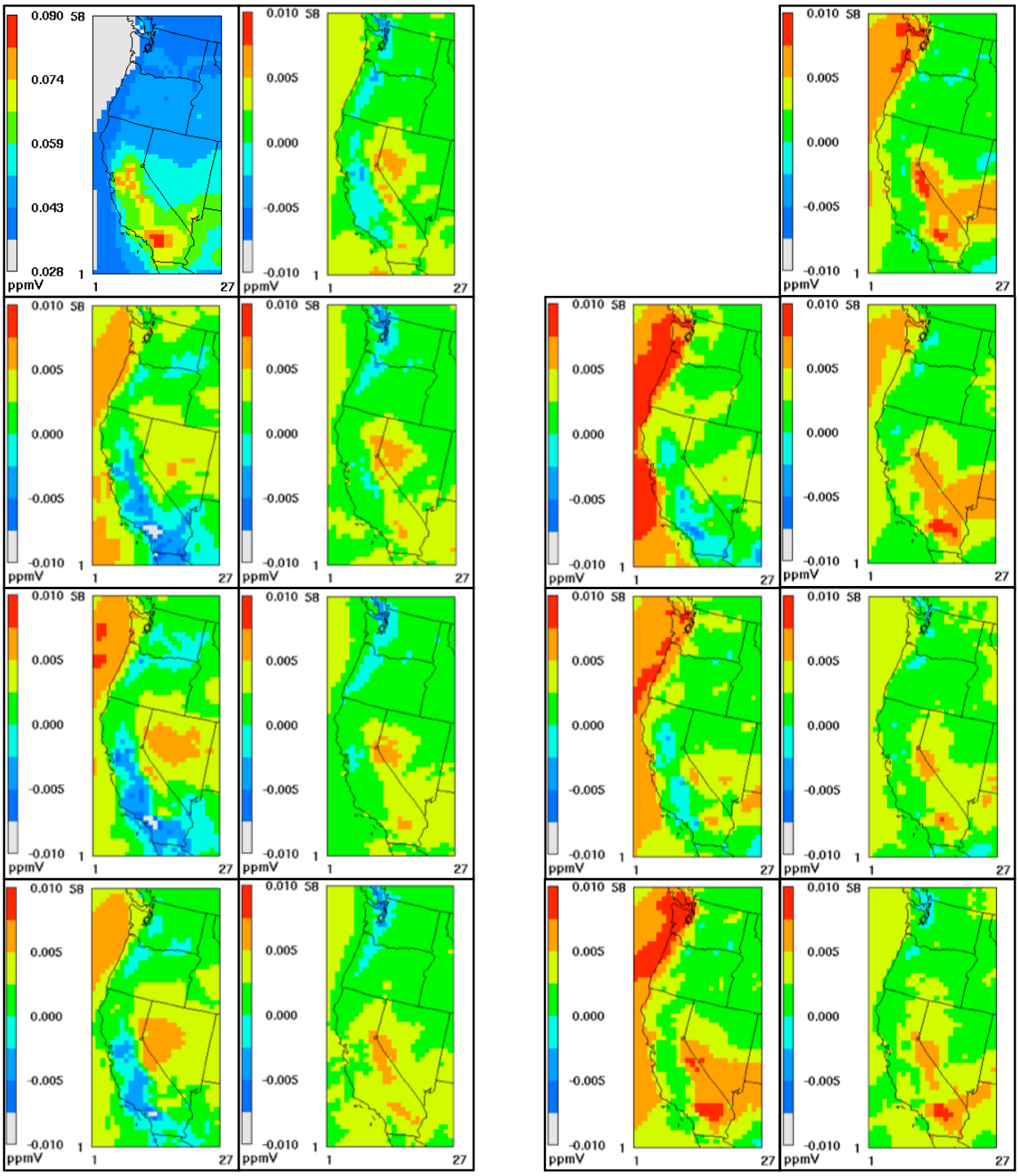

Figure 7.
Present-day summer average daily maximum 1-hr ozone concentration (upper left) and the difference in the daily 1-hr maximum ozone during transport events. Transport events are shown from top to bottom representing events in MOZART rows 12-14 for the left column and 15-18 for the right columns. Mid-troposphere events are shown on the left and lower-troposphere events on the right.

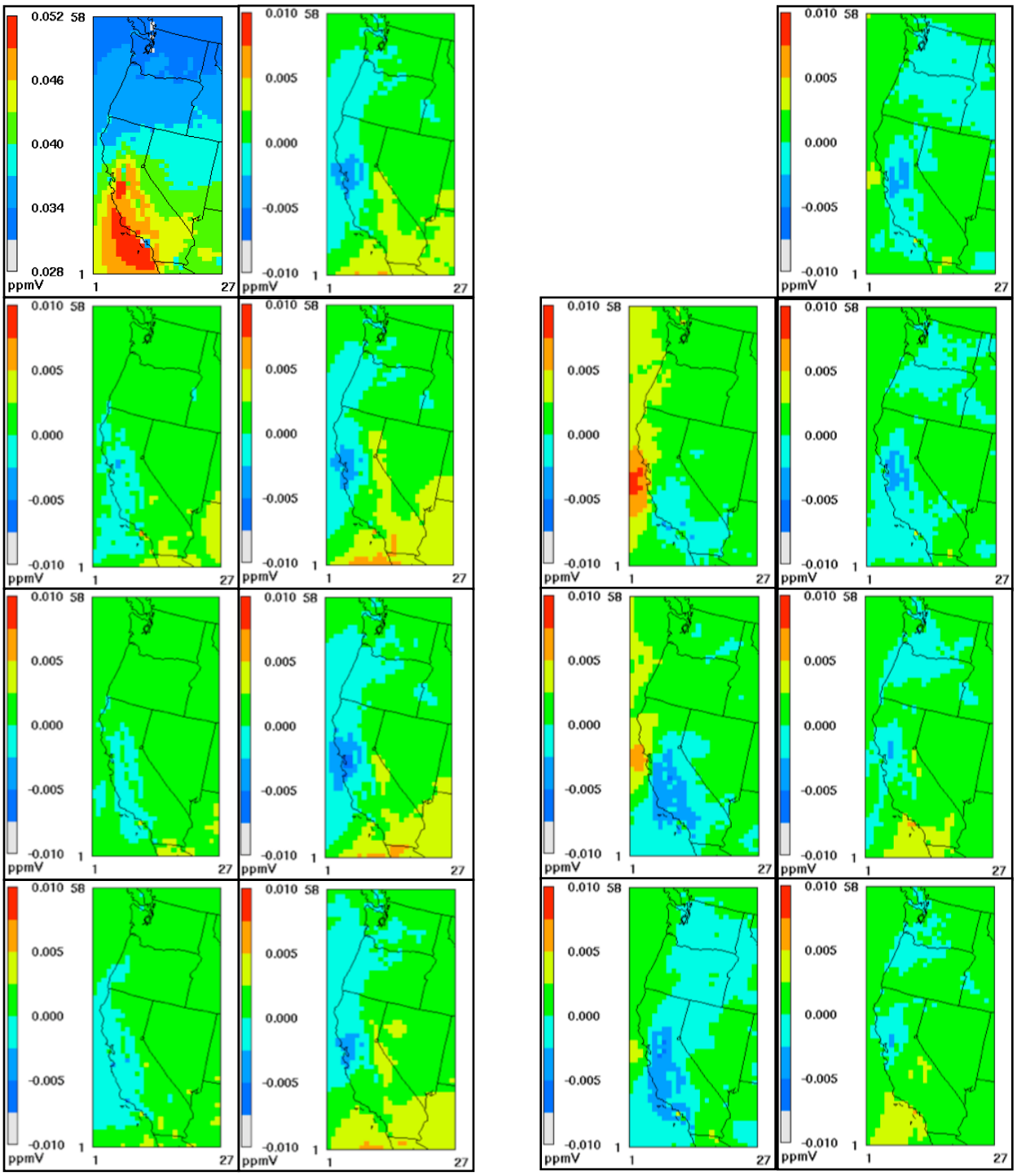

Figure 8.
Present-day fall average daily maximum 1-hr ozone concentration (upper left) and the difference in the daily 1-hr maximum ozone during transport events. Transport events are shown from top to bottom representing events in MOZART rows 12-14 for the left column and 15-18 for the right columns. Mid-troposphere events are shown on the left and lower-troposphere events on the right.

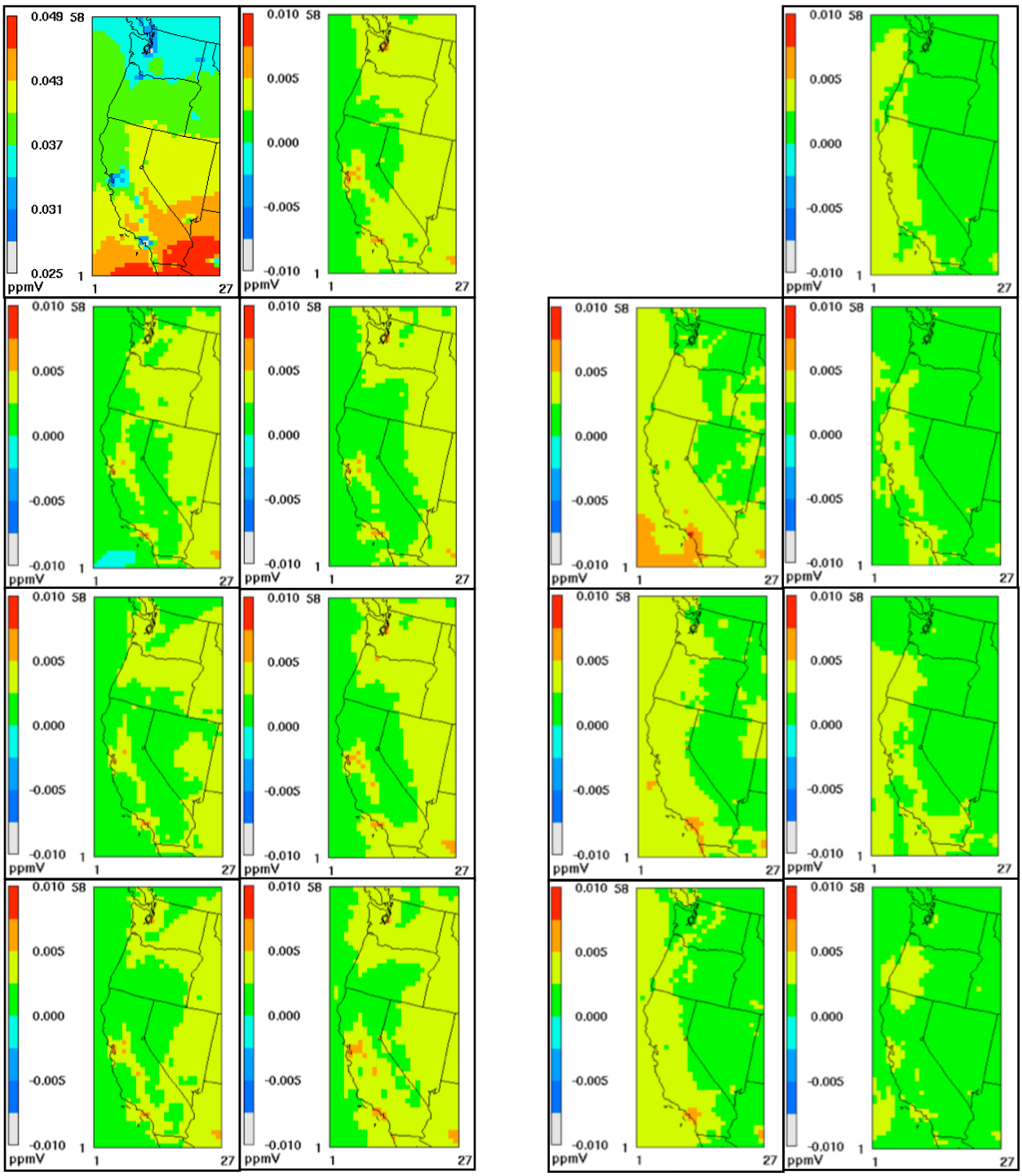

Figure 9.
Future-2050 winter average daily maximum 1-hr ozone concentration (upper left) and the difference in the daily 1-hr maximum ozone during transport events. Transport events are shown from top to bottom representing events in MOZART rows 12-14 for the left column and 15-18 for the right columns. Mid-troposphere events are shown on the left and lower-troposphere events on the right.

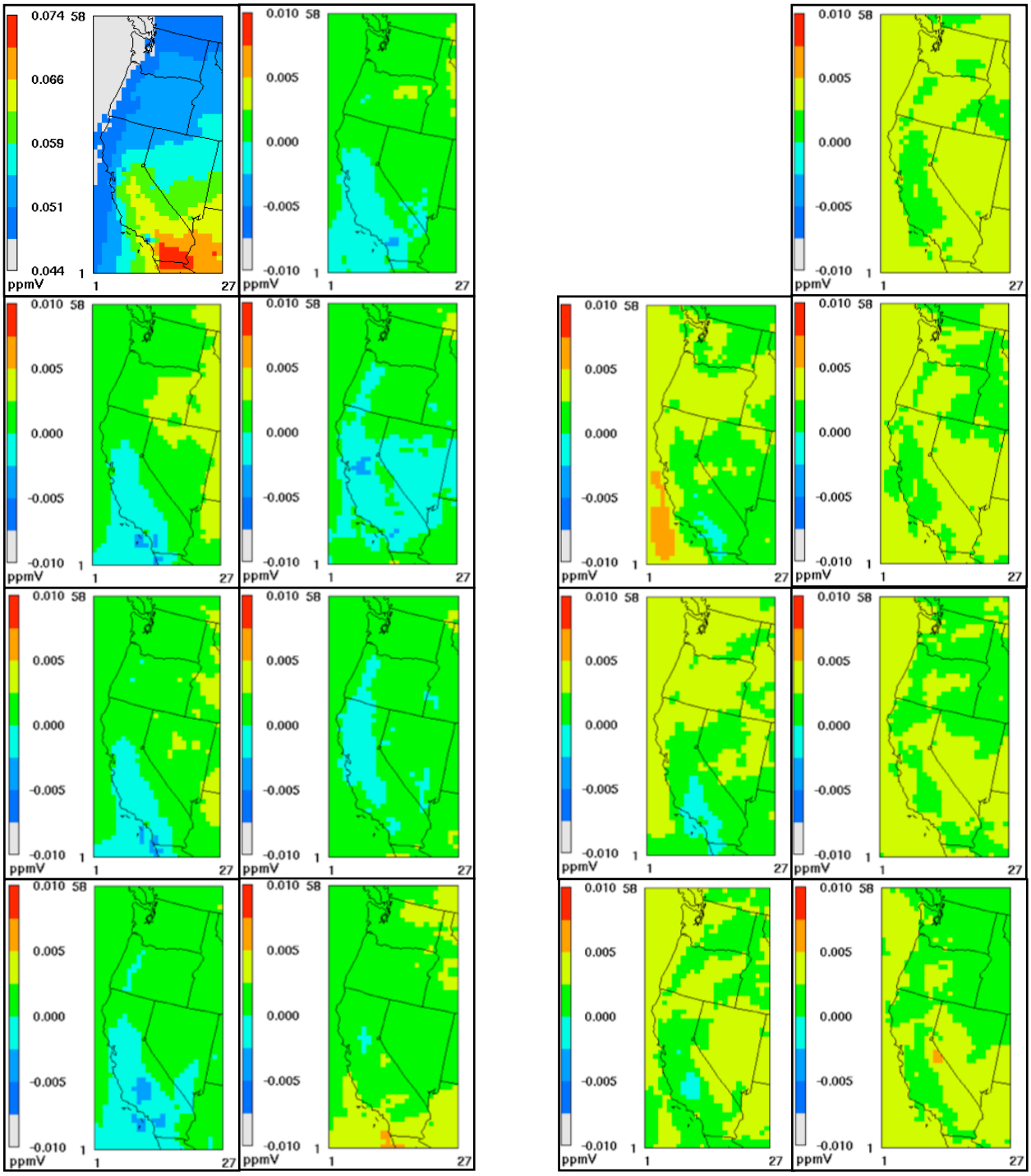

Figure 10.
Future-2050 spring average daily maximum 1-hr ozone concentration (upper left) and the difference in the daily 1-hr maximum ozone during transport events. Transport events are shown from top to bottom representing events in MOZART rows 12-14 for the left column and 15-18 for the right columns. Mid-troposphere events are shown on the left and lower-troposphere events on the right.

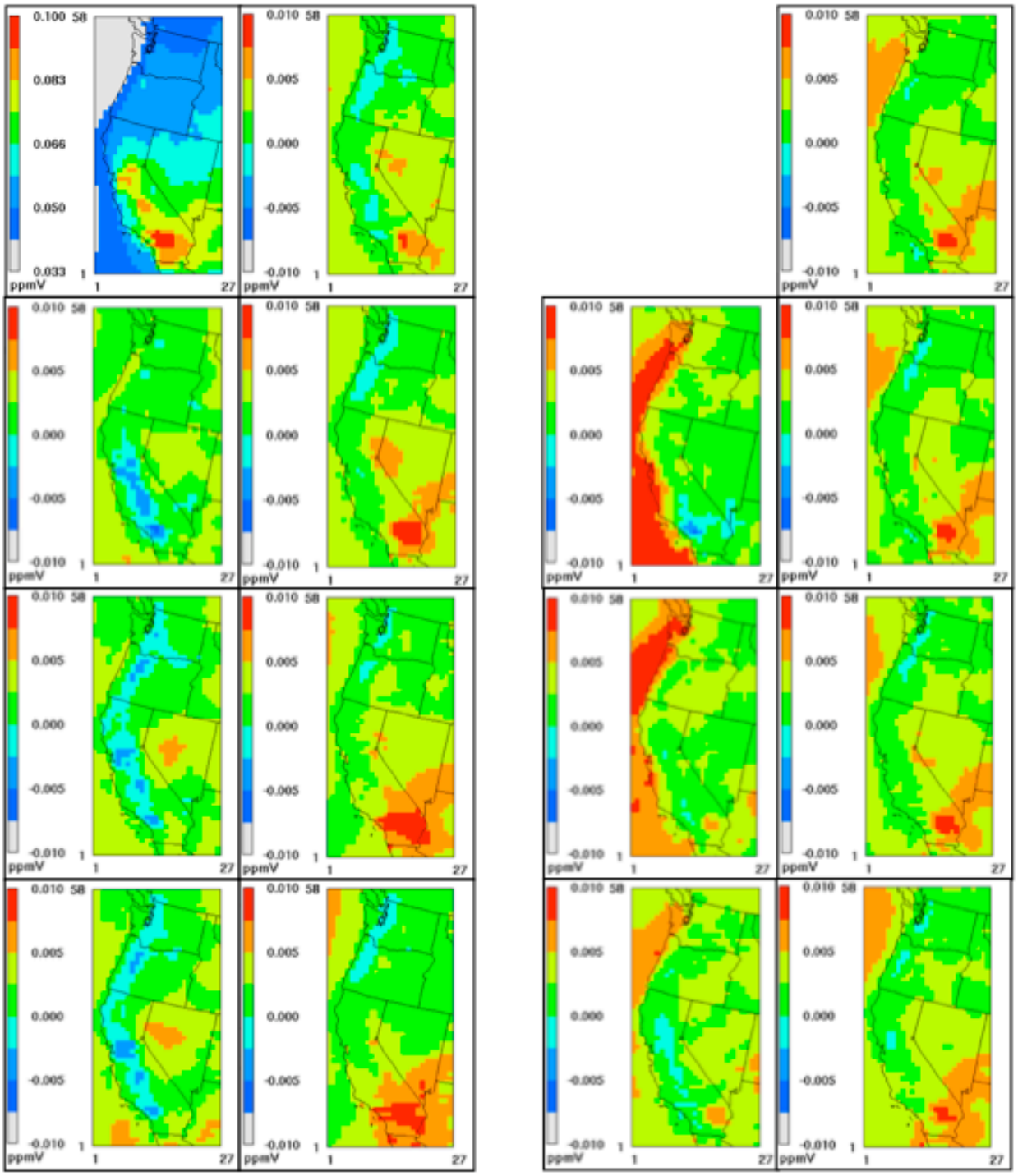

Figure 11.
Future-2050 summer average daily maximum 1-hr ozone concentration (upper left) and the difference in the daily 1-hr maximum ozone during transport events. Transport events are shown from top to bottom representing events in MOZART rows 12-14 for the left column and 15-18 for the right columns. Mid-troposphere events are shown on the left and lower-troposphere events on the right.

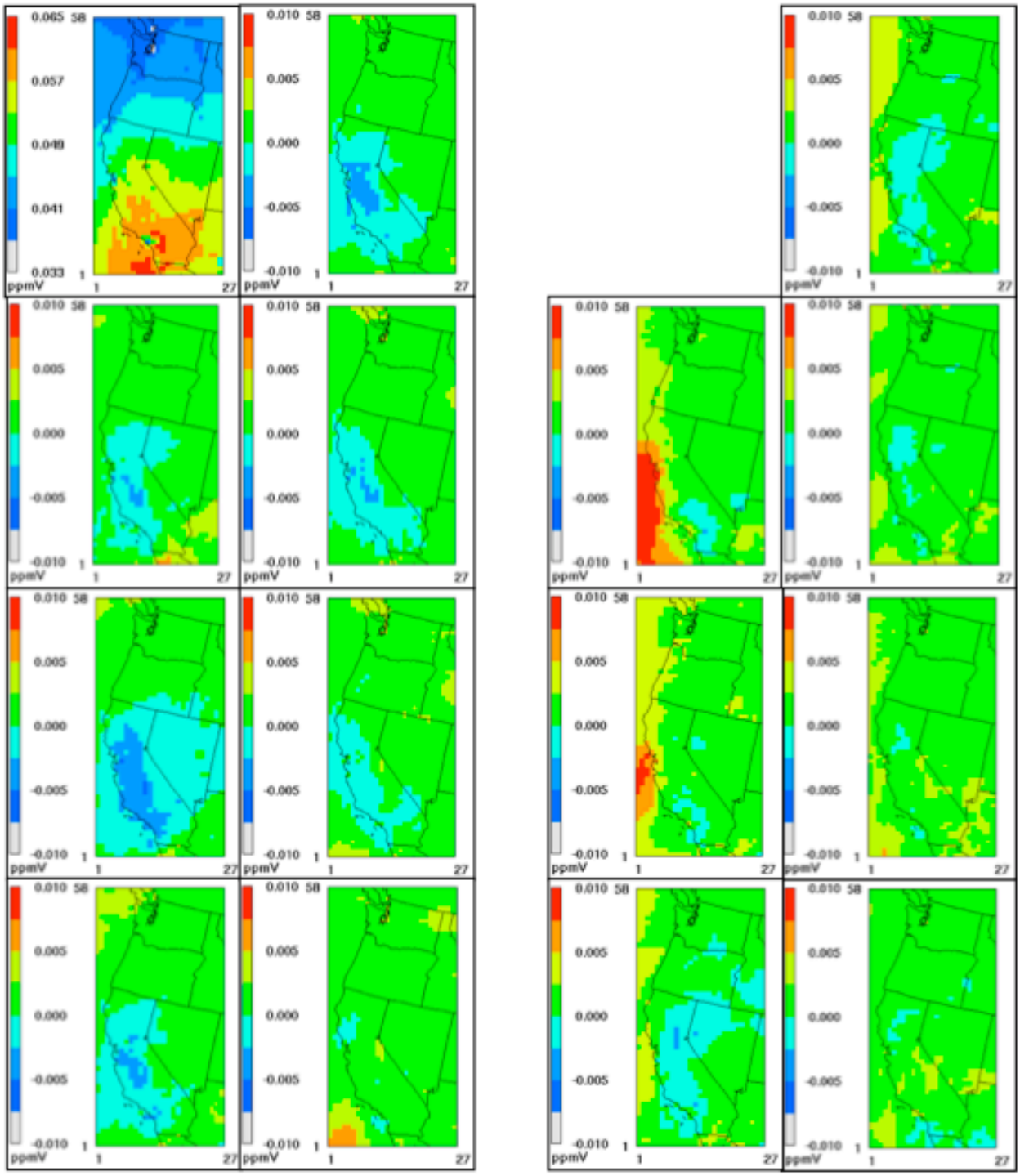

Figure 12.
Future-2050 fall average daily maximum 1-hr ozone concentration (upper left) and the difference in the daily 1-hr maximum ozone during transport events. Transport events are shown from top to bottom representing events in MOZART rows 12-14 for the left column and 15-18 for the right columns. Mid-troposphere events are shown on the left and lower-troposphere events on the right.

Table 1.
Number of long-range transport mid-troposphere (2-6 km) events per month (defined by a minimum of 18 consecutive hours in which the monthly average 85th percentile CO concentration is exceeded) and the percent difference from the present-day (1990-1999) to the future (2045-2054).

	# of present-day events per month (percent difference from present-day to future-2050)			
	winter	spring	summer	fall
row 18	2.1 (-13%)	2.5 (-17%)	2.4 (-14%)	2.2 (+8%)
row 17	2.2 (-9%)	2.4 (-4%)	2.3 (-9%)	2.3 (-3%)
row 16	2.4 (+1%)	2.5 (-7%)	2.0 (+28%)	2.2 (+8%)
row 15	2.2 (+8%)	2.4 (-14%)	1.6 (+63%)	2.1 (+8%)
row 14	2.0 (+25%)	2.7 (-14%)	1.7 (+40%)	1.9 (+14%)
row 13	1.8 (+26%)	2.5 (-1%)	1.5 (+46%)	1.9 (+12%)
row 12	1.9 (+16%)	2.2 (+3%)	1.3 (+41%)	1.7 (+6%)

Table 2.
Number of long-range transport lower-troposphere (0-2 km) events per month (defined by a minimum of 18 consecutive hours in which the monthly average 85th percentile CO concentration is exceeded) and the percent difference from the present-day (1990-1999) to the future (2045-2054).

	# of present-day events per month (percent difference from present-day to future-2050)			
	winter	spring	summer	fall
row 18	1.7 (+17%)	2.3 (-26%)	1.9 (+11%)	2.2 (-15%)
row 17	1.5 (+17%)	2.5 (-28%)	2.0 (+13%)	2.2 (-14%)
row 16	1.7 (+6%)	2.5 (-29%)	1.8 (+16%)	2.1 (-5%)
row 15	1.9 (+21%)	2.3 (-19%)	1.9 (+13%)	2.1 (-14%)
row 14	1.9 (-7%)	2.1 (-5%)	1.6 (+34%)	2.0 (-12%)
row 13	1.9 (-2%)	1.9 (+10%)	1.5 (+41%)	1.6 (+2%)
row 12	1.8 (-2%)	2.2 (-6%)	1.4 (+26)	1.4 (+17%)

Table 3.
Observed and modeled spring-time mean concentrations of CO, PAN, and ozone.

	modeled mean springtime		PHOBEA[a]		ITCT 2K2 North Pacific[b]
	0-2 km	2-6 km	0-2 km	2-6 km	marine free troposphere
CO [ppb]	118	103	139	136	125
PAN [ppt]	340	310	79	195	160
O_3 [ppb]	33	37	47	66	59

[a][Kotchenruther et al., 2001]
[b][Nowak et al., 2004]

Table 4.
Seasonal average CO, PAN, and ozone concentrations for the present-day (1990-1999) and future-2050 (2045-2054). Pollutant enhancements above the seasonal average during CO transport events are shown in parenthesis.

		CO [ppbv]		PAN [ppbv]		O_3 [ppbv]	
		present-day	future-2050	present-day	future-2050	present-day	future-2050
mid-troposphere	winter	106 (+16)	150 (+22)	0.25 (+0.13)	0.43 (+0.25)	31 (-1.6)	40 (-1.2)
	spring	103 (+18)	148 (+23)	0.31 (+0.20)	0.54 (+0.30)	37 (+1.5)	49 (+0.8)
	summer	69 (+15)	102 (+19)	0.11 (+0.10)	0.20 (+0.14)	35 (+6.4)	45 (+6.9)
	fall	84 (+34)	120 (+22)	0.14 (+0.24)	0.25 (+0.16)	35 (-5.5)	47 (+0.5)
low-troposphere	winter	123 (+16)	170 (+22)	0.30 (+0.17)	0.47 (+0.26)	29 (-0.3)	37 (+0.8)
	spring	118 (+17)	166 (+23)	0.34 (+0.25)	0.54 (+0.35)	33 (+2.9)	42 (+3.2)
	summer	78 (+21)	111 (+27)	0.04 (+0.06)	0.05 (+0.08)	23 (+5.9)	28 (+7.6)
	fall	99 (+18)	138 (+26)	0.13 (+0.12)	0.19 (+0.18)	31 (+2.0)	39 (+2.6)

Table 5.
Change in seasonal surface level ozone concentrations during lower-troposphere long-range transport events for the present-day case.

	average daily maximum 1-hr ozone concentration within each region [ppbv] (average of one grid cell)										
	southern CA			northern CA			OR			WA	
season	ave	row 12 event	row 13 event	ave	row 14 event	row 15 event	ave	row 16 event	row 17 event	ave	row 17 event	row 18 event
winter	37	+2	+3	34	+1	+1	31	+2	+2	29	+2	+1
spring	59	-4	-2	52	+0	+0	43	+2	+3	42	+1	+0
summer	90	-4	+0	78	+2	+1	49	+1	+1	48	+0	-1
fall	52	-1	-2	50	-4	-2	38	+0	+1	35	+0	+0

	average daily maximum 1-hr ozone throughout each region [ppbv] (average of entire region)										
	southern CA			northern CA			OR			WA	
season	ave	row 12 event	row 13 event	ave	row 14 event	row 15 event	ave	row 16 event	row 17 event	ave	row 17 event	row 18 event
winter	34	+2	+2	31	+2	+2	30	+1	+2	28	+1	+1
spring	52	-1	+0	44	+1	+1	41	+1	+1	40	+1	+0
summer	68	+0	+1	56	+3	+2	44	+2	+1	42	+1	+1
fall	45	-1	-1	42	-1	+0	36	+0	+0	34	+0	+0

Table 6.
Change in seasonal surface level ozone concentrations during mid-troposphere long-range transport events for the present-day case.

	average daily maximum 1-hr ozone concentration within each region [ppbv] (average of one grid cell)										
	southern CA			northern CA			OR			WA	
season	ave	row 12 event	row 13 event	ave	row 14 event	row 15 event	ave	row 16 event	row 17 event	ave	row 17 event	row 18 event
winter	37	+2	+2	34	+1	+1	31	+2	+2	29	+2	+1
spring	59	-3	-1	52	+0	+0	43	+2	+2	42	+1	+1
summer	90	-8	-5	78	-3	-1	49	+0	+0	48	-2	-1
fall	52	+1	+0	50	-2	-1	38	+1	+1	35	+1	+1

	average daily maximum 1-hr ozone throughout each region [ppbv] (average of entire region)										
	southern CA			northern CA			OR			WA	
season	ave	row 12 event	row 13 event	ave	row 14 event	row 15 event	ave	row 16 event	row 17 event	ave	row 17 event	row 18 event
winter	34	+1	+1	31	+1	+1	30	+1	+1	28	+2	+1
spring	52	-1	+1	44	+0	+0	41	+1	+0	40	+1	+1
summer	68	-3	-3	56	+1	+1	44	+1	+1	42	+0	+0
fall	45	+1	+1	42	+0	+0	36	+0	+0	34	+0	+0

Table 7.
Change in seasonal surface level ozone concentrations during lower-troposphere long-range transport events for the future-2050 case.

	average daily maximum 1-hr ozone concentration within each region [ppbv] (average of one grid cell)											
	southern CA			northern CA			OR			WA		
season	ave	row 12 event	row 13 event	ave	row 14 event	row 15 event	ave	row 16 event	row 17 event	ave	row 17 event	row 18 event
winter	48	+3	+3	43	+3	+3	40	+2	+3	38	+2	+2
spring	74	-1	-1	65	+0	+2	55	+2	+1	53	+2	+2
summer	100	-3	+1	88	-3	+0	59	+2	+3	56	+2	+2
fall	63	+0	+0	60	-2	-1	49	+1	+1	44	+1	+1

	average daily maximum 1-hr ozone throughout each region [ppbv] (average of entire region)											
	southern CA			northern CA			OR			WA		
season	ave	row 12 event	row 13 event	ave	row 14 event	row 15 event	ave	row 16 event	row 17 event	ave	row 17 event	row 18 event
winter	43	+4	+4	40	+3	+2	39	+1	+2	36	+1	+1
spring	65	+1	+0	56	+2	+2	52	+2	+2	50	+2	+2
summer	79	+1	+2	64	+1	+2	53	+2	+2	49	+2	+2
fall	59	+0	+0	52	+0	+0	45	+1	+1	41	+2	+2

Table 8.
Change in seasonal surface level ozone concentrations during mid-troposphere long-range transport events for the future-2050 case.

	average daily maximum 1-hr ozone concentration within each region [ppbv] (average of one grid cell)											
	southern CA			northern CA			OR			WA		
season	ave	row 12 event	row 13 event	ave	row 14 event	row 15 event	ave	row 16 event	row 17 event	ave	row 17 event	row 18 event
winter	48	+2	+2	43	+3	+3	40	+3	+3	38	+3	+3
spring	74	-1	-1	65	-2	-1	55	+0	+0	53	+1	+2
summer	100	-4	+0	88	-5	-1	59	+2	+2	56	+1	+1
fall	63	+1	-1	60	-2	-2	49	+2	+2	44	+1	+1

	average daily maximum 1-hr ozone throughout each region [ppbv] (average of entire region)											
	southern CA			northern CA			OR			WA		
season	ave	row 12 event	row 13 event	ave	row 14 event	row 15 event	ave	row 16 event	row 17 event	ave	row 17 event	row 18 event
winter	43	+3	+3	40	+2	+2	39	+2	+2	36	+3	+3
spring	65	-1	-1	56	-1	+0	52	+0	+0	50	+1	+2
summer	79	+0	+1	64	+0	+2	53	+1	+2	49	+1	+1
fall	59	+0	-2	52	-1	-2	45	+1	+1	41	+2	+2

CHAPTER FOUR

Summary and Future Directions

Global changes are expected to influence regional air quality in ways that have not been explicitly considered by air quality planners. As these planners move forward in developing strategies to improve U.S. air quality, it is essential that they understand how global changes in climate and trace gas emissions will affect their ability to meet their objectives. A necessary tool in developing this type of understanding is the use of meteorological and chemical transport models that can simulate the impact of various global changes on regional air quality. The research presented in this dissertation used global and regional scale modeling systems to project how regional air quality in the U.S. may change in the future due to changes in climate, anthropogenic and biogenic emissions, and the long-range transport of Asian emissions. Analyzing the combined impacts of global changes on future air quality is important, because it gives us a baseline change with which to work with, but it is not particularly useful for air quality planners who need to make decisions on the best way to improve U.S. air quality. A more useful approach, and the one taken with the research discussed in this dissertation, is to analyze the individual impacts of various global changes on air quality, so that we can answer questions such as:

1. How will changes in climate affect future U.S. air quality?
2. What role do changes in regional anthropogenic emissions play in determining future U.S. air quality?
3. How do changes in biogenic emissions due to changes in climate and land management practices affect future U.S. air quality?

4. What is the impact of future global emissions (i.e., chemical boundary conditions) on U.S. air quality?

5. What is the role of the episodic long-range transport of Asian emissions on U.S. air quality, and how will it change in the future?

In the context of this dissertation and the future emission scenario used (IPCC A2), the answers to these questions are:

1. Climate change tends to increase ozone levels in the northeast and in the west central (e.g., Nevada) by up to +2 ppbv, while decreasing ozone to varying degrees in other regions (largest decrease is in the southeast: approximately -8 ppbv). In terms of $PM_{2.5}$, climate change decreases concentration in most regions (largest decrease is in the southeast: approximately -3 $\mu g\ m^{-3}$).

2. Changes in regional anthropogenic emissions tend to increase ozone in all regions (+2 to +5 ppbv), except within large urban areas, while increasing $PM_{2.5}$ concentrations in all regions (+1 to +5 $\mu g\ m^{-3}$).

3. Changes in biogenic emissions have a large impact on ozone and $PM_{2.5}$ concentrations in regions such as the southeast, where there is a large source of biogenic emissions.

4. Changes in global emissions (i.e., chemical boundary conditions) are responsible for significant increases in ozone levels throughout the U.S., but the increases are largest in the west (approximately +6 ppbv). Changes in global emissions also tend to increase $PM_{2.5}$ concentrations, but the increase is minimal (approximately 0.4 $\mu g\ m^{-3}$).

5. The episodic transport of Asian emissions to the U.S. tends to slightly increase ozone levels in the Pacific Northwest, but leads to decreases in California (most likely due to the meteorological conditions associated with transport events). In the future, the impact of these events is expected to become slightly worse.

By answering these questions, we are able to provide guidance to air quality planners in terms of what they should and should not be focusing on for mitigating future air quality issues.

It is important to remember that projections of future global changes are highly uncertain, and the work presented in this dissertation represents only one realization of what the future atmosphere may look like. To illustrate this point, Figure 1 compares results presented in Chapter 2 of this dissertation (see Figure 8 in Chapter 2), with results from two other groups involved in similar modeling work, the EPA's National Exposure Research Laboratory (NERL) and the University of Illinois (Illinois). The variation in the change of summer mean daily maximum 8-hr ozone from each group is due to differences in the future climate and emissions scenarios used, as well as differences in the models used for the simulations. The NERL simulation covered 5 current and future summers using the IPCC A1b scenario and used GISS II for the global climate model simulations, and CMAQ for the regional chemical simulations. In contrast, Illinois employed the PCM model for their global climate simulations and SAQM (SARMAP Air Quality Model) for their regional chemical simulations. Both Illinois simulations cover only one current and future summer, so they do not account for inter-annual variability in climate, which may be an important factor. The Illinois 1 simulation follows the IPCC A1Fi scenario, while the Illinois 2 simulation follows the IPCC B1 scenario. Through various sensitivity simulations, NERL found that decreases in ozone due to future emissions (A1b) offset ozone increases associated with climate change. In contrast, Illinois 1 (A1Fi) found that climate and emissions effects equally contribute to increases in ozone, while Illinois 2 found that emissions effects dominate under the B1 scenario. The differences in the results by NERL, Illinois, and those presented in

this dissertation illustrate how the choice of future climate/emissions scenario can effect results, and that it is necessary to consider a range future scenarios.

In addition, future work should take a systematic approach to projecting future air quality in which projected changes in model inputs (e.g., meteorology/climate, chemical boundary conditions, land-use changes, etc ...) are varied one by one over the range of likely possibilities. This will give regulators a better understanding of which parameters are most likely to have the largest influence on future air quality in any given region, and will allow them to make more informed decisions about how to improve future air quality.

From Figure 8

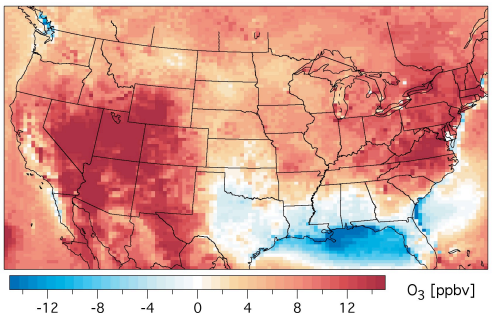

Illinois 1

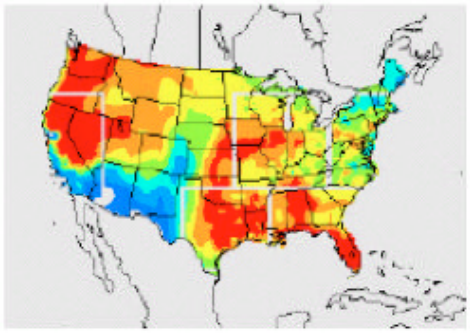

Illinois 2

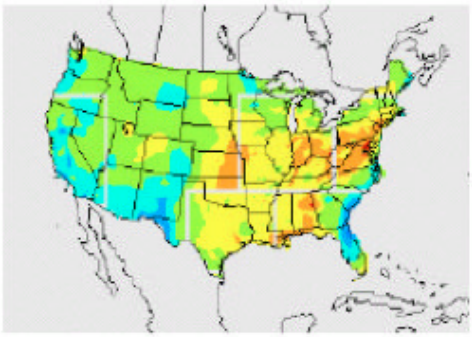

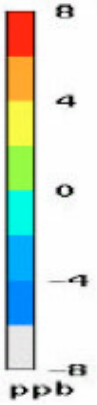

NERL

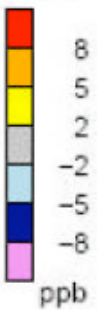

Figure 1. Difference from the 2050's and present-day simulated mean daily maximum 8-hr ozone [adapted from the Draft Review of the U.S. EPA Global Change Research Program Assessment of the Impacts of Global Change on Regional U.S. Air Quality: 2007 Interim Report]. The simulations are based on the following IPCC scenarios: WSU/Figure 8 (A2), Illinois 1 (A1Fi), Illinois 2 (B1), and NERL (A1b).

APPENDIX: Supplementary Material for Chapter Two

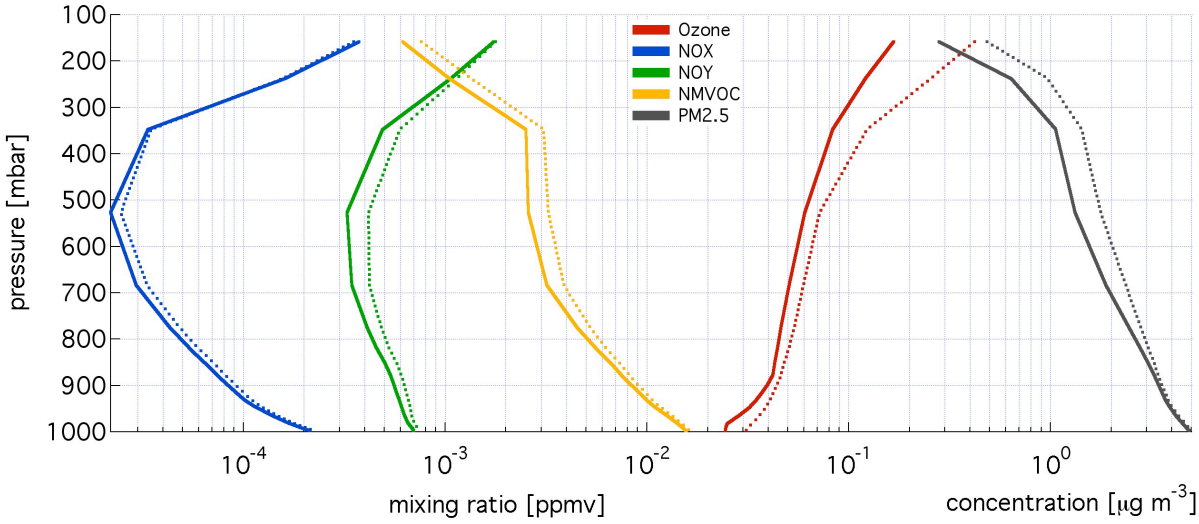

Figure A1.
Comparison of predicted present-day (solid line) to projected future-2050 (dashed line) chemical boundary conditions along the northern boundary of the modeling domain.

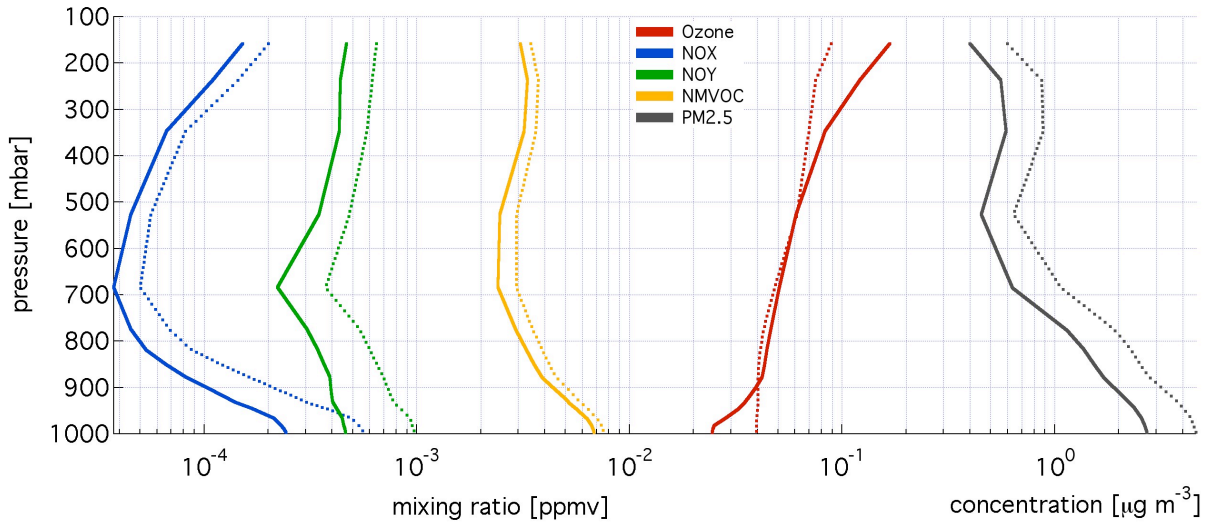

Figure A2.
Comparison of predicted present-day (solid line) to projected future-2050 (dashed line) chemical boundary conditions along the southern boundary of the modeling domain.

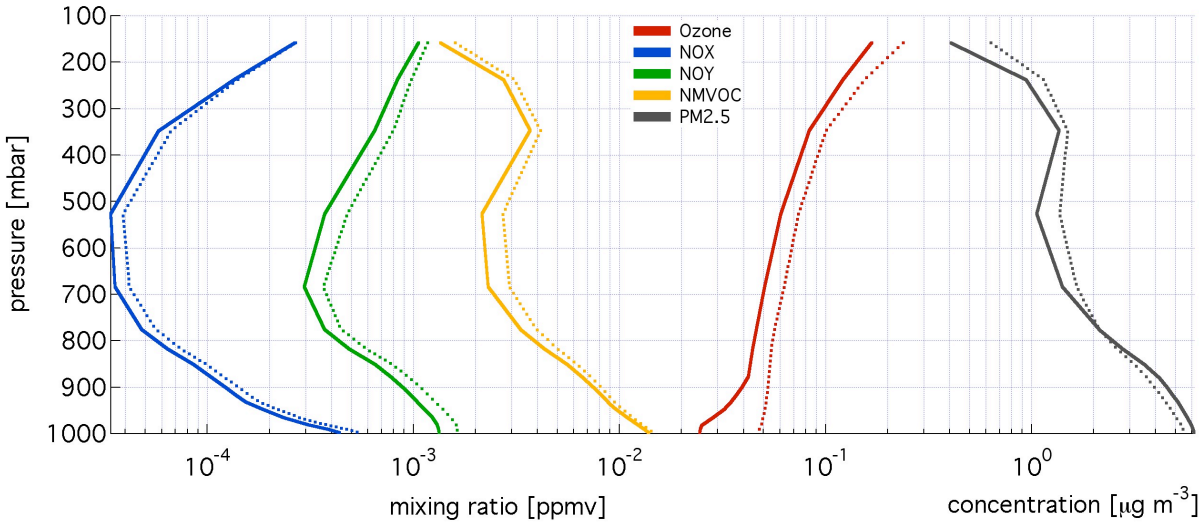

Figure A3.
Comparison of predicted present-day (solid line) to projected future-2050 (dashed line) chemical boundary conditions along the eastern boundary of the modeling domain.

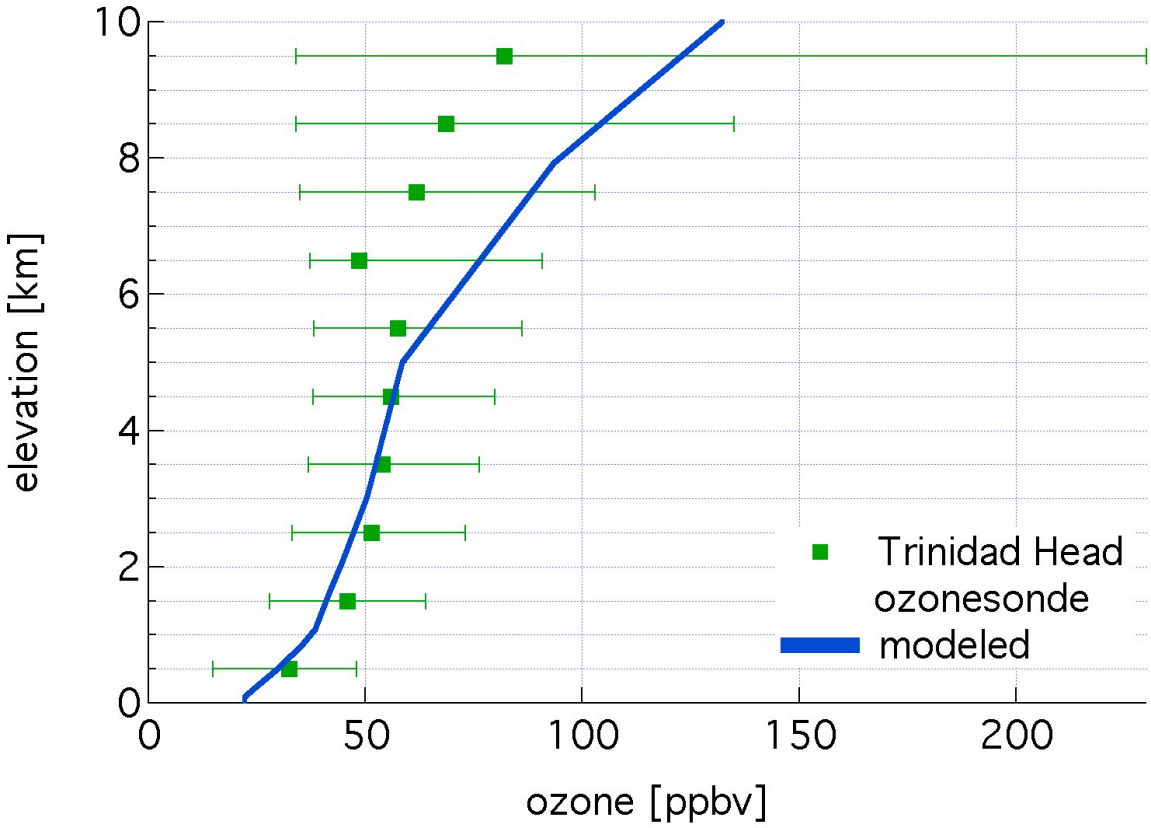

Figure A4.
Comparison of the MOZART ozone vertical profile to ozonesonde measurements at Trinidad Head, CA (URL of the website to access the Trinidad Head data).

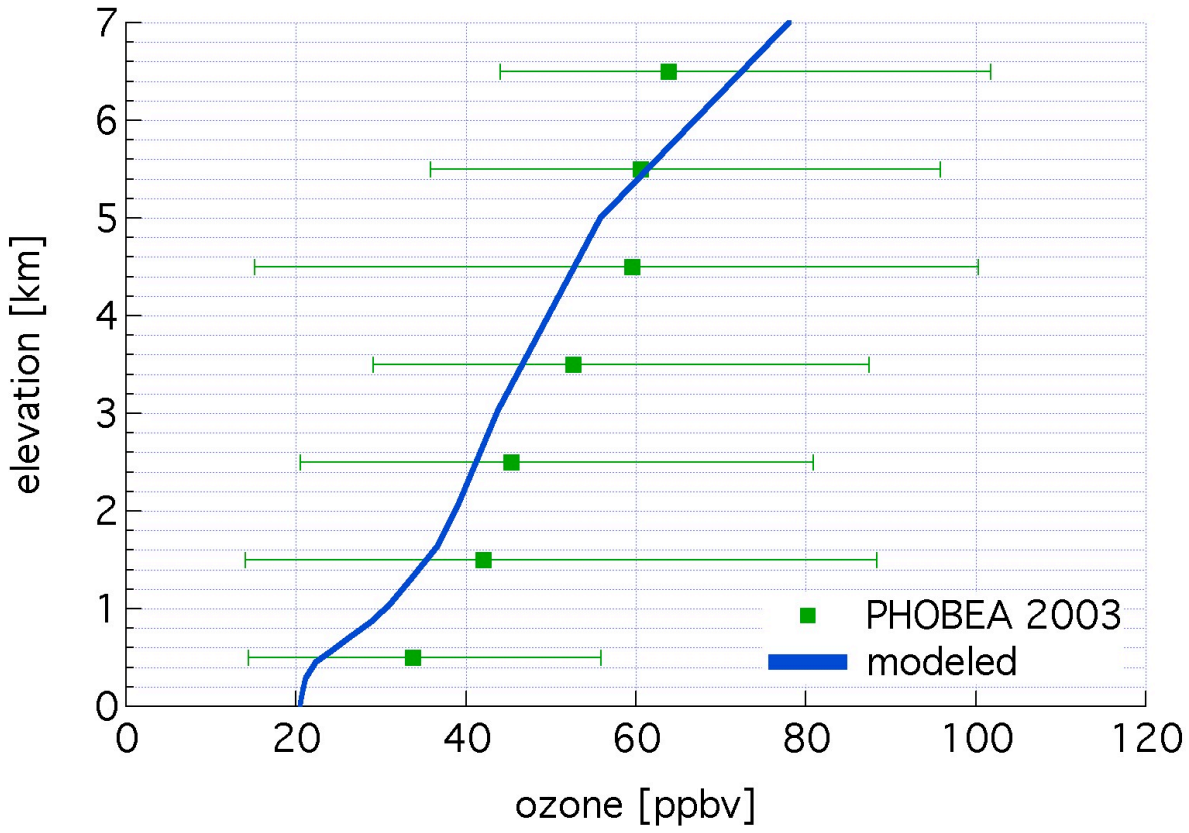

Figure A5.
Comparison of the MOZART ozone vertical profile to measurements made off the Washington State coast during the PHOBEA 2003 field campaign (reference to data).

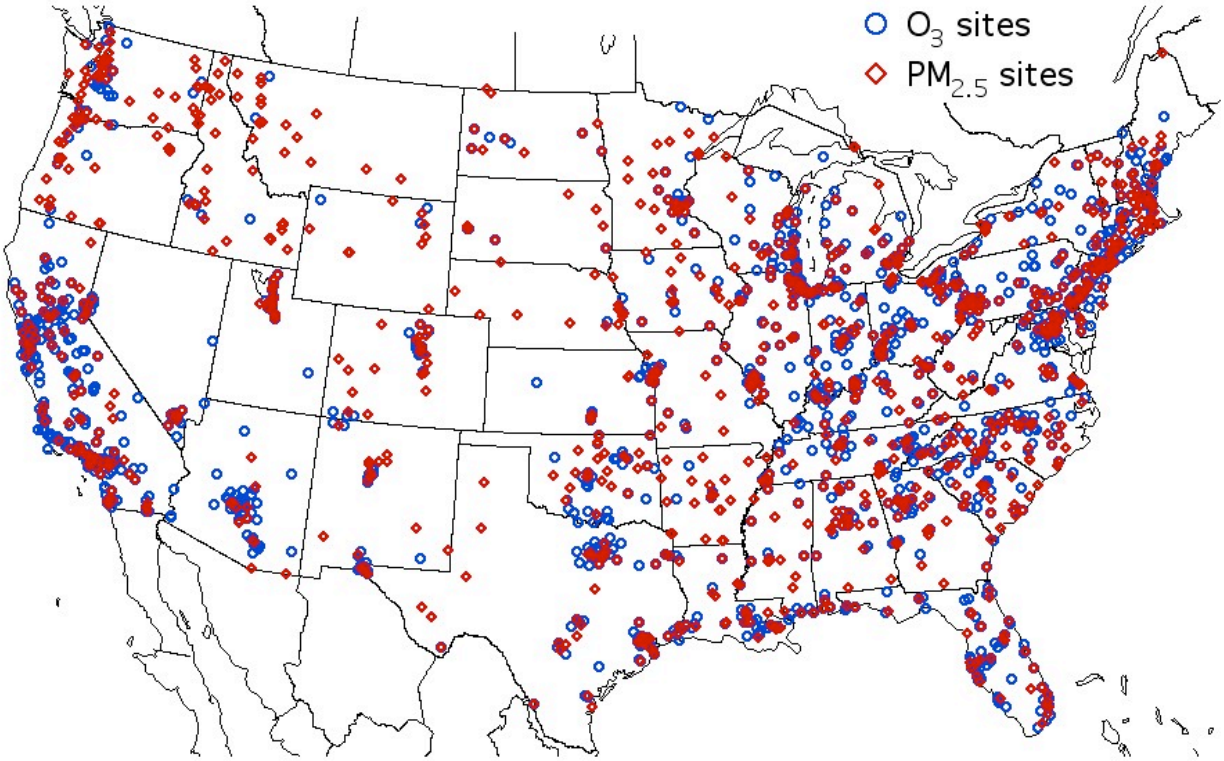

Figure A6.
Observation sites for ozone (1,349 sites) and PM2.5 (1,277 sites) used for comparison to modeled output. Observations obtained from the EPA AIRS database.

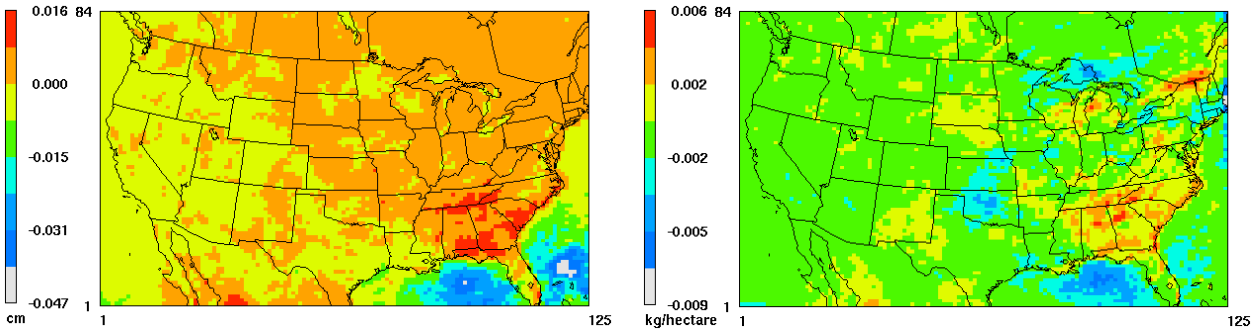

Figure A7.
Difference plots (”future-2050” - “present-day”) for (left) convective precipitation, and (right) $PM_{2.5}$ deposition (futMETcurLU - CURall).

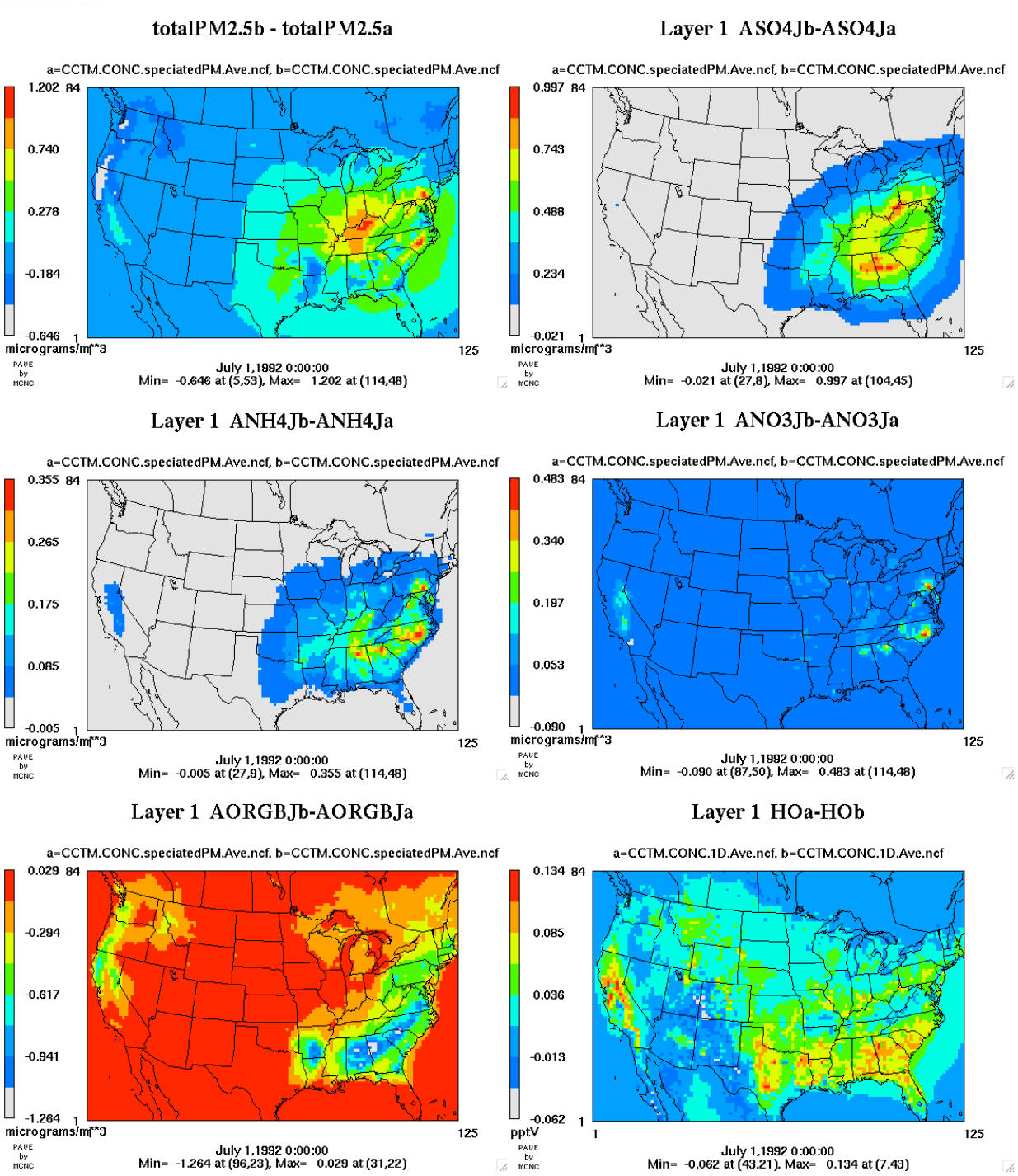

Figure A8.
Difference plots (”futMETfutLU case” - “futMETcurLU case”) for (upper left) total $PM_{2.5}$, (center left) ammonium aerosol, (lower left) biogenic SOA, (upper right) sulfate aerosol, (center right) nitrate aerosol, and (lower right) HO.

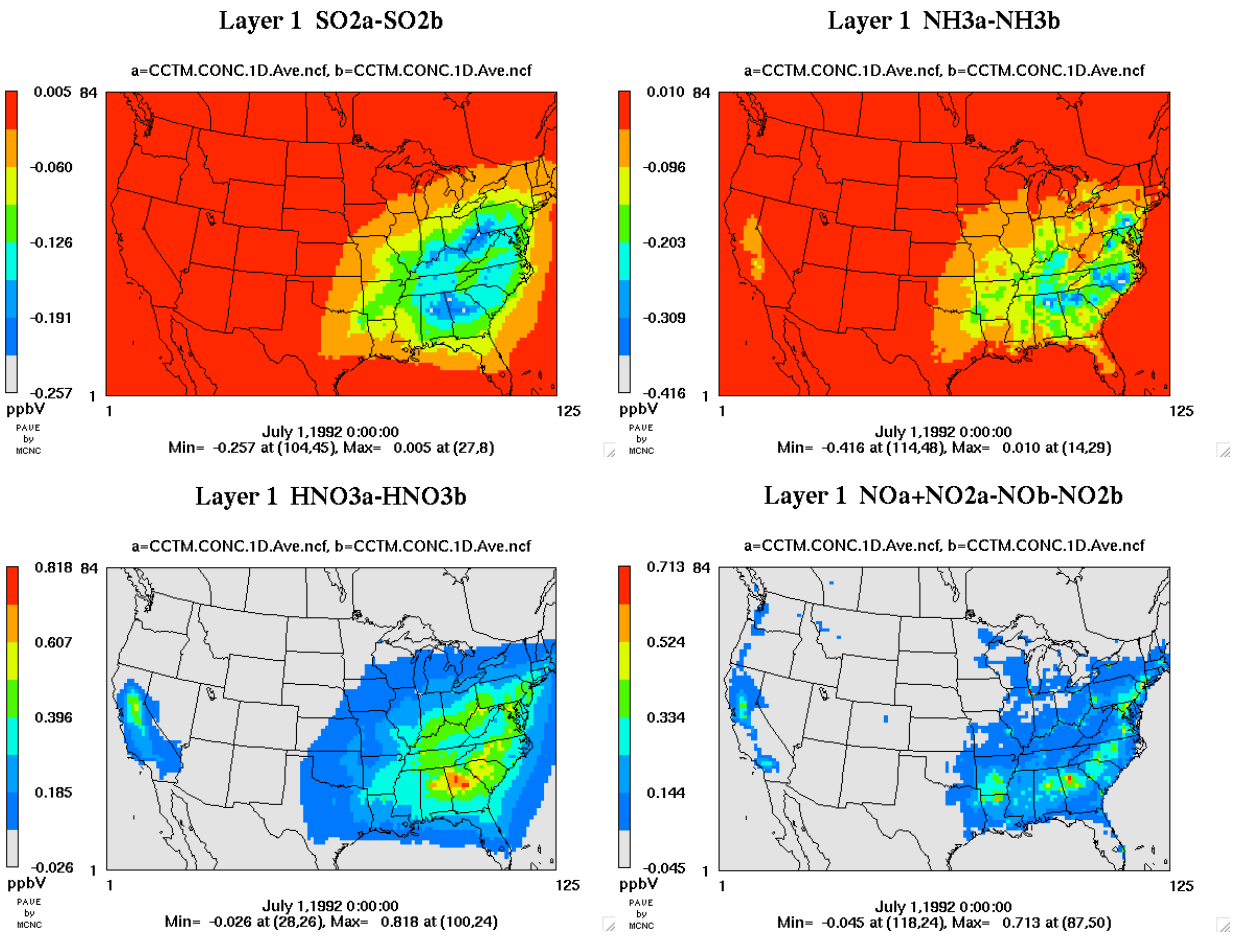

Figure A9.
Difference plots (”futMETfutLU case” - “futMETcurLU case”) for (upper left) SO_2, (lower left) HNO_3, (upper right) NH_3, and (lower right) NO_X.

Table A1.
CMAQ model vertical layer structure and the approximate elevation at layer interface.

Layer Interface	Sigma	Approximate Elevation (m)
18	0.000	12,670
17	0.131	10,300
16	0.175	9,278
15	0.375	5,942
14	0.575	3,522
13	0.725	2,047
12	0.775	1,624
11	0.820	1,302
10	0.850	1,061
9	0.878	860
8	0.900	690
7	0.920	571
6	0.930	454
5	0.950	281
4	0.975	149
3	0.985	82
2	0.995	18
1	1.000	0

Table A2.
Quantitative comparison of the area covered by each USGS land-use category for the current and future simulations.

Description	Present-day USGS (km^2)	Future-2050 USGS (km^2)	Percent Change
Mix Shrubs/Grass	29,808	465,264	+1,461%
Bare Sparse Vegetation	93,312	1,321,920	+1,317
Dryland Crop Pasture	1,486,512	5,456,160	+267
Urban	55,728	169,776	+205
Crop/Grass Mosaic	1,065,312	2,011,392	+89
Crop/Wood Mosaic	578,016	648,000	+12
Water Bodies	10,465,200	9,000,720	-14
Grassland	1,503,360	1,049,760	-30
Evergreen Needleleaf	2,575,152	1,664,064	-35
Savanna	251,424	149,040	-41
Mixed Forest	1,854,576	918,864	-50
Shrubland	1,999,728	575,424	-71
Deciduous Broadleaf	1,041,984	84,240	-92
Irrigated Crop Pasture	82,944	0	-100
Evergreen Broadleaf	23,328	0	-100
Wooded Wetland	86,832	0	-100
Wooded Tundra	317,520	0	-100
Mixed Tundra	2,592	0	-100
Snow or Ice	1,296	0	-100

Table A3.
Comparison of predicted present-day to projected future-2050 chemical boundary conditions. Boundary condition totals are weighted averages up to 500 mbar. The delta change from the present-day is shown in parenthesis.

Species	Units	boundary side			
		west	north	south	east
O_3	ppbv	49 (+10)	50 (+7)	38 (+11)	52 (+10)
$PM_{2.5}$	µg m^{-3}	1.8 (+0.8)	2.3 (+0.4)	1.1 (+0.7)	2.4 (+0.0)
NO_X	pptv	38 (+8)	42 (+8)	71 (+58)	78 (+14)
NO_Y	pptv	354 (+133)	421 (+76)	331 (+228)	539 (+127)
NMVOC	ppbv	1.8 (+0.6)	5.2 (+0.7)	3.3 (+0.6)	4.3 (+0.6)
CH_4	ppmv	1.7 (+0.9)	1.8 (+0.8)	1.7 (+0.8)	1.7 (+0.9)

Table A4.
Observed and percent difference between modeled and observed average daily maximum 8-hr ozone and average of the daily $PM_{2.5}$ ([modeled - observed] / observed).

Region	ozone [ppbv]		$PM_{2.5}$ [µg m^{-3}]	
	Average of the 8-hr daily maximum	98th percentile of the 8-hr daily maximum	Average of the 24-hr average	98th percentile of the 24-hr average
R1-3	57 (+31%)	96 (+14%)	17 (-20%)	58 (-45%)
R04	52 (+39%)	83 (+24%)	17 (-15%)	37 (-10%)
R05	55 (+23%)	87 (+14%)	16 (-15%)	36 (-7%)
R06	48 (+33%)	81 (+19%)	12 (-24%)	26 (-11%)
R07	54 (+22%)	82 (+7%)	14 (-21%)	31 (-17%)
R08	58 (+15%)	79 (+11%)	8 (-44%)	21 (-62%)
R09	57 (+23%)	99 (-2%)	11 (-11%)	26 (-41%)
R10	40 (+22%)	69 (+8%)	7 (-12%)	19 (-43%)

Table A5.
Average 24-hr $PM_{2.5}$ concentration (μg m^{-3}) for each EPA region.

Region	CURall	FUTall	futBC	futEMIS	futMET-curLU	futMET-futLU
R1-3	11	+4	+0.0	+4	+0.2	+0.4
R04	13	+1	+0.3	+5	-3	-3
R05	10	+3	+0.2	+5	-1	-1
R06	6	+2	+0.4	+3	-1	-1
R07	8	+3	+0.3	+4	-1	-1
R08	3	+2	+0.3	+1	+0	+0
R09	5	+2	+0.6	+2	-0.4	-0.5
R10	4	+2	+0.5	+1	-0.2	-0.4
U.S.	7	+2	+0.4	+3	-0.9	-0.8

Table A6.
Average number of 24-hr $PM_{2.5}$ 35 μg m^{-3} exceedances per region per month.

Region	# grid cells	CURall	FUTall	futBC	futEMIS	futMET-curLU	futMET-futLU
R1-3	494	72	+510	+5	+639	-40	+6
R04	788	208	+447	+23	+1604	-187	-166
R05	680	131	+612	+9	+1408	-110	-79
R06	1119	16	+71	+3	+365	-16	-15
R07	558	12	+108	+1	+287	-7	-1
R08	1173	0	+0	+0	+25	+0	+0
R09	774	2	+30	+2	+113	-2	-2
R10	508	0	+0	+0	+0	+0	+0
U.S.	6094	441	+1778	+43	+4441	-362	-257